Fortschritt-Berichte VDI

VDI

Reihe 8

Mess-,
Steuerungs- und
Regelungstechnik

Nr. 1253

Dipl.-Math. techn. Maxim Stuckert,
Ludwigsburg

Theory and Application of the Lang-Gilles Observer for Distillation Processes

Berichte aus der
Aachener Verfahrenstechnik - Prozesstechnik

RWTH Aachen University

Theory and Application of the Lang-Gilles Observer for Distillation Processes

Theorie und Anwendung des Lang-Gilles Beobachters für Destillationsprozesse

Von der Fakultät für Maschinenwesen der Rheinisch-Westfälischen Technischen Hochschule Aachen zur Erlangung des akademischen Grades eines Doktors der Ingenieurwissenschaften genehmigte Dissertation

vorgelegt von
Maxim Stuckert

Berichter: Univ.-Prof. Dr.-Ing. Wolfgang Marquardt
Univ.-Prof. Dr.-Ing. Achim Kienle

Tag der mündlichen Prüfung: 28. Oktober 2016

Fortschritt-Berichte VDI

Reihe 8

Mess-, Steuerungs- und Regelungstechnik

Dipl.-Math. techn. Maxim Stuckert, Ludwigsburg

Nr. 1253

Theory and Application of the Lang-Gilles Observer for Distillation Processes

Berichte aus der
Aachener Verfahrenstechnik - Prozesstechnik

RWTH Aachen University

Stuckert, Maxim
Theory and Application of the Lang-Gilles Observer for Distillation Processes
Fortschr.-Ber. VDI Reihe 8 Nr. 1253. Düsseldorf: VDI Verlag 2016.
168 Seiten, 39 Bilder, 14 Tabellen.
ISBN 978-3-18-525308-9, ISSN 0178-9546,
€ 62,00/VDI-Mitgliederpreis € 55,80.

Keywords: Distillation – Multicomponent mixtures – Nonlinear state observer – Observer convergence – Observer tuning – Tray efficiency – Tray-efficiency estimator – Model predictive control – Plant-model mismatch – Large-scale simulation

This thesis deals with the nonlinear full state observer for distillation processes first introduced by Lang and Gilles in 1990. The observer is very attractive in practice as it requires only few temperature measurements in each section of a distillation column and only few observer parameters need to be tuned. We provide conditions under which this observer converges and derive a simple rule for the tuning of the observer parameters. We also give a method for the on-line estimation of the Murphree tray efficiency. Such on-line methods are rarely found in literature. In a sequence of simulation studies, we investigate the capabilities of the observer for the estimation of the tray efficiency and for model-predictive control. The simulation studies are based on distillation processes for separation of multicomponent mixtures and one of the studies introduces a plant-model mismatch.

Bibliographische Information der Deutschen Bibliothek
Die Deutsche Bibliothek verzeichnet diese Publikation in der Deutschen Nationalbibliographie; detaillierte bibliographische Daten sind im Internet unter http://dnb.ddb.de abrufbar.

Bibliographic information published by the Deutsche Bibliothek
(German National Library)
The Deutsche Bibliothek lists this publication in the Deutsche Nationalbibliographie (German National Bibliography); detailed bibliographic data is available via Internet at http://dnb.ddb.de.

D82 (Diss. RWTH Aachen University, 2016)

ISSN 0178-9546
ISBN 978-3-18-525308-9

Vorwort

Diese Dissertation entstand während meiner Tätigkeit als wissenschaftlicher Mitarbeiter am Lehrstuhl für Prozesstechnik der RWTH Aachen. Viele Personen haben zu deren Gelingen und meiner persönlichen Weiterentwicklung beigetragen. Es ist mir deshalb eine große Freude, ihnen an dieser Stelle danken zu können.

Dabei möchte ich mich ganz besonders bei meinem Doktorvater, Prof. Dr.-Ing. Wolfgang Marquardt, bedanken. Seine seltene Gabe, Schwachstellen in der Argumentation schnell zu erkennen und mögliche Lösungen aufzuzeigen, erlaubte uns stets konstruktive Diskussionen und anschließend gezielte Forschung. Genauso schätzte ich seine vorbildliche Art, tagtäglich im Interesse seiner Mitarbeiter und Doktoranden zu agieren und den interdisziplinären Dialog zu fördern. Ich möchte auch Herrn Prof. Dr.-Ing. Achim Kienle für die Übernahme des Berichts danken. Bei Herrn Prof. Dr.-Ing. Wolfgang Schröder möchte ich mich für die Übernahme des Vorsitzes der Prüfungskommission bedanken.

Für die vielen Diskussionen im Zusammenhang mit dieser Arbeit möchte ich mich herzlich bei meinen ehemaligen Kollegen, Andreas Harwardt, Ionut Muntean, René Schneider und Holger Scheu bedanken.

Für Ideen und Ratschläge zur richtigen Zeit danke ich Dr.-Ing. Adel Mhamdi. Genauso bin ich Prof. Dr.-Ing. Jorge Otávio Trierweiler und Luciane Trierweiler, PhD, dankbar, die ein Jahr am Lehrstuhl verbracht haben und währenddessen mich durch ihre vielseitigen Ansichten bereichert haben.

Den ehemaligen Büro-Kollegen Reinout Romijn, David Kauven, Hans Pirnay und Jennifer Puschke, die stets für das gute Arbeitsklima sorgten, möchte ich hiermit meinen persönlichen Dank ausdrücken. Allen Kollegen am Lehrstuhl sei gedankt – ohne sie wäre meine Zeit am Lehrstuhl um viele schöne Erinnerungen ärmer.

Natürlich wäre die Anfertigung einer Dissertation ohne die Unterstützung meiner Familie sehr beschwerlich. Ich danke deshalb vor allem meinen Eltern, die mich stets bei meinen Vorhaben unterstützt haben. Nicht zuletzt gilt mein Dank meiner Frau, die mit mir diesen langen Weg gegangen ist und durch ihr Verständnis, Geduld und Unterstützung die Fertigstellung dieser Arbeit außerordentlich erleichterte.

Ludwigsburg, Oktober 2016 Maxim Stuckert

Contents

Nomenclature

Abbreviations

ANN	artificial neural network
CMO	constant molar overflow
DMPC	distributed model-predictive control
EQ	equilibrium stage
MPC	model-predictive control
NEQ	nonequilibrium stage
PDE	partial differential equations
PI	proportional-integral controller
PID	proportional-integral-derivative controller
PLS	partial least squares
QP	quadratic programming
RGA	relative gain array
S-DMPC	sensitivity-driven distributed model-predictive control
SP	setpoint
VLE	vapor-liquid equilibrium

Greek letters

α	observer tuning parameter, see Eq. (3.3)
α_i	observer tuning parameter
$\Delta\hat{T}_{k,m}^{pred}$	predicted temperature difference between two trays k and m
$\delta\hat{y}^*$	deviation of the estimated vapor compositions from the estimated equilibrium compositions, see Eq. (3.6)
$\Delta h_{L,0}$	heat of vaporization
δT	vector of temperature differences, see Eq. (3.7)
$\Delta T_{k,m}$	temperature difference between two trays k and m
$\gamma_{i,j}$	activity coefficient of component i

λ_M, λ_V parameters specifying liquid dynamics with respect to holdup and vapor flow rate changes

ν_i^L liquid phase molar volume of component i

$\phi_{i,j}^L$ fugacity coefficient of pure component i in the liquid phase

$\phi_{i,j}^V$ fugacity coefficient of pure component i in the vapor phase

Ψ_j Jacobian of the vapor-liquid equilibrium function

ξ_0, ξ_1 correlation constants in pressure relation

Latin letters

$\bar{f}(\bar{x}, t)$ majorant of $f(x, \hat{x}, t)$, see Eq. (3.14)

$\bar{T}$ vector of all temperature differences in the plant, see Eq. (3.8)

Δx, Δu, Δd, Δy vector deviations in state equation, see Eq. (5.6)

$\hat{D}$ estimated mass transfer matrix, see Eq. (3.4)

$\mathcal{H}$, $\mathcal{F}$, $\mathcal{A}$, $\mathcal{B}$ matrices in QP formulation, see Eq. (5.22)

$\mathcal{T}_x$, $\mathcal{T}_d$, $\mathcal{T}_u$ matrices in prediction equation, see Eq. (5.17)

$f_i^{vap}(\cdot)$ function specifying vapor component i

f^{vle} vapor-liquid equilibrium function

A, B, C matrices in state equation of the plant, see Eq. (2.65)

A_c, B_c, C_c, D_c continuous-time matrices in state equation, see Eq. (5.7)

A_d, B_d, C_d, D_d discrete-time matrices in state equation, see Eq. (5.12)

a_j interfacial area between liquid and vapor phases on tray j

$A_{l_1 l_2}$, $B_{l_1 l_2}$, $C_{l_1 l_2}$ inner matrices in state equation of the plant, see Eq. (2.66)

$a_{r,s,l}$, $b_{r,s,l}$, $c_{r,s,l}$, f^L_{r,l_1,s,l_2}, f^V_{r,l_1,s,l_2} sub-matrices, see Eq. (2.67)

C_l^V, C_l^L efficiency factors with resistance on the vapor and liquid side, respectively

C_l efficiency factor with resistance on the vapor or liquid side

$E_{MV,i,j}$ Murphree tray efficiency for component i on stage j

$E_{MV,j}$ multi-component Murphree tray efficiency on stage j

$E_{OV,i,j}$ Murphree point efficiency for component i on stage j

$E_{OV,j}$ multi-component Murphree point efficiency on stage j

F flow rate through a valve

$f(x, \hat{x}, t)$ redefinition, see Eq. (3.11)

f^L function specifying liquid dynamics

F_j^L feed liquid stream on stage j

f^V function specifying vapor dynamics
F_j^V feed vapor stream on stage j
F_0 distillate flow rate
F_j side stream on stage j
F_{m+1} bottom flow rate
F_{max} maximum flow rate through a valve
h_j^{tot} total height of the liquid on tray j
h_F enthalpy of feed stream F
h_L enthalpy of liquid stream L
h_{S^L} enthalpy of stream S^L
h_{S^V} enthalpy of stream S^V
h_V enthalpy of vapor stream L
J_j interphase stream on stage j
K_j^L matrix of mass transfer coefficients in the liquid phase on tray j
K_j^V matrix of mass transfer coefficients in the vapor phase on tray j
L_j liquid stream leaving stage j
M_j^L liquid holdup on stage j
M_j^V vapor holdup on stage j
m_l number of stages in column l in-/excluding feed stages/condenser and reboiler
$M_{i,j}$ holdup of component i on stage j
m_{sec} number of stages in a distillation column section
$N_{i,j}$ molar flux between the vapor and liquid phases of component i on stage j
$NTU_{L,j}$ matrix of numbers of transfer units for the liquid phase
$NTU_{OV,j}$ matrix of overall number of transfer units on tray j
p_i^{sat} vapor pressure of component i
p_j pressure on stage j
q number of components in the mixture
Q_C heat flow out of condenser
Q_R heat flow into reboiler
$q_{L,0}$ thermal condition of the reflux flow
R ideal gas constant
S_j^L side liquid stream on stage j
S_j^V side vapor stream on stage j
S_j side stream on stage j

S_{actual} current valve stem position

T_j boiling temperature on stage j

U_j internal energy of both phases on stage j

V_j vapor stream leaving stage j

x, y, z vectors of all liquid and vapor compositions in the plant, see Eq. (2.64)

x_l, y_l, z_l vectors of all liquid and vapor compositions in column l, see Eq. (2.63)

$x_{i,j}$, $y_{i,j}$, $z_{i,j}$ molar liquid, vapor or feed fraction of component i on stage j, page 12

$x_{j,l}$, $y_{j,l}$, $z_{j,l}$ vectors of all liquid and vapor compositions in column l on stage j, see Eq. (2.62)

y^* vapor compositions in equilibrium with liquid

Mathematical symbols

$\circ$ Hadamard product

$\dot{(\cdot)}$ time derivative

$\mathbb{R}^n$ vector space over $\mathbb{R}$

$\mathbb{R}^{n\times m}$ $n \times m$ matrix space over $\mathbb{R}$

$L(\cdot)$ linear function

$N(\cdot)$ nonlinear function

Subscripts, superscripts, accents

$(\cdot)^{nom}$ nominal value

$(\cdot)^{rec}$, $(\cdot)^{str}$ refers to a quantity in the rectifying or stripping distillation sections

$(\cdot)^{true}$ refers to a quantity in the plant replacement model

$(\cdot)_{j_i}$ stage number selected from all stages in the distillation column

$\bar{(\cdot)}$ difference between estimated and measured quantities

$\breve{(\cdot)}$ nominal value of the variable

$\hat{(\cdot)}$ an observer variable

1 Introduction

1.1 Distillation, distillation state observers and distillation control

Distillation is a standard process which has been used for centuries in the chemical and petroleum industry for separation of mixtures into their components. This process is based on the different boiling points of the mixture components. The components with lower boiling points evaporate before the components with higher boiling points and accumulate at the top of a distillation apparatus where they are removed. On the other hand, the components with higher boiling points condense before the components with lower boiling points, accumulate therefore at the bottom of the apparatus and can be removed there. If a large amount of a mixture is to be separated by distillation, either a single distillation column or a sequence of distillation columns, is employed. There are various types of distillation columns having quite different designs which are selected with respect to the thermodynamic properties of the mixture, economic considerations, available technology etc. In this work, we consider staged and continuously operated distillation columns. Such columns usually consist of a reboiler at the bottom of the column where heat is added, a condenser at the top where heat is removed, and a number of stages in between that guarantee a desired quality of separation. The mixture enters the distillation column continuously on the feed stage. The separation products are continuously withdrawn from the condenser and the reboiler. Distillation is extensively dealt with in contemporary literature, by Kister (1992), Perry and Green (2008) and many others. With more than 486,000 references[1], it has been one of the most popular research areas in chemical engineering. It is therefore practically impossible to provide a complete overview of distillation and related subjects. In this thesis, we will restrict ourselves to a moderate number of important references.

In order to ensure smooth operation of a distillation column, different quantities have to satisfy certain constraints and, therefore, need to be controlled. Following the classical works of Rademaker et al. (1975) and Buckley et al. (1985), these are liquid levels, pressures, and temperatures or product compositions. Disturbances in the feed flow rate,

[1] References containing the concept "distillation"; found with SciFinder at www.cas.org; March 25, 2012

composition, or thermal condition, as well as in heat supply or removal and ambient temperature may, however, disrupt operation and diminish product qualities.

In distillation columns, pressures, temperatures and liquid levels can usually be measured quickly and reliably. The situation is completely different for product compositions. Their direct measurement is expensive and difficult (Mejdell and Skogestad, 1991a). Besides, only the average tray compositions are typically obtained with a time delay; measurements of the average tray compositions on every tray of a column, not to mention local compositions on every tray, are presently more than a challenge. To overcome the problem of the missing or delayed composition measurements, a lot of research has been devoted to the estimation of product compositions. Static as well as dynamic estimation methods have been proposed. These works include those of Weber and Brosilow (1972), Joseph and Brosilow (1978), Mejdell and Skogestad (1993), Baratti et al. (1995, 1998), Shin et al. (2000a), Kano et al. (2000), Osman and Ramasamy (2010), as well as Olanrewaju et al. (2012). Most of the estimators deal with binary distillation (e.g. Joseph and Brosilow, 1978, Mejdell and Skogestad, 1993, Baratti et al., 1995, Osman and Ramasamy, 2010), but estimators for multicomponent distillation columns are also available (e.g. Lang and Gilles, 1990, Quintero-Marmol et al., 1991, Oisiovici and Cruz, 2001).

To estimate compositions dynamically, state observers have often been used. The term observer was first used by Luenberger (1964). A state observer provides estimates of the state variables from measurements of the input and output of the real system under consideration, i.e., compositions are estimated from flow rate and temperature measurements in a distillation column. Later, a number of different approaches were applied to distillation columns, for example, Kalman filters (Oisiovici and Cruz, 2001, Olanrewaju and Al-Arfaj, 2006), extended Luenberger observers (Quintero-Marmol et al., 1991), geometric observers (Tronci et al., 2005, Álvarez and Fernández, 2009), exponential observers (Deza and Gauthier, 1991), or observers with a physically motivated correction term (Lang and Gilles, 1990). It is well known that the state variables can be fully reconstructed by a state observer from selected measurements if the system is observable. Observability of distillation columns has been investigated by Quintero-Marmol et al. (1991) and Yu and Luyben (1987).

In order to apply state observers in practice, their convergence and robustness with respect to the modeling errors and measurement noise should be verified beforehand. The convergence of linear state observers can usually be proved with relatively little effort for well-selected assumptions. However, the convergence of nonlinear state observers in particular and studies showing their robustness require more effort and are consequently very rare in literature. It is thus not surprising that the convergence properties of linear state observers such as the Kalman filter and the Luenberger observer (Kalman, 1960,

Luenberger, 1964) applied to linear systems are well understood. In contrast, the properties of nonlinear state estimators are less clear. In particular, the convergence of the Lang-Gilles observer (Lang and Gilles, 1990) is still an open question.

In a control environment, composition estimates typically compensate for missing or delayed composition measurements to improve product control. The composition estimates can either be incorporated in the outer (slower) loop of a cascade controller (Barolo and Berto, 1998, Bettoni et al., 2000, Kano et al., 2000, Castellanos-Sahagún and Alvarez, 2004), or, often, they serve as initial values to calculate predictions in a model predictive controller (Brizuela et al., 1996, Diehl et al., 2003, Guo et al., 2009). Often, distillation case studies consider only a single column (Kano et al., 2000, Pannocchia and Brambilla, 2005, Guo et al., 2009). However, since Buckley's pioneering work (Buckley, 1964), a trend towards plantwide control seems inevitable as the research focus shifts to more complex processes (Luyben et al., 1997, Skogestad, 2004, Downs and Skogestad, 2011), in which several distillation columns and also other units may be included. Very few works, even those studying single distillation columns, analyze the effect of parametric plant-model mismatch, e.g., mismatched controller and plant models (Biswas et al., 2009). A structural plant-model mismatch is considered even more rarely. For instance, Olanrewaju and Al-Arfaj (2006) used a linearized model in the Kalman filter and a nonlinear plant model; they also investigated the effect of uncertainties in relative volatilities on control results. Uncertainties in parameters as well as a plant-model mismatch were examined by Baratti et al. (1995), too.

1.2 Scope of the thesis

In the remainder of this work, we investigate several problems that address a certain distillation state observer, the Lang-Gilles distillation observer (Lang and Gilles, 1990). We especially want to shed light on conditions under which this observer converges, and derive a simple rule for the tuning of the observer gains. In a sequence of simulation studies, we will investigate the capabilities of the observer for the estimation of the separation efficiency and for control. The simulation studies are based, except where otherwise stated, on a complex distillation process first developed by Kraemer et al. (2009). This process is introduced in the following.

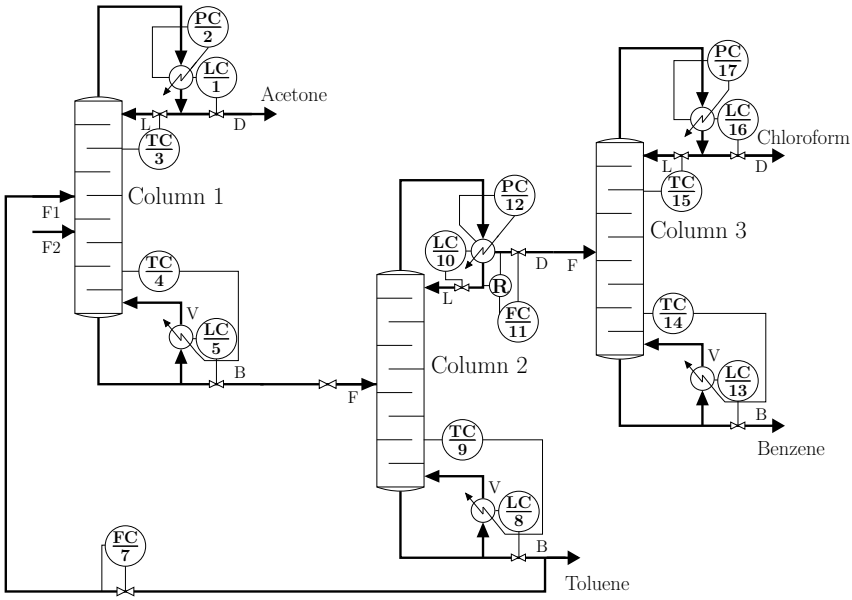

Figure 1.1: The ACBT separation process with a base-control layer; the design of the base-control layer is presented in Section 2.5.2.

1.2.1 A distillation process for the separation of the mixture of acetone, chloroform, benzene and toluene

For the separation of the azeotropic mixture of acetone, chloroform, benzene and toluene, an equimolar feed stream is split into the pure components with a purity of 99 %. The mixture exhibits the binary maximum boiling azeotrope of acetone and chloroform, which gives rise to a distillation boundary. This boundary prohibits separation into the pure components. Kraemer et al. (2009) suggested a process configuration (the ACBT process) in which the curved distillation boundary can be crossed and separation into the pure components is possible with a minimum number of three distillation columns. In this configuration, shown in Fig. 1.1, toluene is recycled to the first column, shifting the total feed of the column and enabling exploitation of the curved boundary in the distillation process. In the first column, pure acetone is separated at the top, followed by separation of pure toluene at the bottom of the second column. The third column separates the binary mixture of chloroform and benzene.

The ACBT process will serve as a plant-replacement model in some simulation studies.

Further, a simpler model of the ACBT process will be used in the Lang-Gilles observer. This will extend the work of Lang and Gilles (1990) who studied the separation of a feed mixture with up to 3 components by a single distillation column. To the best of our knowledge, there are no publications which propose to apply their observer for state estimation of distillation trains. Although the extension to more components seems to be straightforward, the principal obstacles involving the increased numerical workload and integration difficulties may prevent a broader usage of the observer. Lang and Gilles (1990) also do not provide theoretical results for convergence of their observer. Therefore, the convergence properties is one of the problems we will study in this work.

1.2.2 Convergence of the Lang-Gilles observer

The convergence of an observer is defined in terms of the convergence of the difference between the observed and real system-state variables to zero. Under certain assumptions, the propagation of this error is described by the error equation which can be written as

$$\frac{d}{dt}(\hat{x} - x) = A(\hat{x} - x) + f(x, \hat{x}, t), \tag{1.1}$$

where $\hat{x} - x$ is the error between the observed and real state variables, A a system matrix fixed especially by the flow rates and tray holdups, f a function which includes remaining thermodynamical nonlinearities, and t the time variable. One of our main goals will be to define the sufficient conditions under which the error $\hat{x} - x$ in Eq. (1.1) converges to zero. In this context, tuning of the observer gains will also be important.

1.2.3 Separation efficiency estimation in conjunction with the Lang-Gilles observer

There are different definitions of separation efficiencies in distillation columns. A prominent one is unquestionably the Murphree efficiency (Murphree, 1925). The accurate estimation of separation efficiencies, however, plays a very important role in distillation. A good prediction of separation efficiencies helps, for example, to design distillation columns which require lower investment cost. Calculating efficiencies on-line may reduce operating cost because then the plant operator would more easily recognize (un-)favorable operating conditions. Unfortunately, even the estimation of the nominal separation efficiencies is usually a complicated task. It may be even more tricky to calculate these on-line.

In this work, starting from a simplified definition of the multi-component Murphree efficiency $E_{MV,j}$ on stage j,

$$E_{MV,j} = I - (I + C_l \Psi_j^{-1})^{-1}, \tag{1.2}$$

with the Jacobian of the vapor-liquid equilibrium Ψ_j and the lumped separation efficiency parameter C_l, we are interested in a simple on-line method for estimation of the parameter C_l. Only a few temperature measurements should be required and a simple tuning should be sufficient. With this in mind, we will propose a method that combines a parameter estimation method with state estimation by the Lang-Gilles state observer.

1.2.4 Model-predictive control in conjunction with the Lang-Gilles observer

As pointed out in Section 1.1, plantwide control becomes more important when dealing with complex processes. In this thesis, we will investigate the ACBT process for the separation of an acetone-chloroform-benzene-toluene mixture into its components. Since the mixture is azeotropic, its separation is more difficult than that of an ideal mixture as it was outlined in Section 1.2.1. The separation is performed by means of a three-column distillation sequence including a recycle as proposed by Kraemer et al. (2009). This distillation sequence presents us with a challenge in setting up an observer and a model-predictive controller. We are especially interested in answering the following questions for this sequence:

- How can we design the Lang-Gilles observer and how does it perform?
- Does a certain distributed model-predictive controller (Scheu and Marquardt, 2011) have advantages over a decentralized controller?
- How do the designed observer and controllers perform when a structural plant-model mismatch is present?

The results of our simulations are also of particular interest to us as neither the Lang-Gilles observer, nor the proposed model-predictive controller have been tested with azeotropic distillation trains accounting for structural plant-model mismatch before.

1.3 Structure of the thesis

In this thesis we will focus on the following issues:

- dynamic distillation modeling,
- convergence, tuning and performance of the Lang-Gilles observer,

- estimation of the multi-component Murphree efficiency, and
- the use of the Lang-Gilles observer in output feedback control.

These objectives can be roughly assigned to the separate chapters of the thesis.

A detailed study of the existing dynamic distillation models is carried out in Chapter 2. Physically motivated distillation models are the basis for the Lang-Gilles state observer and serve as the plant replacement and controller models in our later case studies. These distillation models adopt the Murphree tray efficiency to take into account the non-ideal behavior of column trays. Here, we first classify distillation models, introduce the Murphree efficiency concept, and present thereafter those particular models for our case studies including a summary of the model parameterization. Finally, we discuss the dynamics of the ACBT process at a nominal operating condition and present the base-control layer for this process.

In Chapter 3, we deal with convergence of the Lang-Gilles observer. Three theorems relying on different assumptions concerning vapor compositions and temperature measurements are stated and proved. After this, we derive from the third theorem a rule for observer tuning. In the subsequent case study, we address an effect influencing the convergence rate of the observer, which is related to the internal flow rates in the distillation columns, that supports the derived tuning rule.

Chapters 4 and 5 cover applications of the Lang-Gilles observer. Chapter 4 introduces a method for estimating the separation efficiency parameter derived in Chapter 2 from the Murphree efficiency model by lumping hardly measurable quantities to one single parameter. This parameter is estimated online in a series of alternate state and parameter estimation steps. The states are estimated by the Lang-Gilles observer and the efficiency parameter is determined by nonlinear parameter estimation. The effectiveness of this sequential approach is again demonstrated in a case study.

Chapter 5 concerns the application of the Lang-Gilles observer in the context of control. First, we recall some theoretical results. Then, a large-scale study is presented in which the Lang-Gilles observer for a distillation train with a plant-model mismatch is used. The high complexity of this study usually avoided in the literature allows us to investigate practically relevant problems especially concerning plant-model mismatch.

Finally, we draw conclusions arising from this work and raise some potential issues for future research.

2 Dynamic distillation modeling

2.1 Introduction

In his book on the history of distillation, Forbes (1970) addressed the origin of distillation and pointed out that Alexandrian chemists were probably first to invent distillation in the first century A.D.. In the following centuries and before industrialization in Europe began, the distillation apparatus was the focus of further development. It was not until 1893 that Sorel (1893) first developed a model of a distillation column comprising a set of algebraic mass and energy balance equations. In these equations, Sorel uses already the so-called K-value to describe the relationship between the liquid and vapor concentrations of alcohol impurities and he recognizes that the K-value depends on the vapor pressure. Surprisingly, he gives no reference to Dalton's and Raoult's laws, known since 1803 and 1886 (Hall, 1999), which can be combined to establish a basic vapor-liquid equilibrium model for ideal vapor and liquid phases that gives explicitly the dependency of the vapor composition on the vapor pressures of the components and the total pressure. However, inside a real distillation column, a vapor-liquid equilibrium is rarely reached. To take this into account, Murphree (1925) introduced a separation efficiency factor named later after him. At that time, the solution of the set of distillation equations was still a problem. This changed in 1925 as McCabe and Thiele (1925) proposed a simple method to solve the equation set *graphically*, and in 1932, Lewis and Matheson (1932) made a first attempt to solve the equations *numerically*. The appearance of analog and especially digital computers marked a milestone in distillation modeling and simulation. In the 1950s researchers first deployed punched card machines for plate-by-plate calculations of distillation columns, e.g. Opler and Heitz (1951). According to Seader (1985) the year 1951 marks the start of using computers for distillation modeling and simulation. Later, countless contributions to distillation modeling appeared which dealt with phenomenological effects and investigated different model structures and solution algorithms (Perry and Green, 2008). For example, a lot of scientific effort was spent to develop new equations of state to detail the K-value model. For non-polar mixtures, some widely used equations of state are the Benedict-Webb-Rubin (Benedict et al., 1940), Redlich-Kwong (Redlich and Kwong, 1949), Soave-Redlich-Kwong (Soave, 1972), and Peng-Robinson (Peng and Robinson, 1976) state

equations. For polar mixtures, the K-value model was extended by additional factors, the activity coefficients. Modern methods for modeling activity coefficients are based on molecular considerations and include the Wilson model (Wilson, 1964) which is adequate for miscible mixtures, the NRTL model (Renon and Prausnitz, 1968) which is especially suitable for non-ideal and partially immiscible mixtures, and the UNIQUAC (Abrams and Prausnitz, 1975) and UNIFAC models (Fredenslund et al., 1975) which are applicable to a variety of miscible and immiscible mixtures. Distillation modeling has also benefited from scientific progress in various fields such as numerical methods and computer science, the demand for new commodities, and new techniques in column design (e.g. Cameron et al., 1986, Gani et al., 1998, Olujić et al., 2009). All these developments boosted novel modeling approaches which now give the engineer a great number of possibilities from which to choose (Taylor, 2007).

In this chapter, dynamical modeling of continuously operated distillation columns or column sequences is presented, including the standard column parts such as reboilers, feed trays, condensers, and stripping and rectifying sections. We will consider equations which apply to a typically configured distillation column as shown in Fig. 2.1 but which may readily be rolled out to column sequences.

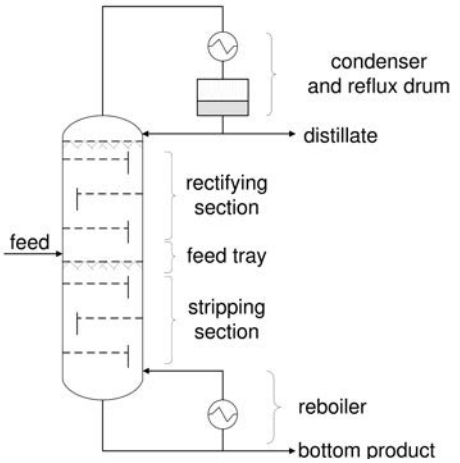

Figure 2.1: A basic configuration for a distillation column

Generally, there are no clear recommendations how the structure of an entire distillation model should be selected. Distinct model structures and correlations were proposed by

various authors (cf. McAvoy and Wang, 1986, Skogestad, 1997, Abdullah et al., 2007, and references therein). Therefore, the approach followed in this thesis is based upon general advice given and partly summarized by Häggblom (1991), Luyben (1992), and Skogestad (1997). Furthermore, correlations which are known to have a sound physical foundation and which result in numerically stable solutions by available modeling environment such as gPROMS (Process Systems Enterprise, 1997-2013) are preferred. Additional considerations made by Pearson (Pearson, 2003), who studied the properties of some nonlinear model structures, are used to justify the choice of nonlinear model structures.

The chapter is organized as follows. In Section 2.2, fundamental, empirical and semi-empirical distillation models are presented. In Section 2.3, we will review distillation efficiency models and derive a parametric form of the multicomponent Murphree efficiency. This efficiency model is incorporated in our plant replacement and controller/observer models. We will derive their equations in Section 2.4 on the basis of Section 2.2. We will also highlight the similarities and differences between the plant replacement and controller/observer models and discuss their parametrization. In Section 2.5, the exemplary dynamics of the distillation models at a nominal operating condition are demonstrated with the help of the ACBT process. We will also introduce the regulatory control for the ACBT process. Finally, we will summarize this chapter.

2.2 Classification of distillation models

Distillation models can be classified in different ways. A plausible way to introduce a classification is to decide which type of information is used to build a model. In this section, we adopt a general classification of distillation models, including fundamental, empirical, and hybrid models. We will emphasize some essential concepts for development of fundamental models, reviewing however model classification and some of the works very much along the lines of Abdullah et al. (2007).

2.2.1 Fundamental models

The term *fundamental* (or first principle) model refers to a model which is derived from physical laws such as mass, energy or momentum balances and the associated constitutive equations. The physical laws are typically represented by nonlinear algebraic and differential equations. Although numerical difficulties and also more development effort are often introduced by nonlinear compared to linear equations, good fundamental models may compensate for these disadvantages with physically meaningful parameters and a superior simulation accuracy. Besides, first principle models usually extrapolate to operating regions not present in the modeling data. Consequently, higher expenses for the

development of a fundamental model are justified if an accurate model is desired. For highly nonlinear distillation processes, the use of such models is very attractive and much valuable work has been conducted on their basis in contemporary research.

In first principle distillation modeling, two concepts, which are used to describe the physical behavior of a tray or a part of a packed column, turned out to be very important: the equilibrium stage (EQ) and the nonequilibrium stage (NEQ) concepts. They will be introduced in the following.

The concept of the equilibrium stage (EQ)

The concept of the equilibrium stage was introduced by Sorel (1893). It is assuming

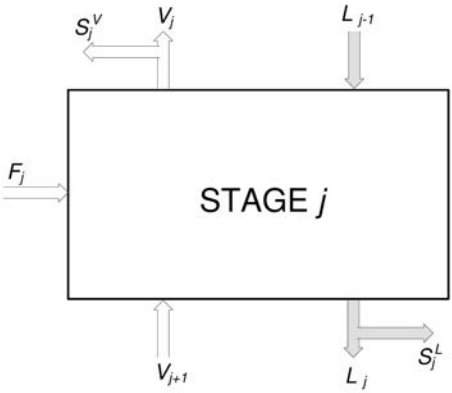

Figure 2.2: The equilibrium stage

that the liquid phase on stage j is well mixed and that vapor and liquid streams leaving the stage, V_j, L_j, S_j^V, S_j^L, are in thermodynamic equilibrium with each other (Fig. 2.2). The assumption of thermodynamic equilibrium is essential as it allows determination of the compositions and temperatures of the streams leaving the stage (Perry and Green, 2008). The differential equations may be formulated for each stage as material balances for components $i = 1, \ldots, q-1$,

$$\frac{dM_{i,j}}{dt} = L_{j-1}x_{i,j-1} - \left(L_j + S_j^L\right)x_{i,j} + V_{j+1}y_{i,j+1} - \left(V_j + S_j^V\right)y_{i,j} + F_j z_{i,j}, \tag{2.1}$$

$$M_{i,j} = M_j^L x_{i,j} + M_j^V y_{i,j}, \tag{2.2}$$

overall material balance,

$$\frac{dM_j}{dt} = L_{j-1} - \left(L_j + S_j^L\right) + V_{j+1} - \left(V_j + S_j^V\right) + F_j, \tag{2.3}$$

$$M_j = M_j^L + M_j^V, \tag{2.4}$$

and energy balance

$$\frac{dU_j}{dt} = L_{j-1}h_{L,j-1} - \left(L_j + S_j^L\right)h_{L,j} + V_{j+1}h_{V,j+1} - \left(V_j + S_j^V\right)h_{V,j} + F_j h_{F,j}. \tag{2.5}$$

Here M_j^L, M_j^V are the holdups of the liquid and vapor phases, respectively. $x_{i,j}, y_{i,j}$, and $z_{i,j}$ denote mole fractions of the liquid phase, the vapor phase, and the feed. U_j is the internal energy of both phases on stage j and $h_{L,j}, h_{V,j}, h_{F,j}, h_{S^L,j}, h_{S^V,j}$ are the enthalpies of the streams $L_j, V_j, F_j, S_j^L, S_j^V$ leaving or entering stage j. Moreover, there are algebraic relations to be included in the model which describe the vapor-liquid equilibrium (VLE), the stage hydraulics and vapor dynamics, i.e.,

$$y_{i,j} = f_i^{vle}(x_{1,j}, \ldots, x_{q-1,j}, T_j, p_j), \tag{2.6}$$

$$L_j = f^L(M_j^L, V_j, \Delta p_j), \tag{2.7}$$

$$V_j = f^V(M_j^L, \Delta p_j), \tag{2.8}$$

where p_j, T_j are the pressure and boiling temperature on stage j. f_i^{vle} is the equilibrium equation valid for the actual mixture. f^L and f^V are some functional relations to be specified with respect to the pressure difference $\Delta p_j = p_{j+1} - p_{j-1}$ over stage j and the plate geometry. A thorough specification of these algebraic functions has been given by Gani et al. (1986), Häggblom (1991), Skogestad (1997), and Wittgens and Skogestad (2000), for example.

In our simulations we will use EQ, where especially the function f_i^{vle} in Eq. (2.6) must be selected. We will calculate this by the so-called γ/ϕ-approach (Perry and Green, 2008). This means that an equation obtained from the equality of the component fugacities in the vapor and liquid phases at vapor-liquid equilibrium,

$$\gamma_{i,j}x_{i,j}\phi_{i,j}^L p_i^{sat} \exp\frac{\nu_i^L(p_j - p_i^{sat})}{RT_j} = \phi_{i,j}^V y_{i,j} p_j, \tag{2.9}$$

is solved for $y_{i,j}$ to obtain

$$y_{i,j} = \gamma_{i,j}x_{i,j}\frac{\phi_{i,j}^L p_i^{sat}}{\phi_{i,j}^V p_j} \exp\frac{\nu_i^L(p_j - p_i^{sat})}{R\ T_j}, \tag{2.10}$$

where R is the ideal gas constant, p_i^{sat} denotes the vapor pressure of component i, ν_i^L is the liquid phase molar volume, $\phi_{i,j}^V$ is the vapor-phase fugacity coefficient of pure component i evaluated at temperature T_j and pressure p_j, $\phi_{i,j}^L$ is the liquid-phase fugacity coefficient

of pure component i evaluated at temperature T_j and pressure p_i^{sat}, and $\gamma_{i,j}$ is the activity coefficient of component i. Moreover, we assume $\phi_{i,j}^V = \phi_{i,j}^L = 1$, i.e, the vapor phase is an ideal gas, and the exponential known as the Poynting factor is neglected. Therefore, Eq. (2.10) reduces to

$$y_{i,j} = \gamma_{i,j} x_{i,j} \frac{p_i^{sat}}{p_j}. \tag{2.11}$$

The vapor pressure p_i^{sat} is calculated by the Extended Antoine equation (Aspen Technology, Inc., 1981-2010),

$$\ln p_i^{sat} = C_{i,1} + \frac{C_{i,2}}{T_j + C_{i,3}} + C_{i,4} + C_{i,5} \ln T_j + C_{i,6} T_j^{C_{i,7}}, \quad C_{i,8} \leq T_j \leq C_{i,9}, \tag{2.12}$$

where $\ln p_i^{sat}$ is extrapolated versus $1/T_j$ if T_j is outside of the temperature bounds. The activity coefficients $\gamma_{i,j}$ account for deviations from ideal behavior in the mixture on stage j. They are functions of temperature and liquid-phase composition. We predict them by the Wilson (1964) equation

$$\ln \gamma_{i,j} = 1 - \ln \left(\sum_{k=1}^{q} \Lambda_{i,k} x_{k,j} \right) - \sum_{k=1}^{q} \frac{\Lambda_{k,i} x_{k,j}}{\sum_{m=1}^{q} \Lambda_{k,m} x_{m,j}}, \tag{2.13}$$

$$\Lambda_{k,m} = \frac{\nu_k^L}{\nu_m^L} \exp - \frac{\lambda_{k,m} - \lambda_{k,k}}{R\, T_j}, \tag{2.14}$$

where the parameters ν_k^L and $\lambda_{k,m}$ must be predetermined for $k, m = 1, \ldots, q$. The dependent concentration $x_{q,j}$, which is required in Eq. (2.13), is calculated from the independent concentrations by the relation $x_{q,j} = 1 - \sum_{i=1}^{q-1} x_{i,j}$. For the Antoine/Wilson parameters of an ACBT mixture as mostly used in this work the reader is referred to Appendix C.1. If the temperature T_j on tray j is required, it is determined as bubble point temperature by solving an implicit function F given as

$$F\left(T_j(p_j, x_1, \ldots, x_q), p, x_1, \ldots, x_q\right) = 0 \tag{2.15}$$

for T_j. For a discussion of bubble point calculations (or flash calculations), the reader is referred to Perry and Green (2008).

If the streams leaving the column tray deviate from equilibrium conditions, the number of theoretical and that of real trays is not the same. Peters, Jr. (1922) was among the first to notice this problem. Thereupon Murphree (1925) suggested a nowadays well-known tray efficiency concept discussed in more detail later in Section 2.3. The use of such an efficiency concept together with the equilibrium stage might sometimes be sufficient to describe a moderate deviation from equilibrium conditions (Murphree, 1925, Klemola, 1997). However, in case of more severe deviations, one should adopt the nonequilibrium stage.

The concept of the nonequilibrium stage (NEQ)

A schematic representation of the nonequilibrium stage is given in Fig. 2.3. Distillation models using NEQ stages are also called rate-based. In contrast to the equilibrium stage,

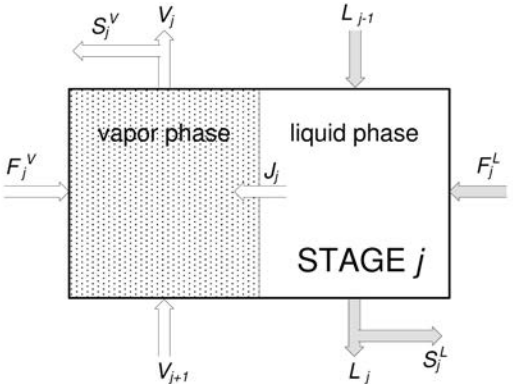

Figure 2.3: The nonequilibrium stage

the nonequilibrium stage j is modeled by writing balance equations for both phases separately. The distinct phases can exchange material and energy by interphase streams J_j (Krishnamurthy and Taylor, 1985).

The dynamic equations corresponding to Fig. 2.3 can be formulated as material balances for components $i = 1, \ldots, q-1$,

$$\frac{dM_{i,j}^L}{dt} = L_{j-1}x_{i,j-1} - \left(L_j + S_j^L\right) x_{i,j} - J_{i,j} + F_j^L z_{i,j}^L, \tag{2.16}$$

$$\frac{dM_{i,j}^V}{dt} = V_{j+1}y_{i,j+1} - \left(V_j + S_j^V\right) y_{i,j} + J_{i,j} + F_j^V z_{i,j}^V, \tag{2.17}$$

$$M_{i,j}^L = M_j^L x_{i,j}, \quad M_{i,j}^V = M_j^V y_{i,j}, \tag{2.18}$$

overall material balances,

$$\frac{dM_j^L}{dt} = L_{j-1} - \left(L_j + S_j^L\right) - J_j + F_j^L, \tag{2.19}$$

$$\frac{dM_j^V}{dt} = V_{j+1} - \left(V_j + S_j^V\right) + J_j + F_j^V, \tag{2.20}$$

$$J_j = \sum_i J_{i,j}, \tag{2.21}$$

and energy balances

$$\frac{dU_j^L}{dt} = L_{j-1}h_{L,j-1} - \left(L_j + S_j^L\right)h_{L,j} - J_j h_{J,j} + F_j^L h_{F^L,j}, \tag{2.22}$$

$$\frac{dU_j^V}{dt} = V_{j+1}h_{V,j+1} - \left(V_j + S_j^V\right)h_{V,j} + J_j h_{J,j} + F_j^V h_{F^V,j}. \tag{2.23}$$

Note that the feed stream is split in two streams, F_j^L (liquid phase) and F_j^V (vapor phase) in the equations above. In general, the vapor and liquid streams leaving the stage are not in equilibrium. However, equilibrium is assumed to hold at the phase boundary. The NEQ stage concept is generic as it can be applied to a stage with any number of phases observed. Even more complex stage models with a mass transfer between the bubbles (phase), the froth (phase) and the spray (phase) were already proposed (Taylor and Krishna, 1993). In contrast to the equilibrium-stage models, tray efficiencies are not used in a rate-based model.

In the following, we discuss rigorous models which may be based upon one of the aforementioned concepts, EQ or NEQ.

Rigorous distillation column models

According to Skogestad the term *rigorous* model usually refers to a staged model as depicted in Fig. 2.4 which includes mass and energy balances on each stage, the liquid flow dynamics, and pressure dynamics (Skogestad, 1997). The EQ concept has been used more frequently than the NEQ concept for distillation modeling although there are situations when the NEQ concept (see p.13) is mandatory (cf. Taylor et al., 2003). Many authors applying the NEQ approach have focused on steady-state models, e.g., Block and Hegner (1976), Müller and Segura (2000), Higler et al. (2004). However, dynamical models were developed, as well, e.g. Gilles and Retzbach (1983). The authors employed an optimal control algorithm including their simplified model of an extractive distillation column in a large-scale plant, where it not only proved its reliability and efficiency in field tests but also in two yeas of continuous operation. A more recent dynamical model was developed by Damartzis and Seferlis (2010). However, the authors emphasize that the employment of NEQ models strongly increases the model size and complexity. For real-time applications simpler approaches are often preferred (Perry and Green, 2008). Therefore, we focus here on distillation models utilizing the EQ stages.

Also for EQ models, Skogestad (1997) reports that no references were found at the time in which the model equations are solved in the rigorous form given in Section 2.2.1. Still, even nowadays, a number of simplifications are commonly employed:

A. Simplifications of the vapor dynamics

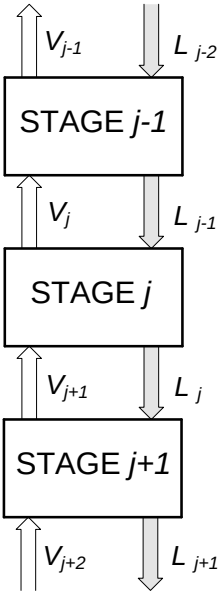

Figure 2.4: A staged distillation section without sidestreams

1. Disregarding vapor holdup

   This assumption is equivalent to requiring $M_j^V = 0$. However, for volatile components, columns operating at high pressures and cryogenic distillation, the difference between vapor and liquid densities becomes smaller. Therefore, under certain circumstances, disregarding vapor holdup may be inadequate. As a consequence of excluding the vapor holdup, a change of the vapor flow at the reboiler immediately changes the vapor flow at every stage of the column.

2. Fixed pressure and disregarding vapor holdup

   As the pressure in a distillation column is usually tightly controlled, it also can be fixed in a simulation. With this approach, a linear or a flow dependent decrease of the pressure along the column can be assumed while at the top of the column the pressure is controlled.

3. Fixed pressure but with vapor holdup

   Vapor holdup should be included if the vapor density becomes relatively high, which often corresponds to operating a distillation column at a pressure higher

than 5 – 10 bar. For example, Luyben (1992) recommends including the vapor holdup if it exceeds 1/6th of the total holdup.

For lower pressures, the vapor holdup should be included if the vapor density becomes greater than 2% of the liquid density. Including the vapor holdup results in more accurate time constants and thus in more reliable predictions of column dynamics (Choe and Luyben, 1987).

B. Simplifications of the liquid flow dynamics

1. Disregarding liquid dynamics

   This case is equivalent to assuming constant liquid holdups. It is a valid assumption if only the dominant response of the composition dynamics is of interest. However, in a control study the initial response of the distillation column, i.e., the response due to the liquid dynamics, is also important. Thus, for control purposes, liquid dynamics must be included in the model.

2. Linearized liquid dynamics

   Linearized liquid dynamics can also be used in a control study if flooding and similar nonlinear effects are not present at the operating condition.

C. Simplifications of the energy balance (in addition to the disregarded vapor holdup and if the internal liquid energy is approximated by the liquid enthalpy)

1. Constant energy holdup

   This common assumption results in an algebraic energy balance. In mathematical notation it is equivalent to assuming $dU_j/dt = M_j dh_{L,j}/dt + h_{L,j} dM_j/dt = 0$ for the left-hand side of the energy balance equation. As this formula suggests, the assumption of a constant energy holdup is valid only if the liquid enthalpy is zero, or both the liquid holdup and the enthalpy are constant. However, in other cases, this is usually a physically wrong assumption and should not be used.

2. Constant liquid enthalpy

   Skogestad remarks that the validity of this assumption, which implies $dU_j/dt = h_{L,j} dM_j/dt$ for the left-hand side of the energy balance equation, depends on the assumed reference state for energy. The reference state should be chosen such that the pure components are saturated liquids at a given reference pressure, which is usually the column pressure. If non-ideal mixtures with large heats of mixing or differences in enthalpy of vaporization are distilled, or the column

pressure varies within wide limits, this assumption is usually very poor (cf. necessary conditions for the derivation of the constant liquid enthalpy assumption in Appendix A.1).

3. Constant molar flows

   When assuming the above reference state for energy, a constant column pressure, the liquid enthalpy equal to zero, and the same heat of vaporization for pure components, it holds $V_j = V_{j+1}$ and at a steady state also $L_j = L_{j+1}$. This corresponds to the constant molar overflow assumption (see Appendix A.2).

As stated by Skogestad (1997), some of the above simplifications are utilized in models which were given different names in the past. Levy et al. (1969) refer to the models incorporating enthalpy (E), mass (M), and components (C) balances as EMC models. Also analogously derived MC and C models have been widely used. There is a link between these models and simplifications outlined by Skogestad and presented above. An EMC model often includes the simplifications A1 and A2, an MC model A2 and C3, and a C model incorporates A2, B1 and C3. Nowadays, due to various advances in computer technology, the computational load is of less importance in distillation simulation and the models C and MC are becoming less relevant. Actual models usually incorporate energy and mass balances in some form (Gani et al., 1986, Häggblom, 1991, Olsen et al., 1997, Biswas et al., 2009, Guo et al., 2009). Often, these equations are referred to as MESH equations, i.e., M equations refer to the material balances, E to the equilibrium equations, S stands for the summation equations of the molar fractions, and H are the enthalpy balance equations. However, the majority of the models based on MESH equations still rely on simplifications, and even so, they may suffer from numerical problems (Perry and Green, 2008, Simulation of distillation processes, pp.13–45).

Finally, we can remark that rigorous models, even the simplified ones, should be classified as fundamental since they incorporate physical laws. However, not all fundamental models are rigorous in the literal sense of Skogestad's definition as there are, for example, non-staged models describing packed distillation columns by a set of partial differential equations (PDE) and reduced models which may retain only some implicit forms of balances. Such reduced models are reviewed in the following.

Reduced models

Model reduction is a mathematical technique which aims at a reduction of the number of differential equations. It is usually employed if the reduced model promises a decrease in computational time. Prior to performing the model reduction, the purpose of the reduction should be defined. Three principal purposes can be distinguished:

a) The reduced model is adopted in real-time applications in order to speed up the optimization or simulation.

b) The reduced model must reduce numerical problems.

c) The reduced model must explain the principal behavior of the plant.

Due to the great importance of these three issues in engineering, it is therefore natural that a considerable amount of research on reduction techniques has been conducted and probably will be conducted in the future (see van den Berg, 2005, Hahn and Edgar, 2002, and references therein).

In the realm of distillation modeling, model reduction became attractive after rigorous simulation was studied in the 1960's (Howard, 1970). First reduced models were linear (Weigand et al., 1972). Thereafter, various mathematical model-reduction techniques were proposed. Among them there are techniques using collocation (Cho and Joseph, 1983), lumping stages to compartments (Benallou et al., 1986), substitution of concentration profiles by waves (Retzbach, 1986, Marquardt, 1988, Kienle, 2000), balancing of empirical Gramians (Hahn and Edgar, 2002), singular perturbation (Kumar and Daoutidis, 2003), and others. Not all of these techniques are equally well suited to each of the purposes a) - c) described above. Besides known problems leading to reduced models which fail to fulfill one of the above purposes, there are other requirements a reduced model should possess. Benallou et al. (1986) formulate these desirable requirements as follows

- the reduced model should retain the physical structure of the process,
- all state variables should remain physically significant,
- all model parameters should be related to the process parameters and should be obtainable from steady state process data.

Compartmental and wave-based models, for example, satisfy these requirements well. On the other hand, collocation-based models are known to produce a discrepancy between the states of the reduced and complete models at steady state. Nevertheless, a true advantage of many reduction techniques is their ability to derive numerically robust models in a structural way. The focus of model reduction, however, may change in the future. While in the past, the need for model reduction often ensued from software limitations and limited computational power (Cho and Joseph, 1983), these obstacles are becoming more and more irrelevant nowadays. Moreover, a "good" reduction method which is necessary to obtain a model of good quality (Marquardt, 2001) also transfers the nonlinear behavior from the non-reduced to the reduced model. This, however, contradicts the goal of model simplification for simulation (Linhart and Skogestad, 2009), especially since the nonlinear

rigorous models can be handled by the actual software and computers quite well. Hence, from the application point of view, a reduction of distillation models will rarely help if high-fidelity (nonlinear) predictions are required.

2.2.2 Empirical models

Empirical modeling is one of the most appealing techniques when no detailed process information is available. In such a case only the input-output behavior of the process may be modeled to prevent time-consuming rigorous modeling procedures.

Although advanced models are available, a very detailed insight into the distillation process seems to be out of reach (Taylor, 2007). The more nonlinear a distillation process is, for example a reactive three-phase distillation, the more laborious it is to create a rigorous model of it which is also adequate to run robustly when using current state-of-the-art solvers. A number of authors responded to this obstacle by empirical modeling of the whole or parts of the distillation process. In particular, the following methods for model derivation have been extensively used:

- identification of a transfer function describing the process or construction of an inferential model,
- design of an artificial neural network (ANN), and
- identification of a block-oriented model.

Identification of a transfer function is a standard system-theoretical approach. Luyben recommends applying an advanced version of this method to highly nonlinear and complex columns for which linearized models can not be obtained easily (Luyben, 1987).

For control of product compositions in a multicomponent distillation column, an inferential model can be constructed which returns estimates of the compositions from on-line measured process variables such as temperatures, the reflux flow rate, the reboiler heat duty and the pressure. Kano et al. (2000, 2003) propose using the partial least squares (PLS) model in a cascade control structure to regress product compositions with measurements instead of using a standard tray temperature control. They also suggest using a dynamic model based on time-series data to improve the estimation capability of the PLS model. However, they recommend fully understanding the process by developing a fundamental model before constructing an inferential model. This helps to validate the usefulness of the inferential model.

An alternative to simple linear models is the use of block-oriented nonlinear models. Three schemes are very popular: the Hammerstein model, the Wiener model, and the feedback block-oriented model (e.g. Bloemen et al., 2001, Nugroho et al., 2004, Gómez and

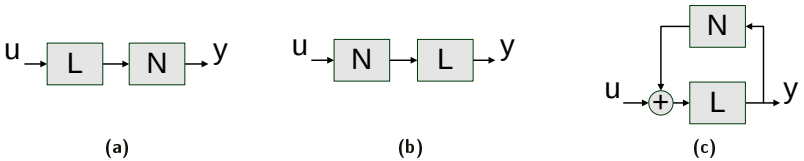

Figure 2.5: (a) Wiener model, (b) Hammerstein model, (c) Feedback block-oriented model

Baeyens, 2004). These models combine a static nonlinear function $N(\cdot)$ with a dynamic linear function $L(\cdot)$ in different ways, see Fig. 2.5. Pearson reports that significant differences in dynamic behavior of these models may appear (Pearson and Pottmann, 2000). The identification process often relies on knowledge of the steady state data which is used to specify the static nonlinear part $N(\cdot)$. The function $L(\cdot)$ is then identified from the input/output data of the process.

The artificial neural network (ANN) is another often-used modeling technique for distillation columns. A popular variant of ANN often applied in distillation modeling is the feedforward neural network where input data propagates through hidden nodes in the direction of the outputs without feedback in the network. There are many publications on distillation modeling with ANN, however, the focus is often on the potential of ANN in the context of control. Different modeling approaches are therefore not compared thoroughly with each other (e.g. Brizuela et al., 1996, Baratti et al., 1997). An overview of the proposed ANN models is given by Abdullah et al. (2007).

2.2.3 Hybrid models

In order to simplify the distillation model, a *hybrid* modeling approach can be preferred. Hybrid modeling refers to the construction of models which comprise a set of fundamental equations and a set of empirical equations. The empirical equations are usually introduced to substitute highly nonlinear and numerically problematic fundamental equations or to describe process parts which are not completely understood while preserving good accuracy of the model.

There are only a few researchers who have published their results on hybrid distillation models (see references in Abdullah et al., 2007). Instead, rigorous equilibrium and non-equilibrium models seem to dominate the distillation literature. However, these models also rely on empirical relations, e.g., the development of more sophisticated models for the phase interface is avoided in practice by including much simpler empirical correlations (Taylor, 2007). For this reason, we proceed without a thorough description of the hybrid models, only noting an approach based on neural networks.

Two articles explicitly dedicated to hybrid distillation modeling are presented by Safavi and Romagnoli (1995), and Safavi et al. (1999). The authors construct a wavelet-based neural network in order to simplify a fundamental binary distillation model. The simplified model consists of simple energy and mass balances. The neural network is developed for the separation factor as a function of reflux and feed flow rates, the reboiler heat duty and feed concentrations. This hybrid model is then adopted in an optimization study where the nominal net profit is optimized.

Generally, model simplifications resulting in a hybrid model can be very useful to reduce the number of model parameters and improve the numerical reliability. However, Pearson (2006) also advises against blind trust in the algorithms performing the simplifications without supervision. Knowledge of the process must be integrated in the modeling procedure to account for important interactions which must not be omitted.

2.3 Distillation efficiency models

The prediction of a distillation model based on the EQ stages is known to depend on tray efficiency. The distillation models presented later in Section 2.4 incorporate the multi-component Murphree tray efficiency, which is a generalization of the well-known Murphree tray efficiency (Murphree, 1925). In the following, we recall some relevant definitions of distillation efficiency and derive a parametric form of the multi-component Murphree tray efficiency including the efficiency factor to be estimated on-line by the algorithm proposed in Chapter 4. Further efficiency models are discussed elsewhere (Taylor and Krishna, 1993, Klemola, 1997).

2.3.1 Murphree point efficiency

Distillation columns with a large diameter usually have concentration gradients in the liquid flowing on trays. For such columns, it is reasonable to define an efficiency at a point. The (vapor-phase) Murphree point efficiency is an approach which allows assigning an efficiency to any point along the flow path of the liquid on a tray. It is defined as the ratio of the *actual* to the *best possible* change in the *local* vapor compositions on two subsequent trays j and $j+1$:

$$E_{OV,i,j} = \frac{y_{i,j} - y_{i,j+1}}{y^*_{i,j} - y_{i,j+1}}. \tag{2.24}$$

This definition requires a phase equilibrium model to compute the equilibrium concentrations $y^*_{i,j}$ of all components $i = 1, \dots q$. Note that $E_{OV,i,j} = 1$, if local thermodynamic equilibrium could be established. It is worth noting that point efficiencies for any component of a binary mixture are identical and range from 0 to 1. In contrast to these, the

point efficiencies in a multi-component mixture are usually different and might take any value between $-\infty$ and ∞ (Klemola, 1997).

2.3.2 Murphree tray efficiency

In the absence of local information, which is usually the case in industrial distillation columns, or for columns with a small diameter, calculation of tray efficiency may be more reasonable. Murphree (1925) proposed a tray efficiency definition very similar to Eq. (2.24) that only requires average vapor compositions on a tray. This (vapor-phase) Murphree tray efficiency for component i on tray j is defined as

$$E_{MV,i,j} = \frac{\bar{y}_{i,j} - \bar{y}_{i,j+1}}{y^*_{i,j} - \bar{y}_{i,j+1}}, \tag{2.25}$$

where the bars over vapor compositions denote now the spatially *averaged* values of the vapor concentrations on trays j and $j+1$. Note that this definition does not respect the interaction effects between the mixture components, such that the Murphree tray efficiency for component i can be calculated from a binary data correlation, e.g., from that proposed by AIChE (1958).

Relations between $E_{OV,i,j}$ and $E_{MV,i,j}$ have been established. In particular, if the liquid and vapor are perfectly mixed on the tray, both are identical (Fair et al., 1983), i.e.,

$$E_{MV,i,j} = E_{OV,i,j}. \tag{2.26a}$$

For plug flow of the liquid across the tray and a perfectly mixed vapor phase, the relation

$$E_{MV,i,j} = \frac{\exp(\lambda E_{OV,i,j}) - 1}{\lambda} \tag{2.26b}$$

holds, where the stripping factor λ and the point efficiency $E_{OV,i,j}$ are assumed to be constant on the tray (Lewis Jr., 1936).

2.3.3 Multi-component Murphree tray efficiency

For multi-component systems, Eq. (2.25) was generalized to implicitly define the multi-component Murphree tray efficiency $E_{MV,j}$ by

$$E_{MV,j}\left(y^*_{:,j} - \bar{y}_{:,j+1}\right) = \bar{y}_{:,j} - \bar{y}_{:,j+1}, \tag{2.27}$$

where the colon denotes the vector of the $q-1$ independent components and $E_{MV,j} \in \mathbb{R}^{(q-1)\times(q-1)}$. The multi-component Murphree tray efficiency in Eq. (2.27) is a generalization of the *component-wise* definition in Eq. (2.25). The former definition implies that the Murphree tray efficiency is a non-diagonal matrix if the mixture components are not very

similar. This is due to the different interaction effects between components which are possible in a multi-component mixture. For example, a component can diffuse when there is no concentration gradient for this component (osmotic diffusion), a component can diffuse in the opposite direction of its concentration gradient (reverse diffusion), or a component does not diffuse at all, although there is a concentration gradient (diffusion barrier) (Taylor and Krishna, 1993). In the general case, the Murphree tray efficiency can have positive or negative entries and is unbounded.

Note that Eqs. (2.26a) and (2.26b) can also be generalized for multi-component systems by introducing the matrix of stripping factors Λ and the multi-component Murphree point efficiency $E_{OV,j}$ (Taylor and Krishna, 1993) to result in

$$E_{MV,j} = E_{OV,j} \tag{2.28a}$$

and

$$E_{MV,j} = \left(\exp\left(E_{OV,j}\Lambda\right) - I\right)\Lambda^{-1}. \tag{2.28b}$$

2.3.4 Multi-component Murphree tray efficiency in parametric form

In this section, we derive a parametric form of the Murphree efficiency based on results from Toor (1964) and discuss some properties of the introduced parameter. Parts of this section have been published before (Stuckert et al., 2012).

Derivation

The multi-component Murphree point efficiency $E_{OV,j}$ is related to $NTU_{OV,j}$, the matrix of overall numbers of transfer units on tray j, by

$$E_{OV,j} = I - \exp\left(-NTU_{OV,j}\right). \tag{2.29}$$

Based on the two-film theory of mass transfer (Lewis and Whitman, 1924), $NTU_{OV,j}$ can be expressed as a function of the matrix of numbers of vapor phase transfer units $NTU_{V,j}$ and the matrix of numbers of liquid phase transfer units $NTU_{L,j}$ as

$$NTU_{OV,j}^{-1} = NTU_{V,j}^{-1} + \Psi_j \frac{V_j}{L_j} NTU_{L,j}^{-1}, \tag{2.30}$$

where Ψ_j is the Jacobian of the vapor-liquid equilibrium function on tray j, calculated as

$$\Psi_j = (\Psi_{m,n})_j = \left(\frac{\partial y_m^*}{\partial x_n}\right)_j \Bigg|_{T,p}, \tag{2.31}$$

where the entry in row m and column n of matrix $(\Psi_{m,n})_j$ refers to the partial derivative of vapor-liquid equilibrium concentration of component m in the vapor phase with respect to the equilibrium concentration of component n in the liquid phase. It is well known that in most distillation columns the resistance to the mass transfer is dominated by the vapor phase (Kister, 1992), i.e., Eq. (2.30) reduces to

$$NTU_{OV,j}^{-1} \approx {NTU_{V,j}}^{-1}. \tag{2.32}$$

On the other hand, at high liquid flow rates the resistance to the mass transfer can be dominated by the liquid phase, i.e., $NTU_{OV,j}$ can be approximated as

$$NTU_{OV,j}^{-1} \approx \Psi_j \frac{V_j}{L_j} {NTU_{L,j}}^{-1}. \tag{2.33}$$

Furthermore, recall the definitions of the matrices of numbers of transfer units for the vapor and liquid phase,

$$NTU_{V,j} = K_j^V a_j h_j^{tot}/V_j, \tag{2.34}$$

$$NTU_{L,j} = K_j^L a_j h_j^{tot}/V_j, \tag{2.35}$$

where K_j^V and K_j^L are the matrices of mass transfer coefficients in the vapor and liquid phase, a_j is the interfacial area per unit volume, and h_j^{tot} denotes the total height of the liquid on tray j. Disregarding diffusional cross effects, i.e., approximating

$$K_j^V \approx k_j^V \cdot I, \qquad K_j^L \approx k_j^L \cdot I, \tag{2.36}$$

with scalars k_j^V and k_j^L and identity matrix I, and lumping with regard to the phase dominating the overall mass transfer as (resistance on the (a) vapor, (b) liquid side)

$$C_{l,j}^V := \frac{k_j^V a_j h_j^{tot}}{V_j}, \tag{2.37a}$$

$$C_{l,j}^L := \frac{k_j^L a_j h_j^{tot}}{V_j} \frac{L_j}{V_j}, \tag{2.37b}$$

the matrix of overall numbers of transfer units, given by Eq. (2.32) (resistance on the vapor side) or Eq. (2.33) (resistance on the liquid side), becomes

$$NTU_{OV,j} \approx \frac{k_j^V a_j h_j^{tot}}{V_j} I = C_{l,j}^V I, \tag{2.38a}$$

$$NTU_{OV,j} \approx \frac{k_j^L a_j h_j^{tot}}{V_j} \frac{L_j}{V_j} \Psi_j^{-1} = C_{l,j}^L \Psi_j^{-1}. \tag{2.38b}$$

Therefore, inserting Eq. (2.38a) into Eq. (2.29) and Eq. (2.38b) into Eq. (2.29) the multicomponent Murphree efficiency matrix simplifies to

$$E_{OV,j} = I - \exp\left(-C_{l,j}^V I\right), \tag{2.39a}$$

$$E_{OV,j} = I - \exp\left(-C_{l,j}^L \Psi_j^{-1}\right). \tag{2.39b}$$

In order to reduce the computational burden, the parameters $C_{l,j}^V$ and $C_{l,j}^L$ can be assumed constant for all trays of the distillation column or, at least, for the trays within a column section (Note that the Murphree tray efficiencies are also often assumed to be constant in a column or column section). Then, Eqs. (2.39a) and (2.39b) become

$$E_{OV,j} = I - \exp\left(-C_l^V I\right) = \left(1 - \exp(-C_l^V)\right) I, \tag{2.40a}$$

$$E_{OV,j} = I - \exp\left(-C_l^L \Psi_j^{-1}\right). \tag{2.40b}$$

In contrast to the parameters $C_{l,j}^V$ and $C_{l,j}^L$, the matrix Ψ_j is not assumed to be constant in Eq. (2.40b). This is due to the fact that we only want $NTU_{L,j}$ be simplified. Since Ψ_j is a factor in the stripping factor, it is left unchanged. To further reduce the computational load, the exponential function can be approximated by the truncated Taylor series up to first order. Hence, Eqs. (2.40a) and (2.40b) reduce to

$$E_{OV,j} = I - (I + C_l^V I)^{-1} = \frac{C_l^V}{1 + C_l^V} I, \tag{2.41a}$$

$$E_{OV,j} = I - (I + C_l^L \Psi_j^{-1})^{-1}. \tag{2.41b}$$

Finally, using Eq. (2.28a), the parametric forms of the multi-component Murphree tray efficiency corresponding to the Murphree point efficiencies given by Eqs. (2.40a), (2.40b), (2.41a), and (2.41b) become

$$E_{MV,j} = \left(1 - \exp\left(-C_l^V\right)\right) I, \tag{2.42a}$$

$$E_{MV,j} = I - \exp\left(-C_l^L \Psi_j^{-1}\right), \tag{2.42b}$$

$$E_{MV,j} = \frac{C_l^V}{1 + C_l^V} I, \tag{2.42c}$$

$$E_{MV,j} = I - (I + C_l^L \Psi_j^{-1})^{-1}. \tag{2.42d}$$

Analogously, using Eq. (2.28b) the parametric forms of the multi-component Murphree tray efficiency corresponding to the Murphree point efficiencies given by Eqs. (2.40a), (2.40b), (2.41a), and (2.41b) are

$$E_{MV,j} = \exp\left(\Lambda - \exp(-C_l^V)\Lambda\right) \Lambda^{-1} - \Lambda^{-1}, \tag{2.43a}$$

$$E_{MV,j} = \exp\left(\Lambda - \exp(-C_l^L \Psi_j^{-1})\Lambda\right) \Lambda^{-1} - \Lambda^{-1}, \tag{2.43b}$$

$$E_{MV,j} = \exp\left(\frac{C_l^V}{1 + C_l^V}\Lambda\right) \Lambda^{-1} - \Lambda^{-1}, \tag{2.43c}$$

$$E_{MV,j} = \exp\left(\Lambda - (I + C_l^L \Psi_j^{-1})^{-1}\Lambda\right) \Lambda^{-1} - \Lambda^{-1}, \tag{2.43d}$$

where $\Lambda = (V_j/L_j)\,\Psi_j$. Note that Eqs. (2.42a) – (2.42d) refer to perfectly mixed liquid and vapor phases, while Eqs. (2.43a) – (2.43d) to plug liquid flow, i.e., non-mixed liquid and perfectly mixed vapor phases.

Properties of the truncated formulae

In distillation models any of the derived Eqs. (2.42a) – (2.42d), or (2.43a) – (2.43d) can be used depending on how well it meets the physics and geometry of the actual distillation column. However, the Eqs. (2.42c), (2.42d) and (2.43c), (2.43d) which were derived using a truncated Taylor series introduce a numerical drawback. For example, consider again Eq. (2.42c). It is derived from Eq. (2.40a) which is equivalent to Eq. (2.42a). However, the domains of definition of Eqs. (2.42c) and (2.42a) are different: Eq. (2.42c) is not defined for $C_l^V = -1$, whereas Eq. (2.42a) is defined everywhere for $C_l^V \in \mathbb{R}$. The diagonal entries of the Murphree tray efficiencies given by Eqs. (2.42a) and (2.42c) are depicted in Figure 2.6. Note the singularity of the truncated formula at $C_l^V = -1$ (dashed line). If noisy estimates

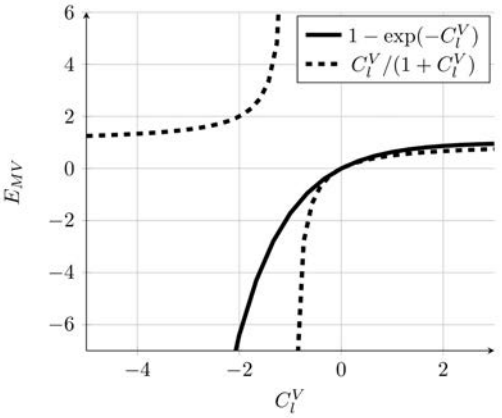

Figure 2.6: Diagonal entries of Murphree efficiency matrices with respect to the parameter C_l^V

of $C_l^V \approx -1$ are used to calculate the Murphree efficiency, the latter could turn out to be inaccurate. Besides, if the actual efficiency is identity, the parameter C_l^V is not unique because of the ambiguity

$$\lim_{C_l^V \to \infty} \frac{C_l^V}{1 + C_l^V} I = \lim_{C_l^V \to -\infty} \frac{C_l^V}{1 + C_l^V} I = I. \tag{2.44}$$

This property is certainly not a concern when calculating the Murphree efficiency from C_l^V because the Murphree efficiency won't change with different algebraic signs of C_l^V.

On the other hand, the range for the Murphree tray efficiency defined by Eq. (2.42c) is between $-\infty$ and $+\infty$, and in contrast to that, the range for the Murphree tray efficiency

defined by Eq. (2.42a) is between $-\infty$ and 1. Therefore, the usage of Eq. (2.42a) is inappropriate under operating conditions for which the Murphree tray efficiencies would have large positive values. This property of Eq. (2.42c) could be even more important in simulation studies than the numeric disadvantages outlined above. Because of this, the truncated Eqs. (2.42c), (2.42d), (2.43c), and (2.43d) should be preferred when choosing a model for the Murphree tray efficiency, if possible.

2.4 Distillation column models for simulation and theoretical analysis

In this section, we discuss some criteria for the selection of the model structure and the level of modeling detail more thoroughly. We will take these criteria into account in the following subsections when choosing our distillation models for simulations.

Modeling of an arbitrary process is a difficult iterative procedure (Foss et al., 1998). The authors summarized the entire modeling process by giving a brief description of a possible task structure. Furthermore, the authors also interviewed several practitioners from academia and industry about modeling habits by using the task list including

a) problem statement and initial data collection,

b) modeling environment selection,

c) conceptual modeling,

d) model representation,

e) implementation,

f) verification,

g) initialization,

h) validation,

i) documentation, and

j) model application.

This list is practical for coarse orientation in any modeling process. Items d) - h) appropriately describe the necessary steps for model selection which were also conducted during the modeling process to prepare this thesis.

The model representation deals with the formal description of the process, i.e., in our case with the modeling equations of the distillation process. Considering the outlined classification of distillation models, we thus only need to choose the appropriate model. However, this appears to be an ambivalent task since the model usefulness is determined by usually contradicting measures (Pearson, 2003):

- approximation accuracy,
- physical interpretation,
- suitability for control, and
- ease of development.

An ideal model should show all these properties but none of the presented fundamental, empiric and hybrid distillation-process models really does. Fundamental models are assumed to have a superior accuracy and to be physically interpretable; however, they are usually less suitable for control due to their complexity and they are more difficult to develop. Empiric models, in contrast to the fundamental ones, are much better suited for control and are easy to formulate. Unfortunately, they usually lack accuracy and physical interpretability. A practicable solution is to consider all four measures of model usefulness by introducing a trade-off between them. Hybrid models will be the result of this modeling effort, offering in the best case a good trade-off between the measures of usefulness. The first three of the measures of usefulness are the most important for this work. Ease of development is indeed less relevant since the models are to be reused in the future. Note that suitability for control also implies that the models should allow stable and fast simulations.

Here, we only introduce equations to model standard parts of a distillation column such as a condenser, a feed tray, section trays, and a reboiler. These are hybrid models in the context of the above classification in Section 2.2.3, including mass and energy balances, whereas the flows, vapor compositions and pressures are subject to phenomenological assumptions. These parts are sufficient to represent the distillation columns which we will encounter later.

In the following, we propose two models, which are well known in literature, in order to consider more realistic scenarios with a plant-model mismatch: a plant replacement and a controller/observer model. We then give an overview over similarities and differences of these models for a better understanding of the introduced mismatch, and for theoretical analysis, we provide a plant-replacement model in state-space form based on the CMO assumption. Finally, the parametrization of the used distillation models is discussed.

2.4.1 Plant-replacement model

Problem statement and initial data

We are interested in a model which is able to simulate the dynamic behavior of a real plant (a distillation column). The problem of model selection for plant replacement is similar to that of model selection when a set of models is known (Verheijen, 2003) and can be formulated as follows:

Assume that all characteristic plant data exists. The purpose of the plant-replacement model is to mimic the principal plant behavior with the highest possible accuracy. Select an adequate model type, structure, and parameters.

The characteristic distillation data is obtained from a rigorous process-design study (Kraemer et al., 2009). It includes stationary data such as liquid and vapor flow rates, compositions and enthalpies of the liquid and vapor phases on each stage, and the heat requirements of the reboiler and condenser. Furthermore, there is complete information on thermodynamics. However, no data on dynamically relevant holdups is available. These and all necessary parameters to describe the liquid dynamics are determined in agreement with Skogestad (1997). The explicit parameterization is explained in Section 2.4.5.

Model equations

The variables on stage j are introduced as follows. M_j^L is the molar holdup of the liquid phase (here equal to the total molar holdup, which is considered to be a valid assumption for pressures less than 10 bar (Luyben, 1992)), $x_{i,j}$ and $y_{i,j}$ are the liquid and vapor concentrations of component i, V_j and L_j are the vapor and liquid flow rates leaving stage j, and $h_{V,j}$ and $h_{L,j}$ are the vapor and liquid enthalpies. Q_C and Q_R are the heat flows out of the condenser and into the reboiler, and p_j is the pressure with the correlation constants ξ_0 and ξ_1. The total number of components is assumed to be q. However, only $q-1$ component concentrations are independent and thus included in mass balance equations. For the plant-replacement model, we especially adopt the EQ stage concept with the following simplifying assumptions from Section 2.2.1:

- vapor dynamics: negligible vapor holdup and pressure controlled at the top of the distillation column (item A.2, p. 16),
- liquid dynamics: linearized liquid flow rate on stages within distillation column sections (item B.2, p. 17),
- energy balance: constant energy holdup (item C.1, p. 17).

For a total condenser, denoted as stage $j = 0$, the equations read as

$$\frac{dM_0^L x_{i,0}}{dt} = V_1 y_{i,1} - (L_0 + F_0)\, x_{i,0}, \quad i = 1, q-1, \tag{2.45a}$$

$$\frac{dM_0^L}{dt} = V_1 - L_0 - F_0, \tag{2.45b}$$

$$0 = V_1 h_{V,1} - (L_0 + F_0)\, h_{L,0} + Q_C, \tag{2.45c}$$

$$0 = p_0 - p_1 + \xi_0 + \xi_1 V_1^2, \tag{2.45d}$$

where F_0 is the distillate liquid flow rate. Note that we use the notation F_0 instead of a more common D to label the distillate flow rate to circumvent notational complexity in the proofs of the theorems in Chapter 3. Eq. (2.45d) describes the "dry tray" pressure drop, i.e., the pressure drop imposed by the geometry of the holes in a tray. The effects of surface tension and froth on a tray are not considered by this equation.

If a partial condenser is used, the equations read as

$$\frac{dM_0^L x_{i,0}}{dt} = V_1 y_{i,1} - L_0 x_{i,0} - F_0 y_{i,0}, \quad i = 1, q-1, \tag{2.46a}$$

$$\frac{dM_0^L}{dt} = V_1 - L_0 - F_0, \tag{2.46b}$$

$$0 = V_1 h_{V,1} - L_0 h_{L,0} - F_0 h_{F,0} + Q_C, \tag{2.46c}$$

$$y_{i,0} = f_i^{vle}(x_{1,0}, \ldots, x_{q-1,0}, p_0, T_0), \quad i = 1, q-1, \tag{2.46d}$$

$$0 = p_0 - p_1 + \xi_0 + \xi_1 V_1^2, \tag{2.46e}$$

where F_0 is the distillate vapor flow rate and the vapor concentration $y_{i,0}$, calculated in Eq. (2.46d) and later by the function f_i^{vle} defined by Eq. (2.11) which is our implementation of Eq. (2.6), is in equilibrium with $x_{i,0}$ at given pressure p_0 and temperature T_0.

For a feed stage, the equations read as

$$\frac{dM_j^L x_{i,j}}{dt} = L_{j-1} x_{i,j-1} - L_j x_{i,j} + V_{j+1} y_{i,j+1} - V_j y_{i,j} + F_j z_{i,j},\ i = 1, q-1, \tag{2.47a}$$

$$\frac{dM_j^L}{dt} = L_{j-1} - L_j + V_{j+1} - V_j + F_j, \tag{2.47b}$$

$$0 = L_{j-1} h_{L,j-1} - L_j h_{L,j} + V_{j+1} h_{V,j+1} - V_j h_{V,j} + F_j h_{F,j}, \tag{2.47c}$$

$$L_j = \lambda_M\big(M_j^L - \breve{M}_j^L\big) + \lambda_V\big(V_{j+1} - \breve{V}_{j+1}\big) + \breve{L}_j, \tag{2.47d}$$

$$y_{i,j} = f_i^{vap}(x_{1,j}, \ldots, x_{q-1,j}, y_{1,j+1}, \ldots, y_{q-1,j+1}, p_j, T_j, C_l^L),\ i = 1, q-1, \tag{2.47e}$$

$$0 = p_j - p_{j+1} + \xi_0 + \xi_1 V_{j+1}^2, \tag{2.47f}$$

where the vapor concentration $y_{i,j}$ is a function of liquid concentration, pressure, temperature, and the efficiency factor C_l^L defined in Section 2.3.4. The liquid flow rate L_j from the feed stage is calculated using a linearization around the nominal liquid holdup $\breve{M}_j^L$ and

the vapor flow rate to the feed stage $\breve{V}_{j+1}$ with the corresponding parameters λ_M and λ_V. The function f_i^{vap} in Eq. (2.47e) and later is obtained by solving Eq. (2.27) for the vector of vapor concentrations $y_{:,j}$ and replacing the vapor-liquid equilibrium function $y_{:,j}^*$ by our implementation of that, f^{vle}, as

$$y_{:,j} = E_{MV,j}\left(f^{vle}(x_{1,j},\ldots,x_{q-1,j},p_j,T_j) - y_{:,j+1}\right) + y_{:,j+1}, \tag{2.48}$$

where the Murphree efficiency $E_{MV,j}$ is calculated by one of Eqs. (2.42a) – (2.42d), or (2.43a) – (2.43d). In our simulation studies, we use Eq. (2.42d). Note that here the function f^{vle} is meant to be a vector function, i.e., $f^{vle} = \left(f_1^{vle};\ldots;f_{q-1}^{vle}\right)$, and f_i^{vap} is defined as the i-th entry of the result vector $y_{:,j}$ in Eq. (2.48).

On each stage j of any column section, the equations read as

$$\frac{dM_j^L x_{i,j}}{dt} = L_{j-1}x_{i,j-1} - L_j x_{i,j} + V_{j+1}y_{i,j+1} - V_j y_{i,j},\ i = 1,q-1, \tag{2.49a}$$

$$\frac{dM_j^L}{dt} = L_{j-1} - L_j + V_{j+1} - V_j, \tag{2.49b}$$

$$0 = L_{j-1}h_{L,j-1} - L_j h_{L,j} + V_{j+1}h_{V,j+1} - V_j h_{V,j}, \tag{2.49c}$$

$$L_j = \lambda_M\left(M_j^L - \breve{M}_j^L\right) + \lambda_V\left(V_{j+1} - \breve{V}_{j+1}\right) + \breve{L}_j, \tag{2.49d}$$

$$y_{i,j} = f_i^{vap}(x_{1,j},\ldots,x_{q-1,j},y_{1,j+1},\ldots,y_{q-1,j+1},p_j,T_j,C_l^L),\ i = 1,q-1, \tag{2.49e}$$

$$0 = p_j - p_{j+1} + \xi_0 + \xi_1 V_{j+1}^2. \tag{2.49f}$$

For a reboiler, denoted as the stage $j = m+1$, the equations read

$$\frac{dM_{m+1}^L x_{i,m+1}}{dt} = L_m x_{i,m} - F_{m+1}x_{i,m+1} - V_{m+1}y_{i,m+1}, \quad i = 1,q-1, \tag{2.50a}$$

$$\frac{dM_{m+1}^L}{dt} = L_m - F_{m+1} - V_{m+1}, \tag{2.50b}$$

$$0 = L_m h_{L,m} - F_{m+1}h_{F,m+1} - V_{m+1}h_{V,m+1} + Q_R, \tag{2.50c}$$

$$y_{i,m+1} = f_i^{vle}(x_{1,m+1},\ldots,x_{q-1,m+1},p_{m+1},T_{m+1}), \quad i = 1,q-1. \tag{2.50d}$$

Note that F_{m+1} refers to the bottom flow rate instead of a more common notation B to simplify the notation in the proofs of the theorems in Chapter 3.

In order to study the effects of flow changes, simplified valves with linear behavior are used for flow control in the pipelines

$$F = S_{actual}F_{max}, \quad 0 \le S_{actual} \le 1, \tag{2.51}$$

where F is the flow rate through the valve, S_{actual} represents the current stem position, and F_{max} is the maximum flow rate through the valve. Headley (2003), for example, suggests using such linear valves for processes with slow dynamics if there is an almost constant pressure drop across a valve. We assume this to be true for our simulations.

The valves are operated automatically. For this task, the PI controllers of the form

$$\text{output}(t) = \text{gain} \cdot \Big(\text{error}(t) + \frac{1}{\text{reset time}} \int_0^t \text{error}(\tau) d\tau\Big) + \text{bias}, \tag{2.52a}$$

$$\text{error}(t) = \text{setpoint} - \text{input}(t), \tag{2.52b}$$

$$\text{output}(t) \in [\text{output}_{min}, \text{output}_{max}], \tag{2.52c}$$

$$\text{input}(t) \in [\text{input}_{min}, \text{input}_{max}], \tag{2.52d}$$

are attached to the valves to set the stem positions without modeling explicitly the valve actuators. Every PI controller may be set in manual mode. In this case, its output and the attached valve's stem position are kept constant. In automatic mode, the controller output is calculated by Eq. (2.52a) and the output limits are preserved by clipping the output value and using a simple integral anti-windup strategy that switches on and off the integral action with respect to the current output value.

The valves and controllers described are also used in the controller model and observer. The controller model which is also used in our state observer is introduced next.

2.4.2 Controller/Observer model

Problem statement and initial data

In contrast to the development of a plant-replacement model, where the main target is *only* to implement a model which accurately represents the plant's behavior, the development of the controller model (which we will also use in the observer introduced in Chapter 3) is more severe: Amrhein et al. (1993) demand from a good model for controller design "the simplest description of the process that captures the essential characteristics relevant for controller design." This idea can be generalized to obtain the problem statement:

Assume that data describing the essential characteristics relevant for controller design exist. The purpose of the controller model to be developed is to capture the essential characteristics of the plant. Select adequate model type, structure, and parameters.

It is worth noting that this problem statement does not give a well-defined problem with a unique controller model as a result but rather comprises a very general idea about the development of the controller model. For simplified modeling of distillation columns, Marquardt and Amrhein (1994) remarked that there is not even "consensus on what constitutes an adequate linear model, on the physical effects to be retained, and on a recommended method for low-order model development". Therefore, in order to obtain our controller model, we need to state our own criteria for development of the controller model.

We choose criteria which give an acceptable trade-off between utility measures outlined in Section 2.4. Especially simplified first-principles models such as those described in

Section 2.2.1 are good candidates. They might capture well essential characteristics of distillation columns (Skogestad, 1997). The resulting controller model is also suitable for observer design.

Necessary parameters for the controller model are adopted from the simulated data for the plant replacement. The explicit parameterization is explained in Section 2.4.5. Note that a plant-model mismatch is introduced in what follows.

Model equations

The variables on stage j are introduced as follows. M_j^L is the mole number in the liquid phase (here equal to the total mole number, which is considered to be a valid assumption for pressures less than 10 bar (Luyben, 1992)), $x_{i,j}$ and $y_{i,j}$ are the liquid and vapor concentrations of component i, V_j and L_j are vapor and liquid flow rates from stage j, and $h_{V,j}$ and $h_{L,j}$ are the vapor and liquid enthalpies. $-Q_C$ and Q_R are the heat flows removed from the condenser and added to the reboiler, T_j is the boiling temperature and p_j is the pressure. The total number of components is assumed to be q. However, only $q-1$ component concentrations are independent and thus included in mass balance equations. For the controller/observer model, we especially adopt the EQ stage concept with the following simplifying assumptions from Section 2.2.1:

- vapor dynamics: negligible vapor holdup and pressure controlled at the top of the distillation column; within distillation column sections between the reboiler and feed stage, and between the feed stage and condenser, a linear pressure decrease assumed (item A.2, p. 16),
- energy balance: constant molar flows within distillation column sections between the reboiler and feed stage, and between the feed stage and condenser (item C.3, p. 18); simplified energy balances in the condensers.

For a total condenser, denoted as stage $j = 0$, the equations read as

$$\frac{dM_0^L x_{i,0}}{dt} = V_1 y_{i,1} - (L_0 + F_0)\, x_{i,0}, \quad i = 1, q-1 \tag{2.53a}$$

$$\frac{dM_0^L}{dt} = V_1 - L_0 - F_0, \tag{2.53b}$$

$$M_0^L \frac{dq_{L,0}}{dt} = (1 - q_{L,0})\, V_1 + \frac{Q_0}{\Delta h_{L,0}}. \tag{2.53c}$$

$$0 = p_0 - p_1 + \xi_0 + \xi_1 V_1^2, \tag{2.53d}$$

where F_0 is the distillate liquid flow rate. Eq. (2.53c) gives the simplified energy balance for the total condenser (it corresponds to Eq. (A.3.9) derived in Appendix A.3). Therein,

$q_{L,0}$ denotes the thermal condition of the reflux flow L_0 which is equal to the thermal condition of the distillate flow F_0 for the total condenser. Eq. (2.53d) describes the "dry tray" pressure drop as in Eq. (2.45d).

If a partial condenser is used, the equations read as

$$\frac{dM_0^L x_{i,0}}{dt} = V_1 y_{i,1} - L_0 x_{i,0} - F_0 y_{i,0}, \quad i = 1, q-1 \tag{2.54a}$$

$$\frac{dM_0^L}{dt} = V_1 - L_0 - F_0, \tag{2.54b}$$

$$0 = \frac{Q_C}{\Delta h_{L,0}} - (V_1 - F_0), \tag{2.54c}$$

$$y_{i,0} = f_i^{vle}(x_{1,0}, \ldots, x_{q-1,0}, p_0, T_0), \quad i = 1, q-1 \tag{2.54d}$$

$$0 = p_0 - p_1 + \xi_0 + \xi_1 V_1^2, \tag{2.54e}$$

where $\Delta h_{L,0}$ is the heat of vaporization, $y_{i,0}$ are the concentrations of the vapor in equilibrium with the liquid at temperature T_0 and pressure p_0 calculated by Eq. (2.11). F_0 is the vapor flow rate leaving the condenser. Eq. (2.54c) corresponds to the energy balance Eq. (A.3.10) derived in Appendix A.3. Eq. (2.54e) describes the "dry tray" pressure drop as in Eq. (2.46e).

For a feed stage, denoted as the stage j, the equations read as

$$M_j^L \frac{dx_{i,j}}{dt} = L_{j-1} x_{i,j-1} - L_j x_{i,j} + V_{j+1} y_{i,j+1} - V_j y_{i,j} + F_j z_{i,j}, \quad i = 1, q-1 \tag{2.55a}$$

$$0 = L_{j-1} - L_j - V_j + V_{j+1} + F_j, \tag{2.55b}$$

$$0 = V_{j+1} h_{V,j+1} - V_j h_{V,j} + L_{j-1} q_{L,0} h_{L,j-1} + F_j h_{F,j} + Q_j, \tag{2.55c}$$

$$y_{i,j} = f_i^{vap}(x_{1,j}, \ldots, x_{q-1,j}, y_{1,j+1}, \ldots, y_{q-1,j+1}, p_j, T_j, C_l^L), \quad i = 1, q-1 \tag{2.55d}$$

where F_j is the feed flow rate and the vapor composition $y_{i,j}$ is a function of the liquid composition, pressure, temperature calculated by Eq. (2.48) and the separation-efficiency factor C_l^L introduced in Section 2.3.4. Note that the liquid holdup M_j^L is assumed to be constant. Therefore, the left-hand side of the mass-balance Eq. (2.55b) is zero and the accumulation term in Eq. (2.55a) reduces to $M_j^L \frac{dx_{i,j}}{dt} = \frac{dM_j^L x_{i,j}}{dt} = M_j^L \frac{dx_{i,j}}{dt} + x_{i,j} \frac{dM_j^L}{dt}$.

On each stage j of a distillation-column section (stages in a rectifying column section are numbered as $j = 1, \ldots, m_{sec}$, in the column sections below, the number of above trays must be added to j), the equations read as

$$M_j^L \frac{dx_{i,j}}{dt} = L_{j-1} x_{i,j-1} - L_j x_{i,j} + V_{j+1} y_{i,j+1} - V_j y_{i,j}, \quad i = 1, q-1 \tag{2.56a}$$

$$L_j = L, \tag{2.56b}$$

$$V_j = V, \tag{2.56c}$$

$$y_{i,j} = f_i^{vap}(x_{1,j}, \ldots, x_{q-1,j}, y_{1,j+1}, \ldots, y_{q-1,j+1}, p_j, T_j, C_l^L), \quad i = 1, q-1 \tag{2.56d}$$

$$p_j = p_0 + (j-1)\,\frac{p_{m_{sec}+1} - p_0}{m_{sec}}, \tag{2.56e}$$

where m_{sec} is the number of stages in the corresponding section. Vapor concentrations $y_{i,j}$ are calculated by Eq. (2.48). The pressure is assumed to be linear in j, where the pressure drop is given by the constant $(p_{m_{sec}+1} - p_0)/m_{sec}$. Note that p_0 in Eq. (2.56e) is understood as the pressure on the first tray above and $p_{m_{sec}+1}$ is the pressure on the first tray below this section.

For a reboiler, denoted as stage $j = m+1$, the equations read as

$$\frac{dM^L_{m+1}x_{i,m+1}}{dt} = L_m x_{i,m} - F_{m+1}x_{i,m+1} - V_{m+1}y_{i,m+1}, \quad i = 1, q-1, \tag{2.57a}$$

$$\frac{dM^L_{m+1}}{dt} = L_m - F_{m+1} - V_{m+1}, \tag{2.57b}$$

$$V_{m+1} = \frac{Q_R}{\Delta h_{L,m+1}}, \tag{2.57c}$$

$$y_{i,m+1} = f_i^{vle}(x_{1,m+1}, \ldots, x_{q-1,m+1}, p_{m+1}, T_{m+1}), \quad i = 1, q-1, \tag{2.57d}$$

where F_{m+1} is the bottom flow rate and $\Delta h_{L,m+1}$ the heat of vaporization of the liquid in the reboiler. The energy balance is given by Eq. (2.57c). Vapor concentrations $y_{i,m+1}$ in Eq. (2.57d) are calculated by Eq. (2.11).

2.4.3 Comparison of plant-replacement and controller/observer models

The plant-replacement and controller models described by Eqs. (2.45a) – (2.50d) and (2.53a) – (2.57d) have much in common. First, they are based on first principles with some simplifications. Second, the models share structurally the same model parts. Finally, they have the same mass balance equations. However, we chose to introduce some differences in the energy balance equations to investigate robustness of the Lang-Gilles observer (Lang and Gilles, 1990, Chapter 3), based on the controller model, towards a structural plant-model mismatch. Lang and Gilles (1990) reported that their observer is very robust towards wrong model parameters or uncertain inputs. However, the authors do not provide any information about the effects of structural mismatches on the robustness of their observer.

What are the main differences between the plant replacement and controller models in detail?

In the plant-replacement model Eqs. (2.45a) – (2.50d) we use the algebraic energy balance Eq. (2.45c) formulated for the condenser. In contrast to this, the energy balance Eq. (2.53c) of the condenser in the controller model is modeled dynamically, but a simpli-

fication is adopted. That reduces especially the numerical load and appears to ease the start-up of a simulation when using the controller model Eqs. (2.53a) – (2.57d)

The energy balances in the reboilers of the plant-replacement and controller models given by Eqs. (2.50c) and (2.57c) are also different. In the plant replacement, Eq. (2.50c) is again algebraic and rigorous, whereas in the controller model, the energy balance Eq. (2.57c) is actually algebraic but in a simplified form. Here, the simplified algebraic relation does not seem to cause numerical problems, probably because the vapor flow rate in the reboiler can be set (almost) independently of all other flows in the column.

The differences in the energy balances of the distillation column sections are more crucial for simulation results than the differences in the energy balances of the condensers and reboilers. In the column sections of the plant-replacement model, the energy balances given by Eq. (2.49c) are algebraic on each stage. In addition, the linearized liquid dynamics Eq. (2.49d) and a polynomial in vapor flow rate of second order for the pressure Eq. (2.49f) are used. On the other hand, the column sections of the controller model have no energy balances (CMO condition) and the pressure in Eq. (2.56e) increases linearly within the section.[1] However, the CMO condition results in a very poor approximation of the composition profiles obtained with the plant-replacement model.

All significant model differences are summarized in Table 2.1.

Table 2.1: Main differences of plant-replacement and controller/observer models

model part	plant-replacement model	controller/observer model
condenser		
1. energy balance	algebraic, rigorous	dynamic, simplified
column sections		
1. energy balance	algebraic, rigorous	not available
2. liquid dynamics	linearized, dependent on liquid holdup and vapor flow rate	liquid/vapor flow rate fixed
3. pressure	polynomial of degree 2 in vapor flow rate	linear approximation of pressure profile
reboiler		
1. energy balance	algebraic, rigorous	algebraic, simplified

The plant-replacement and controller/observer models were implemented in gPROMS

[1] Note that the controller model is in fact a *reduced* model. However, as opposed to a mathematical order reduction, the reduction here is achieved by introducing constraints on model validity for different operating conditions, namely, the controller model is valid for the CMO condition.

(Process Systems Enterprise, 1997-2013). They rely on thermodynamic properties which are calculated by an external software package. For further details, the reader is referred to Appendix B.

2.4.4 Controller model in a compact form for theoretical analysis

In order to prove theoretical results in Chapter 3, we need to give the controller model equations in a compact form. To derive this form, we assume the following conditions:

1. conditions 1–5 from Appendix A.1,
2. conditions 1–2 from Appendix A.2,
3. only total condensers are used,
4. vapor-liquid equilibrium in reboiler and non-ideal column stages with a tray efficiency, and
5. temperatures are functions of tray compositions.

Note that conditions under items 1 and 2 above imply the assumption of constant molar overflow (CMO) as shown in Appendix A.2. Item 3 is given to simplify the analysis of the plant equations, item 4 is a common assumption for distillation columns, and item 5 can be assumed because the column pressures are fixed in line with conditions under item 1.

Our compact form of the controller-model equations is a generalisation of that for a single distillation column based on controller-model Eqs. (2.53a), (2.53b), (2.55a), (2.55b), (2.56a), (2.56b), (2.56c), and (2.57a), (2.57b) from Section 2.4.2. Keep in mind that the latter are composed for numerical reasons of $q-1$ component and one total balance equations per tray and are mainly used in simulation. In contrast to this, now, we want to give equations to investigate the dynamic behavior of distillation trains. A compact form with q component equations is more suitable for such purpose and, therefore, we substitute the equations (2.53b), (2.55b), (2.56b), (2.56c), and (2.57b) from Section 2.4.2 with the corresponding balance equations for component q. For a distillation column with one feed tray j_1, this results in the following set of equations:

$$M_0^L \frac{dx_{i,0}}{dt} = \left(V + \nu_{j_1}^F F_{j_1}\right) y_{i,1} - \left(L + F_0\right) x_{i,0}, \quad i = 1, q, \tag{2.58a}$$

$$\begin{aligned} M_j^L \frac{dx_{i,j}}{dt} &= L\left(x_{i,j-1} - x_{i,j}\right) + \left(V + \nu_{j_1}^F F_{j_1}\right)\left(y_{i,j+1} - y_{i,j}\right), \\ & i = 1, q, \quad j = 1, j_1 - 1, \end{aligned} \tag{2.58b}$$

$$\begin{aligned} M_{j_1}^L \frac{dx_{i,j_1}}{dt} &= L x_{i,j_1-1} - \left(L + \left(1 - \nu_{j_1}^F\right) F_{j_1}\right) x_{i,j_1} + V y_{i,j_1+1} - \\ & \left(V + \nu_{j_1}^F F_{j_1}\right) y_{i,j_1} + F_{j_1} z_{i,j_1}, \quad i = 1, q, \end{aligned} \tag{2.58c}$$

$$\begin{aligned} M_j^L \frac{dx_{i,j}}{dt} &= \left(L + \left(1 - \nu_{j_1}^F\right) F_{j_1}\right)\left(x_{i,j-1} - x_{i,j}\right) + \\ & V\left(y_{i,j+1} - y_{i,j}\right), \quad i = 1, q, \quad j = j_1 + 1, m, \end{aligned} \tag{2.58d}$$

$$M_{m+1}^L \frac{dx_{i,m+1}}{dt} = \big(L + (1-\nu_{j_1}^F)F_{j_1}\big)x_{i,m} - F_{m+1}x_{i,m+1} - Vy_{i,m+1}, \quad i = 1,q, \tag{2.58e}$$

$$y_{i,j} = f_i^{vap}(x_{1,j},\ldots,x_{q-1,j},y_{1,j+1},\ldots,y_{q-1,j+1},p_j,T_j,C_l^L),$$
$$i = 1,q-1, \quad j = 1,m, \tag{2.58f}$$

$$y_{i,j} = f_i^{vle}(x_{1,j},\ldots,x_{q-1,j},p_j,T_j), \quad i = 1,q-1, \quad j = m+1, \tag{2.58g}$$

$$y_{q,j} = 1 - \sum_{i=1}^{q-1} y_{i,j}, \quad j = 1,m+1. \tag{2.58h}$$

In this equation set, Eq. (2.58f) is calculated by Eq. (2.48) with Murphree efficiency E_{MV} depending on the separation efficiency C_l^L as in Eq. (2.42d). The function f_i^{vle} in Eq. (2.58g) is calculated by Eq. (2.11) which is our implementation of Eq. (2.6).

The Eqs. (2.58a) – (2.58e) can be written in compact matrix form as follows (zero elements are omitted, for simplicity; the lines in composition vectors separate from each other the compositions on different stages for better readability):

$$\frac{d}{dt}\begin{pmatrix} x_{1,0} \\ \vdots \\ x_{q,0} \\ \hline x_{1,1} \\ \vdots \\ x_{q,1} \\ \hline \vdots \\ \hline x_{1,j_1} \\ \vdots \\ x_{q,j_1} \\ \hline x_{1,j_1+1} \\ \vdots \\ x_{q,j_1+1} \\ \hline \vdots \\ \hline x_{1,m+1} \\ \vdots \\ x_{q,m+1} \end{pmatrix} = \begin{bmatrix} a_{0,0} & & & & & & & & & \\ a_{1,0} & a_{1,1} & & & & & & & & \\ & \ddots & \ddots & & & & & & & \\ & & a_{j_1,j_1-1} & a_{j_1,j_1} & & & & & & \\ & & & a_{j_1+1,j_1} & a_{j_1+1,j_1+1} & & & & & \\ & & & & \ddots & \ddots & & & & \\ & & & & & a_{m+1,m} & a_{m+1,m+1} & & & \end{bmatrix} \begin{pmatrix} x_{1,0} \\ \vdots \\ x_{q,0} \\ \hline \vdots \\ \hline x_{1,j_1-1} \\ \vdots \\ x_{q,j_1-1} \\ \hline x_{1,j_1} \\ \vdots \\ x_{q,j_1} \\ \hline x_{1,j_1+1} \\ \vdots \\ x_{q,j_1+1} \\ \hline \vdots \\ \hline x_{1,m+1} \\ \vdots \\ x_{q,m+1} \end{pmatrix}$$

$$
+\begin{bmatrix}
0 & b_{0,1} & & & & & & & \\
 & b_{1,1} & b_{1,2} & & & & & & \\
 & & \ddots & \ddots & & & & & \\
 & & & b_{j_1,j_1} & b_{j_1,j_1+1} & & & & \\
 & & & & b_{j_1+1,j_1+1} & b_{j_1+1,j_1+2} & & & \\
 & & & & & \ddots & \ddots & & \\
 & & & & & & & b_{m+1,m+1}
\end{bmatrix}
\left(\begin{array}{c}
y_{1,0} \\ \vdots \\ y_{q,0} \\ \hline \vdots \\ \hline y_{1,j_1} \\ \vdots \\ y_{q,j_1} \\ \hline y_{1,j_1+1} \\ \vdots \\ y_{q,j_1+1} \\ \hline y_{1,j_1+2} \\ \vdots \\ y_{q,j_1+2} \\ \hline \vdots \\ \hline y_{1,m+1} \\ \vdots \\ y_{q,m+1}
\end{array}\right)
$$

$$
+\begin{bmatrix}
0 \\ 0 \\ \\ \\ c_{j_1,j_1} \\ 0 \\ \\ \\ 0
\end{bmatrix}
\begin{pmatrix}
z_{1,j_1} \\ \vdots \\ z_{q,j_1}
\end{pmatrix}, \quad x_{i,j}(0) = x_{i,j}^{init}, \;\; i = 1, q, \;\; j = 0, m+1, \tag{2.59}
$$

where vapor concentrations $y_{i,j}$ are calculated by Eq. (2.58g) and feed concentrations $z_{i,j}$ are time-dependent. During a simulation, the liquid concentrations $x_{i,j}$ are initialized with $x_{i,j}^{init}$. The sub-matrices $a_{r,s}, b_{r,s}$, and $c_{r,s}$ shown in Eq. (2.59) are defined as

$$
a_{r,s} = \begin{cases}
-\frac{1}{M_0^L}\left(L + F_0\right) \cdot I, & r = s = 0, I \in \mathbb{R}^{q \times q}, \\
\frac{1}{M_1^L} L \cdot I, & r = 1, s = 0, I \in \mathbb{R}^{q \times q}, \\
-\frac{1}{M_1^L} L \cdot I, & r = s = 1, I \in \mathbb{R}^{q \times q}, \\
\frac{1}{M_{j_1}^L} L \cdot I, & r = j_1, s = j_1 - 1, I \in \mathbb{R}^{q \times q}, \\
-\frac{1}{M_{j_1}^L}\left(L + (1 - \nu_{j_1}^F) F_{j_1}\right) \cdot I, & r = s = j_1, I \in \mathbb{R}^{q \times q}, \\
\frac{1}{M_{j_1+1}^L}\left(L + (1 - \nu_{j_1}^F) F_{j_1}\right) \cdot I, & r = j_1 + 1, s = j_1, I \in \mathbb{R}^{q \times q}, \\
-\frac{1}{M_{j_1+1}^L}\left(L + (1 - \nu_{j_1}^F) F_{j_1}\right) \cdot I, & r = s = j_1 + 1, I \in \mathbb{R}^{q \times q}, \\
\frac{1}{M_{m+1}^L}\left(L + (1 - \nu_{j_1}^F) F_{j_1}\right) \cdot I, & r = m + 1, s = m, I \in \mathbb{R}^{q \times q}, \\
-\frac{1}{M_{m+1}^L} F_{m+1} \cdot I, & r = s = m + 1, I \in \mathbb{R}^{q \times q},
\end{cases} \tag{2.60a}
$$

$$b_{r,s} = \begin{cases} \frac{1}{M_0^L}\left(V + \nu_{j_1}^F F_{j_1}\right)\cdot I, & r = 0, s = 1, I \in \mathbb{R}^{q\times q}, \\ -\frac{1}{M_1^L}\left(V + \nu_{j_1}^F F_{j_1}\right)\cdot I, & r = 1, s = 1, I \in \mathbb{R}^{q\times q}, \\ \frac{1}{M_1^L}\left(V + \nu_{j_1}^F F_{j_1}\right)\cdot I, & r = 1, s = 2, I \in \mathbb{R}^{q\times q}, \\ -\frac{1}{M_{j_1}^L}\left(V + \nu_{j_1}^F F_{j_1}\right)\cdot I, & r = s = j_1, I \in \mathbb{R}^{q\times q}, \\ \frac{1}{M_{j_1}^L} V\cdot I, & r = j_1, s = j_1 + 1, I \in \mathbb{R}^{q\times q}, \\ -\frac{1}{M_{j_1+1}^L} V\cdot I, & r = s = j_1 + 1, I \in \mathbb{R}^{q\times q}, \\ \frac{1}{M_{j_1+1}^L} V\cdot I, & r = j_1 + 1, s = j_1 + 2, I \in \mathbb{R}^{q\times q}, \\ -\frac{1}{M_{m+1}^L} V\cdot I, & r = s = m + 1, I \in \mathbb{R}^{q\times q}, \end{cases} \tag{2.60b}$$

$$c_{r,s} = \frac{F_{j_1}}{M_{j_1}^L}\cdot I, \quad r = s = j_1, \quad I \in \mathbb{R}^{q\times q}. \tag{2.60c}$$

As stated above, we can generalize Eq. (2.59) to the entire plant, which may consist of several coupled distillation columns, and obtain

$$\frac{dx}{dt} = Ax + By + Cz, \quad x(0) = x^{init}, \tag{2.61a}$$

$$y = f(x, y, p, T, C_l), \tag{2.61b}$$

where x and y are the vectors including all liquid and vapor compositions of the plant, z denotes the vector of external feed compositions, the vector Eq. (2.61b) for calculation of y is composed of Eqs. (2.58f) – (2.58h) which give the vapor compositions on each tray and in each reboiler of the plant columns. The temperatures T_j and consequently the vector T composed of individual temperatures T_j are calculated by Eq. (2.15) with a given fixed pressure p_j. The matrices A, B, and C will be defined below after some additional notation has been introduced.

In order to define the composition vectors x, y, and z for the plant, we first define composition vectors for stage j in column l as

$$x_{j,l} = \begin{pmatrix} x_{1,j,l} \\ \vdots \\ x_{q,j,l} \end{pmatrix} \in \mathbb{R}^q,\ y_{j,l} = \begin{pmatrix} y_{1,j,l} \\ \vdots \\ y_{q,j,l} \end{pmatrix} \in \mathbb{R}^q,\ z_{j,l} = \begin{pmatrix} z_{1,j,l} \\ \vdots \\ z_{q,j,l} \end{pmatrix} \in \mathbb{R}^q, \tag{2.62a}$$

where each entry $y_{i,j,l}$ of vector $y_{j,l}$ is calculated by Eq. (2.58g). Then, the composition vectors for column l with a condenser, a reboiler, and m_l stages including feed tray(s) may be defined as

$$x_l = \begin{pmatrix} x_{0,l} \\ \vdots \\ x_{m_l+1,l} \end{pmatrix} \in \mathbb{R}^{(m_l+2)\cdot q}, \tag{2.63a}$$

$$y_l = \begin{pmatrix} y_{0,l} \\ \vdots \\ y_{m_l+1,l} \end{pmatrix} \in \mathbb{R}^{(m_l+2)\cdot q}, \tag{2.63b}$$

$$z_l = \begin{pmatrix} z_{j_1,l} \\ \vdots \\ z_{j_{k_l},l} \end{pmatrix} \in \mathbb{R}^{k_l \cdot q}, \quad 1 \leq j_1, < \ldots < j_{k_l} \leq m_l, \tag{2.63c}$$

where the index 0 corresponds to the condenser and $m_l + 1$ to the reboiler. Notice that the dimension of vector z_l differs from those of vectors x_l and y_l as it only includes k_l compositions of the existing external feed flows (i.e., feed flows which do not originate from other columns in the plant) $F_{j_1}, \ldots, F_{j_{k_l}}$ on stages j_1 to j_{k_l}. So, the sub-index of variable j ranges from 1 to k_l and denotes the number of the external feed in column l. We define $k_l = 0$ if the column l does not contain any external feeds. In this case, the dimension of vector z_l collapses to zero.

The vectors including all compositions of the plant with n columns are denoted as

$$x = \begin{pmatrix} x_1 \\ \vdots \\ x_n \end{pmatrix} \in \mathbb{R}^{q \sum_{l=1}^{n}(m_l+2)}, \tag{2.64a}$$

$$y = \begin{pmatrix} y_1 \\ \vdots \\ y_n \end{pmatrix} \in \mathbb{R}^{q \sum_{l=1}^{n}(m_l+2)}, \tag{2.64b}$$

$$z = \begin{pmatrix} z_1 \\ \vdots \\ z_n \end{pmatrix} \in \mathbb{R}^{q \sum_{l=1}^{n} k_l}. \tag{2.64c}$$

The matrices A and B from Eq. (2.61a) are introduced as follows

$$A = \left(A_{rs}\right)_{r,s\in\{1,\ldots,n\}} \tag{2.65a}$$

$$B = \left(B_{rs}\right)_{r,s\in\{1,\ldots,n\}} \tag{2.65b}$$

$$C = \left(C_{rs}\right)_{r,s\in\{1,\ldots,n\}} \tag{2.65c}$$

The sub-matrices A_{ll} and B_{ll}, $l \in \{1, \ldots, n\}$, represent the coefficients of the individual columns (including reboiler and (total) condenser) of the column sequence. C_{ll}, $l \in \{1, \ldots, n\}$, is a matrix with non-zero diagonal entries if the column l has external feeds, otherwise C_{ll} and the matrix column and row in C that contain it are removed. The

matrices are defined as

$$A_{ll} = \begin{pmatrix} a_{0,0,l} & 0 & 0 & \dots & 0 \\ a_{1,0,l} & a_{1,1,l} & 0 & \ddots & \vdots \\ 0 & \ddots & \ddots & \ddots & 0 \\ \vdots & \ddots & a_{m_l,m_l-1,l} & a_{m_l,m_l,l} & 0 \\ 0 & \dots & 0 & a_{m_l+1,m_l,l} & a_{m_l+1,m_l+1,l} \end{pmatrix}, \tag{2.66a}$$

$$B_{ll} = \begin{pmatrix} b_{0,0,l} & b_{0,1,l} & 0 & \dots & 0 \\ 0 & b_{1,1,l} & b_{1,2,l} & \ddots & \vdots \\ 0 & 0 & \ddots & \ddots & 0 \\ \vdots & \vdots & \ddots & b_{m_l,m_l,l} & b_{m_l,m_l+1,l} \\ 0 & 0 & \dots & 0 & b_{m_l+1,m_l+1,l} \end{pmatrix}, \tag{2.66b}$$

$$C_{ll} = \begin{pmatrix} c_{j_1,j_1,l} & 0 & 0 \\ 0 & \ddots & 0 \\ 0 & 0 & c_{j_{k_l},j_{k_l},l} \end{pmatrix}. \tag{2.66c}$$

The sub-matrices $A_{l_1l_2}$ and $B_{l_1l_2}$ with $l_1 \neq l_2$ describe possible liquid and vapor streams from distillation column l_2 to distillation column l_1 (i.e. column couplings). These are given by

$$A_{l_1l_2} = \begin{pmatrix} f^L_{0,l_1,j_0,l_2} & 0 & \dots & 0 \\ 0 & f^L_{1,l_1,j_1,l_2} & \ddots & \vdots \\ \vdots & \ddots & \ddots & 0 \\ 0 & \dots & 0 & f^L_{m_{l_2}+1,l_1,j_{m_{l_2}+1},l_2} \end{pmatrix}, \tag{2.66d}$$

$$B_{l_1l_2} = \begin{pmatrix} f^V_{0,l_1,j_0,l_2} & 0 & \dots & 0 \\ 0 & f^V_{1,l_1,j_1,l_2} & \ddots & \vdots \\ \vdots & \ddots & \ddots & 0 \\ 0 & \dots & 0 & f^V_{m_{l_2}+1,l_1,j_{m_{l_2}+1},l_2} \end{pmatrix}. \tag{2.66e}$$

Matrices $C_{l_1l_2}$ with $l_1 \neq l_2$ are equal to zero.

In agreement with Eq. (2.60a), the elements of the generalized sub-matrices $a_{r,s,l}$ read as

$$a_{r,s,l} = \begin{cases} -\frac{L+F_r}{M^L_r} I, & r = s = 0, \\ -\frac{L+\sum_{j_k \leq s}(1-\nu^F_{j_k})F_{j_k}}{M^L_r} I, & 1 \leq r = s \leq m_l, F_r < 0, \\ -\frac{L+\sum_{j_k < s}(1-\nu^F_{j_k})F_{j_k}}{M^L_r} I, & 1 \leq r = s \leq m_l, F_r \geq 0, \\ \frac{L+\sum_{j_k < s}(1-\nu^F_{j_k})F_{j_k}}{M^L_r} I, & r > s, \\ -\frac{F_r}{M^L_r} I, & r = s = m_l + 1, \end{cases} \tag{2.67a}$$

where $I \in \mathbb{R}^{q\times q}$ is the identity matrix. The liquid holdups M_r^L and liquid-flow rates L used in the formulations of $a_{r,s,l}$ belong to the distillation column l. The first entry in Eq. (2.67a) corresponds to the liquid rate of change in the condenser (the minus\plus sign in front of the fraction term stands for a stream leaving\entering the condenser, the same applies to reboiler or other trays in column l). Note that if a partial condenser is included in column l, then $a_{0,0,l} = -L/M_0^L I$. $\nu_{j_k}^F$ is the vapor fraction of the feed-flow rate F_{j_k} on stage j_k. The next three entries in Eq. (2.67a) include the term $\sum_{j_k\leq s}(1-\nu_{j_k}^F)F_{j_k}$ which sums up the feed-flow rates of the liquid feed streams above stage s including ($j_k \leq s$) or excluding ($j_k < s$) the feed on stage s; the first two entries comprise the liquid rates of change due to the liquid leaving stage s distinguished from each other by the algebraic sign of the feed-flow rate F_r on stage $r(=s)$ and the third entry describes the rate of change due to the liquid entering stage s from the stage above. The last entry in Eq. (2.67a) is the rate of change of reboiler due to the leaving liquid.

In agreement with Eq. (2.60b), the generalized sub-matrices $b_{r,s,l}$ are defined as

$$b_{r,s,l} = \begin{cases} 0 \cdot I, & r = s = 0, \\ -\frac{V+\sum_{j_k\geq r}\nu_{j_k}^F F_{j_k}}{M_r^L} I, & r = s \neq 0, F_r < 0, \\ -\frac{V+\sum_{j_k> r}\nu_{j_k}^F F_{j_k}}{M_r^L} I, & r = s \neq 0, F_r \geq 0, \\ \frac{V+\sum_{j_k> r}\nu_{j_k}^F F_{j_k}}{M_r^L} I, & r < s, \end{cases} \tag{2.67b}$$

where $I \in \mathbb{R}^{q\times q}$ is the identity matrix and the vapor flow rate V belongs to the distillation column l. The first entry in Eq. (2.67b) is zero as no vapor is leaving the (total) condenser. Note that if a partial condenser is included in column l, then $b_{0,0,l} = -F_0/M_0^L I$. Similar to $a_{r,s,l}$, the next three entries in Eq. (2.67b) include a term summing up all feed-flow rates for vapor feed streams below stage r including ($j_k \geq r$) or excluding ($j_k > r$) the feed on stage r; the first two entries comprise the vapor rates of change due to the vapor leaving stage r distinguished from each other by the algebraic sign of the feed-flow rate F_r on stage $r(=s)$ and the third entry describes the rate of change due to the vapor entering stage r from the stage below.

In agreement with Eq. (2.60c), the generalized sub-matrices $c_{r,s,l}$ read as

$$c_{r,s,l} = \begin{cases} 0 \cdot I, & r \neq s, \\ \frac{F_r}{M_r^L} I, & r = s, \end{cases} \tag{2.67c}$$

where the non-zero entry corresponds to the existing external feeds on stage s in column l.

Finally, the generalized sub-matrices f_{r,l_1,s,l_2}^L and f_{r,l_1,s,l_2}^V describing the couplings between individual distillation columns in the plant and being used in Eqs. (2.66d) and (2.66e) are defined as

$$f_{r,l_1,s,l_2}^L = (1-\nu_s^F)F_s^{l_2}/M_r^{L,l_1} I, \tag{2.67d}$$

$$f^V_{r,l_1,s,l_2} = \nu^F_s F^{l_2}_s / M^{L,l_1}_r I. \tag{2.67e}$$

The definitions f^L_{r,l_1,s,l_2} and f^V_{r,l_1,s,l_2} indicate the direction and phase of the corresponding coupling stream, namely the liquid or vapor stream from stage s of column l_2 to the stage r of column l_1. The stream $F^{l_2}_s$ is withdrawn from stage s of column l_2 and the term M^{L,l_1}_r denotes the liquid holdup on stage r of column l_1. If there are no streams between the columns l_2 and l_1, then $f^L_{r,l_1,s,l_2} = f^V_{r,l_1,s,l_2} = 0$.

2.4.5 Determination of model parameters

In this thesis, several simulation studies will be considered. Due to the lack of real process data, the parameters of the models must either be estimated from design data, tuned manually, or assigned some reasonable values taken from literature. An overview of all available parameters, the models in which these occur, and the methods used for their determination, are depicted in Table 2.2. Parameters describing the thermodynamic properties of the mixture are extracted from Aspen Plus (Aspen Technology, Inc., 1981-2011), for further details see Sections C.1 and C.2 in the Appendix, and hence excluded from Table 2.2. The pressure correlation constants ξ_0 and ξ_1 in Eqs. (2.45d), (2.46e), (2.47f),

Table 2.2: Model parameters and methods for their determination

model parameter	model	method
ξ_0	plant replacement	least squares
ξ_1	plant replacement	least squares
λ_M	plant replacement	empirical value
λ_V	plant replacement	empirical value
$\breve{M}^L_j$	plant replacement	empirical value
$\breve{L}_j$	plant replacement	column design (nominal)
$\breve{V}_j$	plant replacement	column design (nominal)
C_l	all	tuning
M^L_j	controller/observer	empirical value
L	controller/observer	column design (mean)
V	controller/observer	column design (mean)
$p_{m_{sec}+1}$	controller/observer	plant (steady state)
p_0	controller/observer	plant (steady state)

(2.49f), (2.53d), and (2.54e) are determined for each distillation column by minimization of the least squares error assuming a dry-tray pressure drop of $p_{j+1} - p_j = 6$ mbar which

lies within the operating region of a bubble-cap tray (cf. Atteridg et al. (1956)) and taking nominal vapor flow rates $\breve{V}_j$ calculated by Kraemer et al. (2009) as follows

$$\min_{(\xi_0,\xi_1)} \left\| \left(p_{j+1} - p_j\right)_{j=0,m} - \begin{bmatrix} 1 & \breve{V}_{j+1}^2 \end{bmatrix}_{j=0,m} \begin{pmatrix} \xi_0 \\ \xi_1 \end{pmatrix} \right\|_2^2 . \tag{2.68}$$

The inverse of the hydraulic time constant λ_M in Eq. (2.47d) varies typically from 0.5 to 15 seconds and the vapor constant λ_V in Eq. (2.47d) ranges between -5 and 5 (Wittgens and Skogestad, 2000). The nominal liquid holdup $\breve{M}_j^L$ in Eq. (2.47d) is proportional to a multiple of the feed flow rate F, as usual $30 \cdot F$, but may vary considerably (Skogestad, 1997). Starting with any initial values within proposed ranges, λ_M, λ_V, and $\breve{M}_j^L$ are manually fine-tuned for stable simulations. The reader is also referred to Wittgens and Skogestad (2000) who provide some details on how these parameters are identified in practice.

For our models, the nominal liquid and vapor flow rates $\breve{L}_j$ and $\breve{V}_j$ in Eq. (2.47d) are set according to the values obtained by Kraemer et al. (2009) in their design study. Unlike the nominal flow rates, the separation efficiency factor C_l^L in Eqs. (2.47e), (2.49e), (2.55d), and (2.56d) is not determined in the design study. Instead it is also manually tuned.

The liquid holdups on trays of the controller/observer model M_j^L in Eq. (2.56a) are taken equal to the nominal holdups in the plant replacement $\breve{M}_j^L$. The liquid and vapor flow rates L and V in Eqs. (2.56b) and (2.56c) are estimated from column design data obtained by Kraemer et al. (2009) by taking the mean value of the corresponding flow rates in each of the column sections. The pressures on the stages located above the top and bottom stages of a column section p_0 and $p_{m_{sec}+1}$ in Eq. (2.56e) fix the pressure profile within this column section and are equated with the corresponding pressures of the plant replacement in a stationary state. In the column section, the pressures are assumed to increase linearly from the top stage downwards.

2.5 Dynamics and basic control of the ACBT process

The dynamics and base control layer of distillation models are demonstrated with the help of the ACBT process.

2.5.1 ACBT process dynamics at the nominal state

Here, we compare the dynamics of the linearized plant-replacement model based on equations from Section 2.4.1 with those of the linearized controller model based on equations from Section 2.4.2 at the nominal state to establish the appropriateness of the controller model for control purposes at the nominal steady state. Both models emulate the ACBT

process depicted in Fig. 1.1 from Section 1.2.1. The nominal state refers to the steady state obtained with the nominal design data which are referenced in Section 5.4 and summarized in Appendix C.6.

The dynamics of the linear state-space models are characterized by the eigenvalues of their (continuous-time) system matrices. Figure 2.7 depicts the eigenvalues of both the linearized plant-replacement and the controller/observer models at the nominal state. There are obviously fewer eigenvalues of the controller/observer model than of the plant-replacement model. The former overlap the slower part of the spectrum of the plant replacement. The additional eigenvalues of the plant replacement represent faster dynamics introduced by the liquid and pressure dynamics which are modeled by algebraic relations in the controller/observer model. Fortunately, the principal dynamics (dynamics of concentrations) are not represented by these additional eigenvalues since otherwise the controller model would be inadequate. This is also in agreement with Skogestad (1997) who notices that

> [...] This very common assumption (disregarding liquid dynamics - author's note) is partly justified by the fact that the dominant composition dynamics are much slower than the flow dynamics and nearly unaffected by the flow dynamics [...]

However, it is even more important to ensure that the most dominant eigenvalues, i.e., the eigenvalues representing the poles of the system closest to the imaginary axis in the s-plane and giving rise to the longest lasting transient responses of the system, are equal, as also mentioned by Rommes and Martins (2006) (see transfer function modal equivalent). Figure 2.8 shows the 5 most dominant eigenvalues for the controller/observer (three real and one conjugate-complex pair of eigenvalues) and 6 most dominant eigenvalues for the plant-replacement (two real and two conjugate-complex pairs of eigenvalues) models. It is clear that a perfect overlapping of the eigenvalues is hardly possible. Therefore, we can only expect that all eigenvalues lie close to each other as it is the case for the distillation process as shown in Figure 2.8. Note also that both models are stable at the nominal state although the controller/observer model possesses a poorly damped pair of conjugate complex poles what complicates its use for predictions over a longer time horizon.

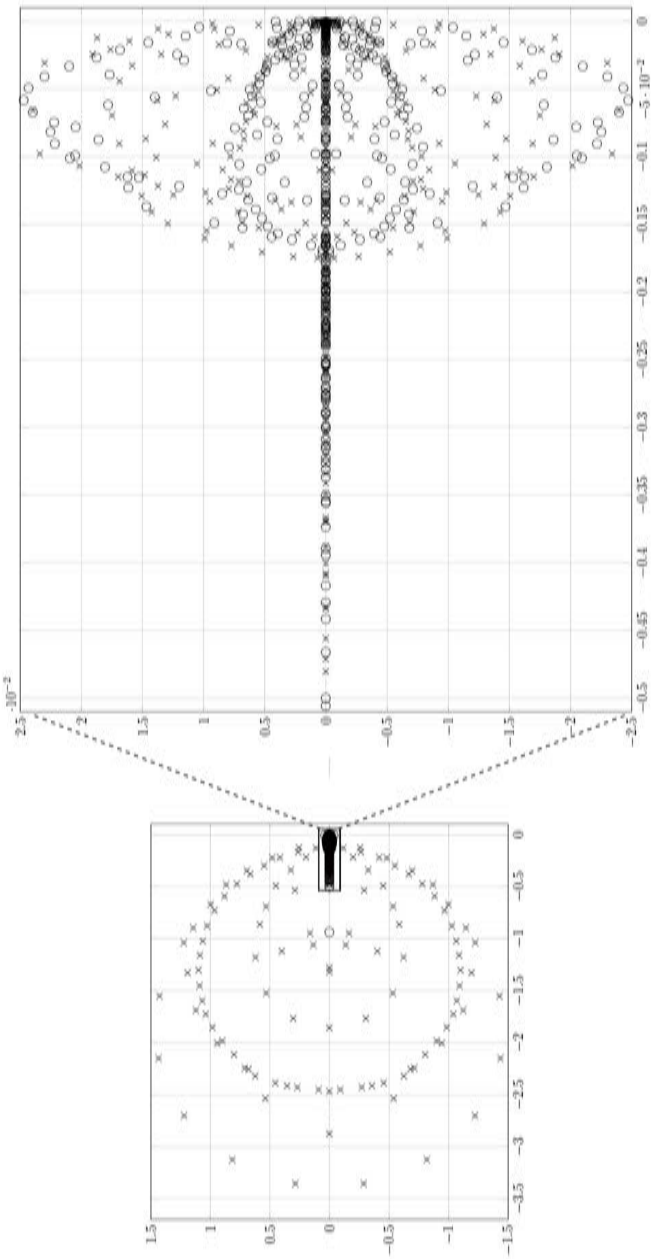

Figure 2.7: Eigenvalue spectra of the linearized plant-replacement (x) and controller/observer (o) models

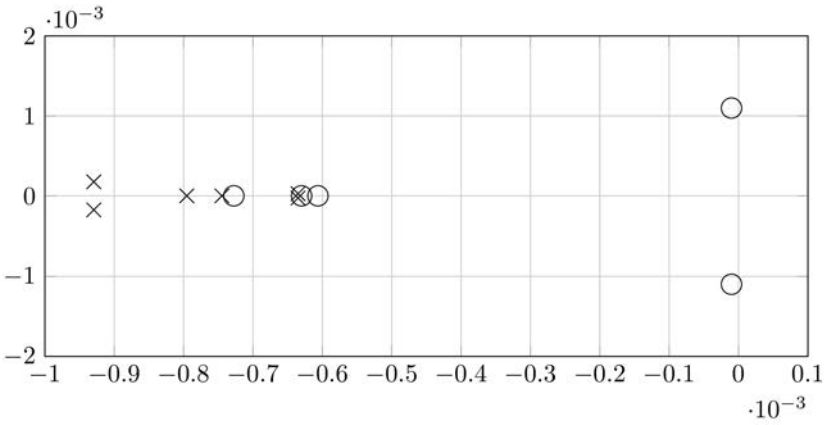

Figure 2.8: Dominant spectra of the linearized plant-replacement (x) and controller/observer (o) models

2.5.2 Regulatory control of the ACBT process

The function of regulatory control loops is to provide basic control of a process, i.e., they ensure a safe start-up, operation at a required target, and shut-down of the process. Furthermore, regulatory control should reduce the effects of load disturbances.

Here, we introduce the regulatory control for the ACBT process shown in Fig. 1.1 from Section 1.2.1. The production rate is set at the inlet to the plant by fixing the feed flow rate $F2$. Controlled and manipulated variables are chosen based on the standard control configurations typically used in distillation columns (Kister, 1990). All regulatory controllers are implemented as PI regulators specified by Eqs. (2.52a) – (2.52d). The objective of the regulatory control for the ACBT process is to stabilize the plant for varying flow rate and composition of the feed by using the following 16 PI controllers:

- pressures are controlled by manipulating the rates of heat removal in the condensers with controllers 2, 12, and 17,
- condenser levels are controlled by manipulating distillate and reflux flow rates with controllers 1, 10, and 16,
- reboiler levels are controlled by manipulating bottoms flow rates with controllers 5, 8, and 13,

- temperatures are controlled by manipulating either reflux flow rates with controllers 3 and 15, or by manipulating the reboiler heat inputs with controllers 4, 9, and 14,
- the flow rate in the recycle is set by the controller 7, and the distillate flow rate of the second column is controlled by a distillate-to-reflux ratio controller 11.

Note that the second column has a partial condenser which requires a different basic control scheme from that used in the total condensers of columns 1 and 2. The controller tuning parameters are tabulated in Table C.5 in Appendix C.3.

2.6 Chapter summary

In this chapter, we presented three variants of distillation-column models: fundamental, empirical, and hybrid. We especially focused on the fundamental models to be used in the following chapters. In this context, the concept of the equilibrium stage with an associated vapor-liquid equilibrium function was introduced. The equilibrium stage is employed in our distillation columns for modeling individual trays; the vapor-liquid equilibrium function is known to affect crucially the quality of the distillation-column model.

For non-ideal mixtures, the vapor-liquid equilibrium function must be extended with an efficiency concept. For this purpose, we presented the well-known Murphree point and tray efficiencies and gave the link between them. Based on the multi-component Murphree tray efficiency we derived a parametric efficiency model. The independent parameter of this efficiency model is an efficiency factor that lumps together several hardly measurable quantities. To estimate this factor on-line, an algorithm will be proposed later in Chapter 4.

Moreover, based on the fundamental models, two different models to be used as the plant replacement and controller/observer models were chosen for the studies and analysis in the next chapters. By this choice, a structural plant-model mismatch that concerns the energy balances in particular can be introduced where necessary. The case study in Chapter 5, for example, was carried out with that type of mismatch. Of course, parametric plant-model mismatches can also be investigated with either of the plant replacement and controller models, e.g., a mismatch of tray holdups, flows or the parameters involved in the vapor-liquid equilibrium model. For subsequent analysis, we also derived a generalized compact form of an arbitrary plant model with several possibly coupled distillation columns assuming the CMO conditions. The CMO conditions simplify the plant model such that its compact form is suitable for mathematical analysis in Chapter 3.

Finally, a comparison of model dynamics of the linearized plant replacement and controller models with the layout introduced in Section 1.2.1 is presented and the regulatory control of the ACBT process is introduced in Section 2.5.2. The principal dynamics of

these models are determined by their dominant poles and concern the outcomes of our later control studies. Dominant poles of both models are shown to lie close to each other; a poorly damped pair of poles in the controller model was found which will play again a negative role in findings of Chapter 5.

3 Analysis of the Lang-Gilles observer

In this chapter, some theoretical results on convergence of the Lang-Gilles observer will be presented.

3.1 Introduction

Due to its industrial importance, distillation is the subject of many papers in the process control literature. Many researchers have demonstrated that successful control of distillation columns can lead to significant improvements in energy efficiency, process safety, and profit. However, in order to apply these beneficial control techniques in practice, accurate distillation column models and carefully designed state observers are typically required.

Since Kalman (Kalman, 1960) and Luenberger (Luenberger, 1964) developed their famous state estimators for linear systems in the 1960s, the capabilities of computers have risen significantly and modern numerical methods allow the accurate solution of nonlinear differential equations with improved extrapolation quality. Consequently, a number of nonlinear state estimation schemes were proposed and some of them were eventually applied to nonlinear distillation column models. The remainder of this section provides some references concerned with nonlinear state estimation in distillation columns.

To start with, the well-known Extended Kalman Filter (EKF) (Jazwinski, 1970) was studied for binary distillation by Diehl et al. (2003). The authors developed a variant of a full-state EKF for a distillation column with 40 stages to be used in a model-predictive controller (MPC). Three temperature measurements are used in the EKF which also incorporates state and parameter ranges in form of bounds. However, the authors do not give the explicit model equations and no thorough discussion of the filter performance. The provided information on the prediction quality of this EKF suggests a possible error in temperature prediction of up to ± 4 K. A more thorough investigation of an EKF designed for a ternary mixture was presented by Baratti et al. (1998). The authors developed a distillation column with 30 stages assuming CMO conditions. In order to calculate the activity coefficients of the VLE equation, the NRTL equations are used. On each stage,

a constant Murphree tray efficiency is assumed. Furthermore, a constant linear pressure profile along the column is included in the model. The EKF is studied for disturbances on steam, reflux and feed flow rates. It uses temperature measurements to update its states and the measurements are taken only at two points of a real pilot plant. The authors note that additional temperature measurements do not improve essentially the prediction quality of their EKF. Even these two measurements are sufficient to predict temperatures with an accuracy of up to ± 2 K. The authors do not investigate larger distillation columns or column trains, though. A similar work with a focus on the effect of additional temperature measurements on EKF's convergence behavior and prediction accuracy was done by Oisiovici and Cruz (2000). These authors developed a model for a multi-component batch distillation process also based on the CMO conditions and assumed a constant column pressure. The columns in their examples have 10 to 30 stages. They claim that the EKFs designed for fast distillation processes require more temperature measurements than necessary in theory to be observable (the number of required measurements is equal to the number of mixture components minus one) to improve convergence and prediction quality. However, the authors give only some probable reasons for this EKF property without providing reasonable derivations. Also here, it is not clear how an adequate number of temperature measurements can be determined for larger columns or column trains.

Quintero-Marmol et al. (1991) applied full and reduced-order Extended Luenberger Observers (ELO) to a batch distillation process. They developed a model on the basis of CMO conditions with the tray temperatures calculated by Antoine equation and constant relative volatilities. For this, they gave a complete procedure for observer design and studied a ternary column with 20 trays. The authors investigated, in particular, the effect of initial conditions on convergence and found that using more temperature measurements for the state correction makes the observer less sensitive to the mismatch between the plant and model initial conditions. However, except for the presented procedure for observer design, no further derivations confirming the findings were given. Barolo and Berto (1998) pointed out some shortcomings of the ELO as used by Quintero-Marmol et al. (1991). To show the problems of this observer, the authors used essentially the same distillation model but introduced a plant-model mismatch in feed composition, neglected the tray hydraulics, and assumed noise in temperature measurements. They found that the larger the number of trays in the column, the harder it becomes to tune the observer and the number of temperature measurements should be increased. For a large amount of noise in measurements they advised to use a Kalman filter. Regrettably, in the case of tuning problems it is not made clear what a "large" number of trays could be as no derivations were presented.

In order to estimate continuous and non-continuous variables of a system while taking into account some constraints on these variables, moving horizon estimation (MHE) can be

deployed. For example, Olanrewaju et al. (2012) developed a CMO model with constant relative volatilities and tray temperatures calculated by Antoine equation. For their case study, the authors presented a hybrid MHE (HMHE) which estimates simultaneously all states by a method incorporating a Kalman filter and a nonlinear optimizer and tested it on a binary pilot plant with 5 trays. Changing the vapor boilup, they obtained very accurate estimates of the product mole fraction with an accuracy of ± 0.01. The small model in this case study is a big drawback. A consequence thereof could be that difficulties, e.g., with the tuning/convergence of the Kalman filter or the choice of the right measurement positions which can appear for larger columns and restrict the use of the HMHE, were not detected.

A high-gain observer with guaranteed exponential convergence was presented by Deza and Gauthier (1991) for distillation of a binary mixture when vapor composition measurements are available. This observer has a Luenberger-like structure. In contrast to the Luenberger observer, the observer gain matrix of the high-gain observer is updated on-line by solving an additional differential equation. The distillation column model is based on the assumption of CMO conditions. The authors presented a sketch of the proof where they apply the Lyapunov theory to show the convergence of the high-gain observer. Furthermore, the authors suppose that this observer is useful for low-dimensional systems; the assumptions of the proof might be violated in high-dimensional systems due to the stronger nonlinearities.

Another Luenberger-like observer, the so-called geometric estimator (GE), was studied by Tronci et al. (2005) and Álvarez and Fernández (2009). The gain of the GE is also updated on-line, however in contrast to the high-gain observer (Deza and Gauthier, 1991), Lie derivatives of the system model output are used to calculate the gain matrix. The main drawback of the GE is that the order of the Lie derivatives in the gain grows with the order of the system model. This makes the estimator less robust and impractical as a full-state estimator. Tronci et al. (2005) suggested, therefore, a design procedure to reduce the observer order. The authors used the same distillation model as Baratti et al. (1998) that was mentioned above. They tested their reduced-order estimator on a pilot-plant binary column with 32 trays. However, the proposed design procedure is complex and the advantage of GE over conventional observers is not clear.

Observers based on neural networks are presented by Brizuela et al. (1996), Baratti et al. (1997) and Fortuna et al. (2005). Neural networks are different from the observers discussed above in that they are data-driven and require a large amount of data to identify the model parameters. These neural models represent correlations between input and output arguments and not differential equations modeling a system behavior updated with some measurements as it is the case, e.g., for the Luenberger observer. We want to emphasize

the work of Fortuna et al. (2005). These authors developed soft sensors to estimate the top and bottom product concentrations in a real debutanizer column as an alternative to the gas chromotographs introducing long time delays. Real historical data as well as expert plant knowledge were used to train and validate the neural networks. A comparison with the installed gas chromotographs was made where the soft sensors achieved an accuracy of ± 0.5 wt%. This study not only shows that neural networks can work well in complex systems but also that expert system knowledge is compulsory to develop a good neural network.

Based on the wave theory introduced by Marquardt (1988), a profile position observer was developed by Han and Park (1993). A position observer consists of one differential equation per column section and has a Luenberger-like structure. The main idea behind this observer is that a concentration profile retains its constant-pattern form while moving around its position in the column where the position of the profile is defined by the point of inflection. Han and Park (1993) developed their observer only for binary columns as the wave theory for multi-component distillation was missing at that time. For the observer correction term, the concentration measurements were used, and this observer behaved robustly in cascade control applied to a distillation column taken from the literature. A similar study was done by Shin et al. (2000b). Instead of the concentration measurements, these authors used temperature measurements which are known to follow from the compositions for binary mixtures. Kienle (2000) extended the wave theory to multi-component distillation. Based on that, Grüner et al. (2004) developed a position observer for multi-component columns. Here, one profile position observer for each independent concentration profile was derived and the authors reported a good performance of the observer in control of a ternary distillation column. Their observer is in principle usable for all multi-component columns, however, from the practical point of view, the application of the observer to the columns with more than three components might be demanding as the complexity of profile dynamics rises with the number of mixture components.

Finally, one particular approach to accurate nonlinear distillation column modeling and observer design was proposed by Lang and Gilles (1990). The observer relies on a nonlinear, high-order dynamic process model for prediction, and uses temperature measurements in regions of high mass-transfer for the correction of the predicted temperature profile along the column. Appropriate design is based on physical insight and requires only a few tuning parameters. In simulation, the observer obtained was found to exhibit good and sufficiently robust dynamic behavior.

While some of the authors above have successfully tested their observers in experiments, there are remarkably few papers that give theoretical convergence guarantees for the specific nonlinear distillation observer. There are even less convergence results for coupled

column trains. In particular, to the best of our knowledge no proof of convergence has been reported for the attractive nonlinear distillation column model and observer proposed by Lang and Gilles (1990). In this thesis we give general proofs for asymptotic convergence of the observer's states to the true states for varying requirements on the initial estimation error. The proofs are general in that they hold not only for the particular distillation column model used by Lang and Gilles (1990) but for a more general class of distillation column trains.

3.2 Lang-Gilles observer

There are many approaches worthy of consideration when developing a state observer for distillation columns (Birk, 1992, Tronci et al., 2005). We utilize a full state observer (Lang and Gilles, 1990) based on the model presented in Section 2.4.2. This observer has a simple Luenberger-like structure and the choice of its feedback term is based on the physical insight that a temperature front moves with the region of high mass transfer. As shown below, the mass balance equations are corrected by the observer feedback. The observer model captures well the principal dynamics of a distillation process (Marquardt, 1988, Skogestad, 1997).

3.2.1 Problem statement and initial data

Having chosen the state observer of Lang and Gilles relieves us of selecting a model for the observer. We formulate the task of selecting a model for the observer in a similar way to that adopted for the controller model but, in addition, require the plant to be observable:

Assume that data describing the essential characteristics relevant for observer design exist and the plant is observable. The purpose of the observer model to be developed is to capture the essential characteristics of the plant. Select adequate model type, structure, and parameters.

Selecting the same model for both the controller and state observer allows us to also use the same data for their initialization and for determining their parameters. For the same reason, in the following we consider only those model equations which are different for the observer.

3.2.2 Observer correction term

In the observer model, state variables are corrected. These corrections concern the liquid compositions in the column sections only. Eq. (2.56a) specifying the mass balance in a column section of the controller model is corrected and the remaining Eqs. (2.56b) – (2.56e)

of the column section are left unchanged. In the condenser, feed trays, and reboiler, corrections of the compositions are dropped in favor of a model simplification, i.e., the equations are the same as Eqs. (2.53a) – (2.53d), (2.55a) – (2.55d), (2.57a) – (2.57d) in the controller model. This observer simplification is in agreement with Lang and Gilles (1990).

On each stage j of a column section, the equations read as

$$\begin{aligned}
\frac{d\hat{x}_{i,j}}{dt} &= \frac{1}{M_j^L}\big(\hat{L}_{j-1}\hat{x}_{i,j-1} - \hat{L}_j\hat{x}_{i,j} + \hat{V}_{j+1}\hat{y}_{i,j+1} - \hat{V}_j\hat{y}_{i,j}\big) \\
&\quad - \alpha_i\hat{N}_{i,j}\big(\tilde{T}_{j_i} - \hat{T}_{j_i}\big), \quad i = 1, q-1, && \text{(3.1a)} \\
\hat{L}_j &= L, && \text{(3.1b)} \\
\hat{V}_j &= V, && \text{(3.1c)} \\
\hat{N}_{1:q-1,j} &= NTU_{OV,j} \cdot \big(\hat{y}_{1:q-1,j} - \hat{y}^*_{1:q-1,j}\big)\,, && \text{(3.1d)} \\
\hat{y}_{i,j} &= f_i^{vap}(\hat{x}_{1,j}, \ldots, \hat{x}_{q-1,j}, \hat{y}_{1,j+1}, \ldots, \hat{y}_{q-1,j+1}, p_j, \hat{T}_j, C_l^L), \quad i = 1, q-1, && \text{(3.1e)} \\
\hat{y}^*_{i,j} &= f_i^{vle}(\hat{x}_{1,j}, \ldots, \hat{x}_{q-1,j}, p_j, \hat{T}_j), \quad i = 1, q-1, && \text{(3.1f)} \\
p_j &= p_0 + (j-1)\,\frac{p_{m_{sec}+1} - p_0}{m_{sec}}. && \text{(3.1g)}
\end{aligned}$$

where the hat highlights observer variables. $\hat{x}_{i,j}$ and $\hat{y}_{i,j}$ are the liquid and vapor concentrations of component i. $\hat{y}^*_{i,j}$ are the concentrations of vapor in equilibrium with liquid. M_j^L is the mole number in the liquid phase. $\hat{L}_j$ and $\hat{V}_j$ are liquid and vapor flow rates leaving stage j. The term $\alpha\hat{N}_{i,j}$ is the observer gain, where α_i denotes the observer tuning parameter and $\hat{N}_{i,j}$ is the predicted molar flux between the vapor and liquid phases of component i on stage j calculated by Eq. (3.1d). Therein, the matrix of overall numbers of transfer units $NTU_{OV,j}$ is obtained from Eq. (2.38b). Note that the colon notation in term $\hat{N}_{1:q-1,j}$ (also in $\hat{y}_{1:q-1,j}$ and $\hat{y}^*_{1:q-1,j}$) denotes a vector of length $q-1$ with its elements $\hat{N}_{i,j}$ ($\hat{y}_{i,j}$ and $\hat{y}^*_{i,j}$) for $i \in \{1, \ldots, q-1\}$. $\tilde{T}_{j_i}$ and $\hat{T}_{j_i}$ are the measured and predicted temperatures on stage j_i. The indices j_i with sub-indices $i \in \{1, \ldots, i_{max}\}$ point to the stages selected from all available stages of a single column. These must be chosen such that the corresponding temperatures are strongly related to single components, i.e., the temperatures must lie within the regions of high mass transfer of corresponding components. The maximum sub-index i_{max} is a design parameter equal to the number of temperatures used in the observer feedback. m_{sec} is the number of stages in the corresponding column section. The pressure p_j on stage j is assumed to be linear in j, where the pressure drop is given by the constant $(p_{m_{sec}+1} - p_0)/m_{sec}$.

3.2.3 Plant observer in a compact form for theoretical analysis

Here, we introduce the plant observer for estimating state variables of the plant replacement which was given in compact form by Eqs. (2.61a) and (2.61b). This observer is based on the equations of the controller model with corrected mass balances in column sections as it was explained in Section 3.2.2. Note that equations corresponding to stage j are formulated for q (not $q-1$) components for reasons stated in Section 2.4.4.

Assuming $\hat{A} = A$, $\hat{B} = B$, $\hat{C} = C$, and $\hat{z} = z$ for the sake of simplicity to allow further mathematical analysis, the state equation for the observer corresponding to an entire plant can be written as

$$\frac{d\hat{x}}{dt} = \hat{A}\hat{x} + \hat{B}\hat{y} + \hat{C}\hat{z} + \alpha\, \hat{N} \circ \delta T, \quad \hat{x}(0) = \hat{x}^{init}, \tag{3.2a}$$

$$\hat{N} = \hat{D}\, \delta\hat{y}^*, \tag{3.2b}$$

$$\hat{y} = f(\hat{x}, \hat{y}, p, \hat{T}, C_l^L), \tag{3.2c}$$

$$\hat{y}^* = f^{vle}(\hat{x}, p, \hat{T}), \tag{3.2d}$$

$$\hat{T} = \hat{T}(p, \hat{x}), \tag{3.2e}$$

where $\circ$ is the entrywise product (Hadamard product). The three composition vectors from the observer $\hat{x}$, $\hat{y}$ and $\hat{z}$ are determined by following the same steps as for x, y and z from Eq. (2.61a). The matrices A, B, and C are those defined by Eqs. (2.65a), (2.65b), and (2.65c). The vector $\hat{N}$ in Eq. (3.2b) is a generalisation of that in Eq. (3.1d) for the entire plant where $\hat{D}$ is assumed for simplicity to be a constant matrix of overall numbers of transfer units. Eq. (3.2c) corresponds to Eq. (2.61b) and Eq. (3.2d) combines all vapor concentrations in equilibrium with liquid on each tray calculated by Eq. (2.11) which is our implementation of Eq. (2.6). p is the vector of pressures on column trays. C_l^L is the vector of separation efficiencies for column sections. $\hat{T}$ is the vector of all tray temperatures where each element is calculated by Eq. (2.15). It should be understood that the notation in Eqs. (3.2b) – (3.2e) suggests the calculation of the vector elements of $\hat{N}, \delta\hat{y}^*, \hat{y}, \hat{y}^*$, and $\hat{T}$ by taking the corresponding elements from the vectors $\hat{x}, \hat{y}, p, \hat{T}$, and C_l^L. In the following, we introduce in more detail the specific observer variables $\alpha, \hat{D}, \hat{y}^*, \delta\hat{y}^*$, and δT.

The observer tuning parameter α in Eq. (3.2a) is a diagonal matrix, where values corresponding to each tray from one column section are equal. It is defined as

$$\alpha = \mathrm{diag}(\mathrm{diag}(\alpha_1), \mathrm{diag}(\alpha_2), \ldots, \mathrm{diag}(\alpha_n)) \in \mathbb{R}^{q\sum_{l=1}^{n}(m_l+2)\times q\sum_{l=1}^{n}(m_l+2)}, \tag{3.3a}$$

where $\mathrm{diag}(\alpha_1), \ldots, \mathrm{diag}(\alpha_n)$ are diagonal sub-matrices assigned to n distillation columns

and

$$\alpha_{j,l} = \begin{pmatrix} \alpha_{1,j,l} \\ \vdots \\ \alpha_{q,j,l} \end{pmatrix} \in \mathbb{R}^q, \quad j = 0, m_l + 1, \quad l = 1, n, \tag{3.3b}$$

$$\alpha_l = \begin{pmatrix} \alpha_{0,l} \\ \vdots \\ \alpha_{m_l+1,l} \end{pmatrix} \in \mathbb{R}^{(m_l+2)\cdot q}, \quad l = 1, n. \tag{3.3c}$$

The tuning parameters $\alpha_{i,j,l}$ in Eq. (3.3b) that correspond to different species i on stage j in column l are assumed to be equal, i.e. $\alpha_{1,j,l} = \ldots = \alpha_{q,j,l}$ (Lang and Gilles, 1990), whereas the parameter vectors corresponding to different stages j in column l, $\alpha_{j,l}$, can be equal in each column section but vary for different column sections. When no observer correction is used on a certain stage (e.g. reboiler and condenser), then the corresponding α-values will be zero.

$\hat{D}$ in Eq. (3.2b) is a bounded matrix which corresponds to the finite mass transfer between the liquid and vapor phases. It is denoted as

$$\hat{D} = \mathrm{diag}(\hat{D}_1, \hat{D}_1, \ldots, \hat{D}_n) \in \mathbb{R}^{q\sum_{l=1}^{n}(m_l+2)\times q\sum_{l=1}^{n}(m_l+2)}, \tag{3.4a}$$

$$\hat{D}_j \in \mathbb{R}^{(m_l+2)q\times(m_l+2)q}. \tag{3.4b}$$

Note that claiming the boundedness of $\hat{D}$ is required for mathematical proofs later.

The vector of estimated vapor compositions in equilibrium with the liquid is denoted as

$$\hat{y}^*_{j,l} = \begin{pmatrix} \hat{y}^*_{1,j,l} \\ \vdots \\ \hat{y}^*_{q,j,l} \end{pmatrix} \in \mathbb{R}^q, \quad j = 0, \ldots, m_l + 1, \quad l = 1, \ldots, n, \tag{3.5a}$$

$$\hat{y}^*_l = \begin{pmatrix} \hat{y}^*_{0,l} \\ \vdots \\ \hat{y}^*_{m_l+1,l} \end{pmatrix} \in \mathbb{R}^{(m_l+2)\cdot q}, \quad l = 1, n, \tag{3.5b}$$

$$\hat{y}^* = \begin{pmatrix} \hat{y}^*_1 \\ \vdots \\ \hat{y}^*_n \end{pmatrix} \in \mathbb{R}^{q\sum_{l=1}^{n}(m_l+2)}, \tag{3.5c}$$

and the deviation of the estimated current vapor compositions from corresponding estimated equilibrium compositions as

$$\delta\hat{y}^* = \hat{y} - \hat{y}^*. \tag{3.6}$$

In order to update the component mass balances on a stage of the column l, the feedback term of Eq. (3.2a) includes the vector of k temperature differences, $\delta T_{j_1:j_k,l}$, defined as

$$\delta T_{j_1:j_k,l} = \begin{pmatrix} \bar{T}_{j_1,l} \\ \vdots \\ \bar{T}_{j_k,l} \\ 0 \\ \vdots \\ 0 \end{pmatrix} \in \mathbb{R}^q, \quad k \leq q, \quad l = 1, n, \tag{3.7a}$$

where $\bar{T}_{j,l} = \hat{T}_{j,l} - \tilde{T}_{j,l}$ denotes the difference between the estimated ($\hat{T}_{j,l}$) and measured ($\tilde{T}_{j,l}$) temperatures on stage j in the distillation column l. The temperature $\hat{T}_{j,l}$ is calculated by Eq. (2.15). As the definition of the vector $\delta T_{j_1:j_k,l}$ suggests, if $k < q$, then the vector is filled up with zeros to have q entries. However, it must be noted that faster convergence is expected for a larger k. In order to update the component mass balances of the entire column l, the following vector is defined:

$$\delta T_l = \begin{pmatrix} \delta T_{j_1:j_k,l} \\ \vdots \\ \delta T_{j_1:j_k,l} \end{pmatrix} \in \mathbb{R}^{(m_l+2)q}, \quad l = 1, n. \tag{3.7b}$$

Finally, the vector of temperature differences used in Eq. (3.2a) is defined as

$$\delta T = \begin{pmatrix} \delta T_1 \\ \vdots \\ \delta T_n \end{pmatrix} \in \mathbb{R}^{q \sum_{l=1}^{n} (m_l+2)}, \tag{3.7c}$$

where each entry of this vector has its own set of indices $\{j_1, \ldots, j_k\}$.

For concise formulation of our theorems, it is also convenient to define the following vector of all temperature differences in the plant as

$$\bar{T} = \begin{pmatrix} \bar{T}_1 \\ \vdots \\ \bar{T}_n \end{pmatrix} \in \mathbb{R}^{\sum_{l=1}^{n} (m_l+2)}, \tag{3.8a}$$

where the vector of temperature differences in the column l is given as

$$\bar{T}_l = \begin{pmatrix} \bar{T}_{0,l} \\ \vdots \\ \bar{T}_{m_l+1,l} \end{pmatrix} \in \mathbb{R}^{m_l+2}, \quad l = 1, n. \tag{3.8b}$$

3.3 Convergence analysis

Here, convergence of the state observer is analyzed in terms of stability of the differential equation which is derived for the error between the observer states and the states of the plant. The states comprise all q liquid compositions on each of the $m_l + 2$ (including condenser and reboiler compositions) stages of a column l and are represented by a state vector of length $q \cdot (m_l + 2)$. The state observer of the plant, e.g., a distillation column or a distillation train, generally combines several column observers into one. In what follows, we consider the observer for the entire plant.

3.3.1 The state error equation

Subtracting Eq. (2.61a) from (3.2a), the state error equation for the entire plant is introduced as

$$\frac{d\bar{x}}{dt} = A\bar{x} + B\bar{y} + \alpha\ \hat{D}\ \delta\hat{y}^* \circ \delta T. \tag{3.9}$$

Therein, we define the error vectors as

$$\bar{x} = \hat{x} - x, \tag{3.10a}$$

$$\bar{y} = \hat{y} - y, \tag{3.10b}$$

where $\hat{y}$ and y are given by Eqs. (3.2c) and (2.61b). The variables x, A, B were introduced in Section 2.4.4. The variables $\alpha, \hat{D}, \delta\hat{y}^*, \delta T$ are given in Section 3.2.3 by Eqs. (3.3a), (3.4a), (3.6), and (3.7c). To prepare a notation compatible with the auxiliary theorems used in our proofs, we define

$$f(x, \hat{x}, t) = B\bar{y} + \alpha\ \hat{D}\ \delta\hat{y}^* \circ \delta T. \tag{3.11}$$

Note that in Eq. (3.11) f is interpreted as a function of $x, \hat{x}$, and t only because with fixed pressure p and efficiency constants C_l^L the temperature and vapor concentration vectors $T, \hat{T}, \delta T$ and $y, \hat{y}, y^*, \hat{y}^*$ are all functions of $x, \hat{x}, t$. Thus, we can rewrite Eq. (3.9) as

$$\dot{\bar{x}} = A\bar{x} + f(x, \hat{x}, t). \tag{3.12}$$

Keep in mind that at a given pressure in both plant and observer, $f(x, \hat{x}, t) \to 0$ for $\hat{x} \to x$.

3.3.2 Preliminary results

In order to prove our convergence theorems, we will apply Theorem D.2 in the Appendix to an equation which is related to Eq. (3.12) by the majorant criterion for integrals[1].

[1] This criterion claims that for the functions f and g with $f(x) \leq g(x)$ the inequality is also retained for integrals of these functions (cf. Walter (1995)).

As a consequence of the majorant criterion, the solution of Eq. (3.12) will converge to zero because the former equation converges to zero under specific conditions, too. The assumptions for this convergence behavior are summarized in Lemma 1. We must also show that the matrix A in Eq. (3.12) has eigenvalues with negative real parts. This result is summarized in Lemma 2.

Lemma 1. *Let*

$$\dot{\bar{x}} = A\bar{x} + f(x, \hat{x}, t), \quad \bar{x}(0) = \bar{x}_0 \tag{3.13}$$

be the system from Eq. (3.12)*. Moreover, let*

$$\dot{\bar{x}} = A\bar{x} + \bar{f}(\bar{x}, t), \quad \bar{x}(0) = \bar{x}_0 \tag{3.14}$$

be a second system, where the function $\bar{f}$ is a majorant of function f from Eq. (3.13)*, and the variables $\bar{x}, A$ be defined as those in Eq.* (3.13)*. If the solution $\bar{x}$ of Eq.* (3.14) *converges towards zero, then the solution $\bar{x}$ of Eq.* (3.13) *converges towards zero.*

Proof. Since $\bar{f}$ is a majorant of function f, this can be written, by definition, as an element-wise inequality

$$|f(x, \hat{x}, t)| \leq \bar{f}(\bar{x}, t). \tag{3.15}$$

Adding $A\bar{x}$ to each side of inequality (3.15), we obtain

$$A\bar{x} + f(x, \hat{x}, t) \leq A\bar{x} + |f(x, \hat{x}, t)| \leq A\bar{x} + \bar{f}(\bar{x}, t). \tag{3.16}$$

Furthermore, the solution of Eq. (3.13) can be given as

$$\bar{x}(t) = \bar{x}_0 + \int_0^t A\bar{x}(s) + f\big(x(s), \hat{x}(s), s\big)\, ds, \tag{3.17}$$

and that of (3.14) as

$$\bar{x}(t) = \bar{x}_0 + \int_0^t A\bar{x}(s) + \bar{f}\big(\bar{x}(s), s\big)\, ds. \tag{3.18}$$

Since the inequality (3.16) is preserved by integration (also for improper integrals), we obtain

$$\int_0^t A\bar{x}(s) + f\big(x(s), \hat{x}(s), s\big)\, ds \leq \int_0^t A\bar{x}(s) + \bar{f}\big(\bar{x}(s), s\big)\, ds, \tag{3.19}$$

and using Eq. (3.19), the terms on the right-hand sides of Eqs. (3.17) and (3.18) can be brought into relation to each other as

$$\bar{x}_0 + \int_0^t A\bar{x}(s) + f\big(x(s), \hat{x}(s), s\big)\, ds \leq \bar{x}_0 + \int_0^t A\bar{x}(s) + \bar{f}\big(\bar{x}(s), s\big)\, ds. \tag{3.20}$$

Finally, let the solution of Eq. (3.14), given by Eq. (3.18), converge towards zero, then

$$\begin{aligned} 0 \quad &\leq \quad \left\| \bar{x}_0 + \int_0^t A\bar{x}(s) + f\big(x(s), \hat{x}(s), s\big)\, ds \right\| \\ &\overset{(3.20)}{\leq} \left\| \bar{x}_0 + \int_0^t A\bar{x}(s) + \bar{f}\big(\bar{x}(s), s\big)\, ds \right\| \to 0. \end{aligned} \tag{3.21}$$

Eq. (3.21) guarantees that also the solution of Eq. (3.13) converges to zero. □

Lemma 2. *Let $A = G + E$ be a decomposition of the matrix A from Eq.* (2.65a) *such that G is the lower triangular matrix and E the strictly upper triangular matrix. If $\|E\|_2$ is sufficiently small, then all eigenvalues of the matrix A in Eq.* (2.65a) *have negative real parts.*

Proof. Let $A = G + E$ be a decomposition of the matrix A from Eq. (2.65a) such that G is the lower triangular matrix (including the diagonal entries) and E the strictly upper triangular matrix (excluding the diagonal entries).

First, notice that diagonal entries of the matrix G are equal to those of the matrix A. Because G is triangular, its diagonal entries, i.e., the values $a_{r,s,l}$ in Eq. (2.67a) for $r = s$, are also its eigenvalues. These are negative as otherwise, i.e., for a zero numerator in $a_{r,s,l}$, there would be no liquid flow on stage r in distillation column l what is only possible in the case of a malfunction.

Then, Theorem D.1 in the Appendix applied to G ensures that the eigenvalues of A are close to those of G if $\|E\|_2$ is sufficiently small ($\|\cdot\|_2$ is here the spectral norm), i.e., if the streams between different distillation columns are sufficiently small. □

Note that the matrix A can be arranged such that only recycle streams are described by the matrix E and therefore required to be sufficiently small in terms of the above Lemma. This lemma also gives only sufficient conditions which might be too strict in general.

3.3.3 Convergence results

In this section, we state and prove three theorems to demonstrate how different assumptions imply convergence of the state observer. To this end we will usually use non-specific vector

and matrix norms. In some cases, it will be more convenient to use a norm of the class of p-norms, defined as

$$\|x\|_p = \sqrt[p]{\sum |x_i|^p}, \quad 1 \leq p < \infty$$
$$\|x\|_\infty = \max_{1 \leq i \leq n} |x_i|,$$

for a vector $x \in \mathbb{R}^n$. For matrices, we will use natural norms induced by p-norms and defined as

$$\|A\|_p = \max_{x \neq 0} \frac{\|Ax\|_p}{\|x\|_p}, \quad 1 \leq p \leq \infty,$$

especially the row sum norm

$$\|A\|_\infty = \max_i \sum_{j=1}^{n} |a_{ij}|$$

and the spectral norm

$$\|A\|_2 = \sqrt{\lambda_{max}(A^H A)},$$

where λ_{max} is the maximum eigenvalue of $A^H A$ and A^H is the conjugate transpose of A. However, as norms in finite-dimensional spaces are equivalent, the qualitative results are essentially the same for either norm.

Theorem 1. *Let $A = G + E$ be a decomposition of A and $\|E\|_2$ be sufficiently small in the context of Lemma 2. Furthermore, let the diagonal gain matrix α with $\alpha_{i,i} > 0$ be arbitrarily chosen, and $\exists K_1, K_2 \in \mathbb{R} : \|\bar{y}\|_\infty \leq K_1 \|\bar{x}\|_\infty^{1+\beta_1}$, $\|\bar{T}\|_\infty \leq K_2 \|\bar{x}\|_\infty^{1+\beta_2}$, where $\beta_1 > 0$ and $\beta_2 > 0$. Then there is a $\delta > 0$ such that for every initial observer state $\hat{x}(0)$ with $\|\hat{x}(0) - x(0)\|_\infty \leq \delta$ the solution $\hat{x}$ of the observer system* (3.2a) *converges asymptotically towards the solution x of the system* (2.61a).

Proof. In order to prove the statement, it is sufficient to show that there is a system as in Eq. (3.14) for which all assumptions of Theorem D.2 in the Appendix are fulfilled.
(i) All eigenvalues of A have negative real parts.
This is shown for a sufficiently small value of $\|E\|_2$ by Lemma 2.
(ii) It holds $\exists K > 0\ \exists \delta > 0$: $\left\|\bar{f}(\bar{x}, t)\right\|_\infty \leq K \|\bar{x}\|_1$, $\forall \|\bar{x}\|_1 \leq \delta$, $t \geq 0$.
First, we derive a majorant $\bar{f}(\bar{x}, t)$ for $f(x, \hat{x}, t)$ from Eq. (3.11) and show finally that *(ii)* is fulfilled.

Due to subadditivity

$$\|f(x, \hat{x}, t)\|_\infty \leq \|B\bar{y}\|_\infty + \left\|\alpha \hat{D} \delta \hat{y}^* \circ \delta T\right\|_\infty \tag{3.22}$$

holds. For the first term on the right hand side of Eq. (3.22), we obtain by the assumption $\|\bar{y}\|_\infty \leq K_1 \|\bar{x}\|_\infty^{1+\beta_1}$, $\beta_1 > 0$ that

$$\|B\bar{y}\|_\infty \leq K_1 \|B\|_\infty \|\bar{x}\|_\infty^{1+\beta_1}. \tag{3.23}$$

The second term in Eq. (3.22) also has an upper bound. Note that

$$\left\|\alpha\hat{D}\delta\hat{y}^* \circ \delta T\right\|_\infty = \left\|\alpha\hat{D}\delta\hat{y}^* \circ \left(P\,\bar{T}\right)\right\|_\infty, \tag{3.24}$$

where the matrix P is selected (*selection* matrix) such that

$$P\,\bar{T} = \delta T. \tag{3.25}$$

Furthermore, the Hadamard product can be resolved by virtue of equivalence of norms in finite-dimensional spaces and the Cauchy-Schwarz (CS) inequality

$$\left\|\alpha\hat{D}\delta\hat{y}^* \circ \left(P\,\bar{T}\right)\right\|_\infty \leq \left\|\alpha\hat{D}\delta\hat{y}^* \circ \left(P\,\bar{T}\right)\right\|_1 \overset{CS}{\leq} \left\|\alpha\hat{D}\delta\hat{y}^*\right\|_2 \left\|P\,\bar{T}\right\|_2 \leq C \left\|\alpha\hat{D}\delta\hat{y}^*\right\|_\infty \left\|P\,\bar{T}\right\|_\infty, \tag{3.26}$$

where C is the corresponding constant of the equivalence relation. By the assumption $\left\|\bar{T}\right\|_\infty \leq K_2 \|\bar{x}\|_\infty^{1+\beta_2}$, $\beta_2 > 0$ and as $\delta\hat{y}_i^*$ are bounded functions of $\hat{x}$, i.e., $\exists K_3 \in \mathbb{R} : \|\delta\hat{y}^*\|_\infty \leq K_3$, the latter term can be further reduced to result in

$$\left\|\alpha\hat{D}\delta\hat{y}^* \circ \delta T\right\|_\infty \leq C K_2 K_3 \left\|\alpha\hat{D}\right\|_\infty \|P\|_\infty \|\bar{x}\|_\infty^{1+\beta_2}. \tag{3.27}$$

Hence, for

$$K := K_1 \|B\|_\infty + C K_2 K_3 \left\|\alpha\hat{D}\right\|_\infty \|P\|_\infty \tag{3.28}$$

one obtains for $\bar{x}$ with $\|\bar{x}\|_\infty \leq \delta \leq 1$

$$\|f(x,\hat{x},t)\|_\infty \leq K \|\bar{x}\|_\infty^{1+\min(\beta_1,\beta_2)} \leq K \|\bar{x}\|_\infty. \tag{3.29}$$

Then, a trivial majorant for $f(x,\hat{x},t)$ is given by

$$\bar{f}(\bar{x},t) := \left(K \|\bar{x}\|_\infty^{1+\min(\beta_1,\beta_2)}, \ldots, K \|\bar{x}\|_\infty^{1+\min(\beta_1,\beta_2)}\right)^T \in \mathbb{R}^{q\sum_{l=1}^n (m_l+2)}. \tag{3.30}$$

Then, it follows using Eq. (3.29) for the first and second inequalities and norm definitions of $\|\cdot\|_\infty$ and $\|\cdot\|_1$ for the third inequality

$$\|f(x,\hat{x},t)\|_\infty \leq \left\|\bar{f}(\bar{x},t)\right\|_\infty \leq K \|\bar{x}\|_\infty \leq K \|\bar{x}\|_1. \tag{3.31}$$

(iii) It holds $\forall \varepsilon > 0\ \exists \delta > 0\ \exists t_e > 0$: $\left\|\bar{f}(\bar{x},t)\right\|_\infty \leq \varepsilon \|\bar{x}\|_1$, $\forall \|\bar{x}\|_1 \leq \delta$, $t \geq t_e$.
Let $\varepsilon > 0$ be arbitrarily chosen. If $\varepsilon \geq K$ then *(iii)* is obvious due to Eq. (3.31). Otherwise, define

$$\delta := (\varepsilon/K)^{1/\min(\beta_1,\beta_2)} \tag{3.32}$$

and require $\|\bar{x}\|_1 \leq \delta$ to conclude

$$K \|\bar{x}\|_1^{\min(\beta_1,\beta_2)} \leq K\delta^{\min(\beta_1,\beta_2)} = \varepsilon \tag{3.33}$$

and, using the third inequality in Eq. (3.31),

$$\left\|\bar{f}(\bar{x},t)\right\|_\infty = K \|\bar{x}\|_\infty^{1+\min(\beta_1,\beta_2)} \overset{(3.31)}{\leq} K \|\bar{x}\|_1^{1+\min(\beta_1,\beta_2)} \overset{(3.33)}{\leq} \varepsilon \|\bar{x}\|_1 . \tag{3.34}$$

Now using Lemma 1, we conclude the convergence of Eq. (3.13) to zero and consequently the statement of the theorem. □

Remark 1. The assumptions of Theorem 1 on functions $\bar{y}$ and $\bar{T}$ seem to be rather complex at first glance. Their effect can be illustrated by means of a simplified example. Assume that $\hat{y} = y$ and $\hat{T} = \tilde{T}$ describe the vapor-liquid equilibrium and the boiling temperature on a tray as functions of the liquid concentration of one component in a binary pseudo-mixture, i.e., $y = y(x)$ and $\hat{T} = \hat{T}(x)$ are one-dimensional functions of $x \in (0,1) \subset \mathbb{R}$. Furthermore, assume that $\hat{y}$ and $\hat{T}$ are analytic, i.e., they can be represented by convergent Taylor series. Then for $\bar{x} \to 0$

$$\bar{y}(\hat{x},x) = \hat{y}(\hat{x}) - y(x) = \hat{y}(x+\bar{x}) - y(x) = \dot{y}(x) \cdot \bar{x} + \mathcal{O}\left(\bar{x}^2\right), \tag{3.35}$$

$$\bar{T}(\hat{x},x) = \hat{T}(\hat{x}) - \tilde{T}(x) = \hat{T}(x+\bar{x}) - \tilde{T}(x) = \dot{\hat{T}}(x) \cdot \bar{x} + \mathcal{O}\left(\bar{x}^2\right), \tag{3.36}$$

where the last terms in Eqs. (3.35) and (3.36) result from Taylor expansions of $\hat{y}(x+\bar{x})$ and $\hat{T}(x+\bar{x})$ at x with subtracted $y(x)$ and $\tilde{T}(x)$, respectively. If, in addition to Eqs. (3.35) and (3.36), we make the assumptions $\exists K_1, K_2 \in \mathbb{R} : \|\bar{y}\|_\infty \leq K_1 \|\bar{x}\|_\infty^{1+\beta_1}$, $\left\|\bar{T}\right\|_\infty \leq K_2 \|\bar{x}\|_\infty^{1+\beta_2}$ with $\beta_1 = \beta_2 = 0.5$, we obtain

$$\left|\dot{y}(x) \cdot \bar{x} + \mathcal{O}\left(\bar{x}^2\right)\right| \leq K_1 |\bar{x}|^{1.5}, \tag{3.37}$$

$$\left|\dot{\hat{T}}(x) \cdot \bar{x} + \mathcal{O}\left(\bar{x}^2\right)\right| \leq K_2 |\bar{x}|^{1.5}. \tag{3.38}$$

However, Eqs. (3.37) and (3.38) are only valid if $\dot{y}(x) = \dot{\hat{T}}(x) = 0$. We show this by contradiction: if $\dot{y}(x) \neq 0$ and $\dot{\hat{T}}(x) \neq 0$, then for $\bar{x}$ close to zero, the linear terms $\dot{y}(x) \cdot \bar{x}$ and $\dot{\hat{T}}(x) \cdot \bar{x}$ on the left grow faster than those on the right of Eqs. (3.37) and (3.38). This means that reverse inequality signs in Eqs. (3.37) and (3.38) are true what is a contradiction. So, we obtain

$$\bar{y}(\hat{x},x) = \mathcal{O}\left(\bar{x}^2\right), \tag{3.39}$$

$$\bar{T}(\hat{x},x) = \mathcal{O}\left(\bar{x}^2\right). \tag{3.40}$$

Eqs. (3.39) and (3.40) are technically less realistic, since we require from the derivative of the function modeling the vapor composition and temperature to be zero on every stage of

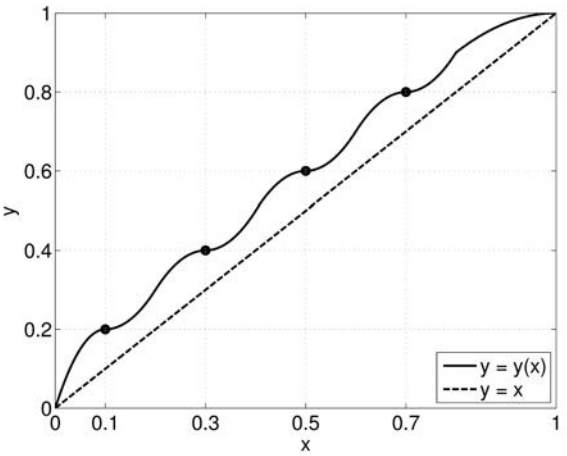

Figure 3.1: Example of a function $y = y(x)$ modeling the vapor-liquid equilibrium of a binary pseudo-mixture and defined by some piece-wise quadratic functions with zero-derivatives at liquid concentrations $x_1 = 0.1, x_2 = 0.3, x_3 = 0.5, x_4 = 0.7$ as indicated by Eq. (3.39)

each distillation column in the plant (cf. Fig. 3.1). From the mathematical point of view, these assumptions are even stronger than the *local* Lipschitz continuity (it can be easily verified that $\min(\beta_1, \beta_2) > 0$ is sufficient for y and T to be locally Lipschitz). A better choice is to require y and T be differentiable with respect to x and to have bounded first derivatives, which is equivalent to requiring y and T be Lipschitz, i.e., $\beta_1 = \beta_2 = 0$. For example, consider an often used approach for modeling vapor-liquid equilibrium

$$y = K(p, T)x, \tag{3.41}$$

where the so-called "K-value" is a function of pressure p and temperature T only. If y in Eq. (3.41) is assumed to be Lipschitz in x then K has to be bounded which is in agreement with the fixed range of y given by theory. However, the Lipschitz continuity is not sufficient to show the third item in the proof which relies on the assumption $\min(\beta_1, \beta_2) > 0$. Consequently, in the following theorems the stronger assumptions $\beta_1 > 0$ and $\beta_2 > 0$ are gradually replaced by the Lipschitz continuity while introducing additional assumptions.

Theorem 2 assumes that the temperature T is Lipschitz while the vapor composition y fulfills the requirements of Theorem 1.

Theorem 2. *Let $A = G + E$ be a decomposition of A and $\|E\|_2$ be sufficiently small in the context of Lemma 2. Suppose $\exists K_1 \in \mathbb{R} : \|\bar{y}\|_\infty \leq K_1 \|\bar{x}\|_\infty^{1+\beta_1}$, where $\beta_1 > 0$. Let T*

be Lipschitz continuous, i.e., $\exists K_2 : \left\|\bar{T}\right\|_\infty \leq K_2 \left\|\bar{x}\right\|_\infty$. *Then there are a* $\delta > 0$ *and a diagonal gain matrix* α *with* $\alpha_{i,i} > 0$ *such that for every initial observer state* $\hat{x}(0)$ *with* $\left\|\hat{x}(0) - x(0)\right\|_\infty \leq \delta$ *the solution* $\hat{x}$ *of the observer system* (3.2a) *converges asymptotically towards the solution* x *of the system* (2.61a).

Proof. The idea of the proof is the same as for Theorem 1. Therefore, we must prove statements *(i), (ii)* and *(iii)*. *(i)* and *(ii)* hold as in the proof of Theorem 1. We only need to show the statement *(iii)*.
(iii) $\forall \varepsilon > 0\ \exists \delta > 0\ \exists \alpha > 0\ \exists t_e > 0$: $\left\|\bar{f}(\bar{x}, t)\right\|_\infty \leq \varepsilon \left\|\bar{x}\right\|_1, \forall \left\|\bar{x}\right\|_1 \leq \delta, t \geq t_e$.
For

$$K := K_1 \left\|B\right\|_\infty \tag{3.42}$$

one obtains, analogously to the proof of Theorem 1 (cf. derivations of Eqs. (3.28), (3.29)),

$$\left\|f(x, \hat{x}, t)\right\|_\infty \leq K \left\|\bar{x}\right\|_\infty^{1+\beta_1} + CK_2K_3 \left\|\alpha\hat{D}\right\|_\infty \left\|P\right\|_\infty \left\|\bar{x}\right\|_\infty . \tag{3.43}$$

Hence, a trivial majorant for $f(x, \hat{x}, t)$ is

$$\begin{aligned}\bar{f}(\bar{x}, t) := \Big(&K \left\|\bar{x}\right\|_\infty^{1+\beta_1} + CK_2K_3 \left\|\alpha\hat{D}\right\|_\infty \left\|P\right\|_\infty \left\|\bar{x}\right\|_\infty, \ldots, \\ &K \left\|\bar{x}\right\|_\infty^{1+\beta_1} + CK_2K_3 \left\|\alpha\hat{D}\right\|_\infty \left\|P\right\|_\infty \left\|\bar{x}\right\|_\infty\Big)^T \in \mathbb{R}^{q\sum_{l=1}^{n}(m_l+2)}.\end{aligned} \tag{3.44}$$

Let $\varepsilon > 0$ be arbitrarily chosen. If

$$K + CK_2K_3 \left\|\alpha\hat{D}\right\|_\infty \left\|P\right\|_\infty \leq \varepsilon, \tag{3.45}$$

then *(iii)* is obvious with any $\delta \leq 1$ due to Eq. (3.43).
Otherwise, define

$$\delta := (\varepsilon/(2K))^{1/\beta_1}, \tag{3.46}$$

$$\alpha_{i,i} := \varepsilon / \left(2CK_2K_3 \left\|\hat{D}\right\|_\infty \left\|P\right\|_\infty\right). \tag{3.47}$$

From $\left\|\bar{x}\right\|_\infty \leq \delta$, $\beta_1 > 0$ and K from Eq. (3.42) we can conclude

$$K \left\|\bar{x}\right\|_\infty^{\beta_1} \leq K\delta^{\beta_1}. \tag{3.48}$$

Replacing δ in Eq. (3.48) with that from Eq. (3.46) results in

$$K \left\|\bar{x}\right\|_\infty^{\beta_1} \leq \varepsilon/2. \tag{3.49}$$

Finally, substituting Eqs. (3.47) and (3.49) into Eq. (3.43), we obtain

$$\begin{aligned}\left\|f(x, \hat{x}, t)\right\|_\infty \leq \left\|\bar{f}(\bar{x}, t)\right\|_\infty &\leq K \left\|\bar{x}\right\|_\infty^{1+\beta_1} + \alpha_{i,i}CK_2K_3 \left\|\hat{D}\right\|_\infty \left\|P\right\|_\infty \left\|\bar{x}\right\|_\infty \\ &\leq \varepsilon/2 \left\|\bar{x}\right\|_\infty + \varepsilon/2 \left\|\bar{x}\right\|_\infty = \varepsilon \left\|\bar{x}\right\|_\infty \leq \varepsilon \left\|\bar{x}\right\|_1 .\end{aligned} \tag{3.50}$$

Now using Lemma 1, we conclude the convergence of Eq. (3.13) to zero and consequently the statement of the theorem. □

Remark 2. Theorem 2 shows that swapping the assumption $\beta_2 > 0$ of Theorem 1 for $\beta_2 = 0$ and at the same time restricting the observer gains $\alpha_{i,i}$ by Eq. (3.47), which corresponds to some gain tuning, also ensures convergence. While this explains the role of gain tuning, y is still assumed to satisfy $\|\bar{y}\|_\infty \leq K_2 \|\bar{x}\|_\infty^{1+\beta_1}$ and $\beta_1 > 0$. Using the Direct Lyapunov method, we can state the next theorem which only requires the Lipschitz continuity of y.

In Theorem 3, the Euclidean norm is used for vectors and the spectral norm for matrices indicated by $\|\cdot\|_2$.

Theorem 3. *Let $A = G + E$ be a decomposition of A and $\|E\|_2$ be sufficiently small in the context of Lemma 2 and the diagonal gain matrix α with $\alpha_{i,i} > 0$ be appropriately chosen. Let y and T be Lipschitz continuous, i.e., suppose $\exists K_1, K_2 \in \mathbb{R} : \|\bar{y}\|_2 \leq K_1 \|\bar{x}\|_2, \left\|\bar{T}\right\|_2 \leq K_2 \|\bar{x}\|_2$. If there is a sufficiently small constant K_α such that $\|f(x, \hat{x}, t)\|_2 \leq K_\alpha \|\bar{x}\|_2$, then for every initial observer state $\hat{x}(0)$ the solution $\hat{x}$ of the observer system* (3.2a) *converges asymptotically towards the solution x of the system* (2.61a).

Proof. Recall Eq. (3.12)

$$\dot{\bar{x}} = A\bar{x} + f(x, \hat{x}, t). \tag{3.51}$$

The matrix A was shown to have eigenvalues with negative real parts in Lemma 2 under mild assumptions. Then, by a well-known theorem (e.g. Liao et al. (2007), Th. 2.3.8), the Lyapunov matrix equation

$$SA + A^T S = -I, \tag{3.52}$$

where I is the identity matrix, has a unique positive definite, symmetric solution S. Hence, the function

$$V(\bar{x}, t) = \bar{x}^T S \bar{x} \tag{3.53}$$

can be defined which obeys the items 1 and 2 of Theorem D.3 in the Appendix. Moreover, differentiating V with respect to time, we obtain

$$\frac{dV(\bar{x}, t)}{dt} = \bar{x}^T \left(SA + A^T S\right) \bar{x} + 2\bar{x}^T S f(x, \hat{x}, t). \tag{3.54}$$

For the term on the right hand side of Eq. (3.54) we show the validity of the inequality

$$\bar{x}^T \left(SA + A^T S\right) \bar{x} + 2\bar{x}^T S f(x, \hat{x}, t) \leq -\bar{x}^T \bar{x} + 2\lambda_{\max}(S) K_\alpha \|\bar{x}\|_2^2, \tag{3.55}$$

where $\lambda_{\max}(S)$ is the largest eigenvalue of S and the constant K_α is derived below. First, due to the supposed Lipschitz inequalities for y and T, it follows, analogously to Eqs. (3.28) and (3.29) in the proof of Theorem 1, that

$$\|f(x, \hat{x}, t)\|_2 \leq K_\alpha \|\bar{x}\|_2 \tag{3.56}$$

with

$$K_\alpha := K_1 \|B\|_2 + CK_2K_3 \left\|\alpha\hat{D}\right\|_2 \|P\|_2, \tag{3.57}$$

where the constants K_1, K_2, K_3, C are different from those in Eq. (3.28) since we use the 2-norm. Second, by Eq. (3.52) we obtain

$$\bar{x}^T \left(SA + A^T S\right) \bar{x} = -\bar{x}^T \bar{x}. \tag{3.58}$$

Third, using the Cauchy-Schwarz inequality we obtain

$$\begin{aligned} 2\bar{x}^T S f(x, \hat{x}, t) &\leq 2 \left|\bar{x}^T S f(x, \hat{x}, t)\right| \overset{CS}{\leq} 2 \left\|\bar{x}^T\right\|_2 \|Sf(x, \hat{x}, t)\|_2 \\ &\leq 2 \left\|\bar{x}^T\right\|_2 \|S\|_2 \|f(x, \hat{x}, t)\|_2 \overset{(3.56)}{\leq} 2 \left\|\bar{x}^T\right\|_2 \|S\|_2 K_\alpha \|\bar{x}\|_2 \\ &= 2\lambda_{\max}(S) K_\alpha \|\bar{x}\|_2^2. \end{aligned} \tag{3.59}$$

Finally, Eq. (3.55) follows from Eqs. (3.58) and (3.59).

To fulfill the remaining items 3 and 4 of Theorem D.3 in the Appendix and complete our proof we must provide $\mathcal{K}$-class functions β, γ and δ (cf. Definition D.1, Appendix D). Therefore, we define

$$\beta(\chi) := \lambda_{\min}(S)\chi^2, \tag{3.60a}$$

$$\gamma(\chi) := \lambda_{\max}(S)\chi^2, \tag{3.60b}$$

$$\delta(\chi) := (1 - 2K_\alpha \lambda_{\max}(S))\chi^2, \tag{3.60c}$$

where $\lambda_{\min}(S)$ is the smallest eigenvalue of S. Note that the values $\lambda_{\min}(S), \lambda_{\max}(S)$ and $1 - 2K_\alpha\lambda_{\max}(S)$ are positive as required by the definition of a $\mathcal{K}$-class function; $\lambda_{\min}(S)$ and $\lambda_{\max}(S)$ are positive eigenvalues of S since the matrix S is positive definite and the value $1 - 2K_\alpha\lambda_{\max}(S)$ is positive if the constant K_α satisfies

$$K_\alpha < \frac{1}{2\lambda_{\max}(S)}. \tag{3.61}$$

Moreover, the inequality

$$\lambda_{\min}(S) \leq \frac{\bar{x}^T S \bar{x}}{\bar{x}^T \bar{x}} \leq \lambda_{\max}(S),\ \bar{x} \neq 0 \tag{3.62}$$

holds due to Theorem D.4. Hence, multiplying Eq. (3.62) by $x^T x$, we obtain

$$\beta(\|\bar{x}\|_2) = \lambda_{\min}(S)\bar{x}^T\bar{x} \leq \bar{x}^T S \bar{x} \leq \lambda_{\max}(S)\bar{x}^T\bar{x} = \gamma(\|\bar{x}\|_2). \tag{3.63}$$

This fulfills the item 3 of Theorem D.3. Furthermore, with δ defined by Eq. (3.60c) the item 4 of Theorem D.3 is also fulfilled because of Eqs. (3.54) and (3.55). Now, all assumptions of Theorem D.3 are met and its statement completes our proof. □

Remark 3. Note that according to Eq. (3.57) the infimum of K_α is given by $K_1 \|B\|_2$. This lower bound can be attained if $\alpha \to 0$. Varying α to reduce K_α might be even necessary to fulfill Eq. (3.61) and make the observer converge in the context of the theorem. This is what we mean in the theorem statement by requiring α to be *appropriately chosen*.

As we can see from the proof of this theorem, if at all, the observer convergence is only guaranteed if the infimum $K_1 \|B\|_2$ also fulfills the condition stated by Eq. (3.61). In other words, tuning of α is possible to a certain degree and is necessary to guarantee the observer convergence. Note that the proof does not mean that the observer can't converge for values of α which do not fulfill Eq. (3.61). The reason is that the term $2\bar{x}^T S f(x, \hat{x}, t)$ in Eq. (3.54) can be negative while its upper bound $2\lambda_{\max}(S)K_\alpha \|\bar{x}\|_2^2$ and even the term $(-1 + 2\lambda_{\max}(S)K_\alpha)\|\bar{x}\|_2^2$, which is an upper bound for the right-hand side in Eq. (3.54), is positive (i.e., Theorem 3 provides only *sufficient* conditions for the observer convergence). In the next section, a tuning method combining these findings is presented.

3.3.4 A tuning method for Lang-Gilles observer

The tuning method in this section is based on Theorem 3. We derive the method for a column section, assuming that $L = L_j$, $M = M_j^L$, $V = V_j$, $M_j^V = 0$. A derivation of a method for the entire observer is also possible, however, the required approximations therein and the tuning results would be looser.

If we extract from matrix A in Eq. (2.59) the matrix corresponding to a specific column section A_{sec} (e.g. rectifying section), we obtain

$$A_{sec} = \begin{bmatrix} -\frac{L}{M} & & & \\ \frac{L}{M} & -\frac{L}{M} & & \\ & \ddots & \ddots & \\ & & \frac{L}{M} & -\frac{L}{M} \end{bmatrix} = \frac{L}{M} \begin{bmatrix} -1 & & & \\ 1 & -1 & & \\ & \ddots & \ddots & \\ & & 1 & -1 \end{bmatrix} = \frac{L}{M} \bar{A}_{sec}. \tag{3.64}$$

Thus, Eq. (3.52) becomes

$$S_{sec} A_{sec} + A_{sec}^T S_{sec} = -I, \tag{3.65}$$

or

$$\bar{S}_{sec} \bar{A}_{sec} + \bar{A}_{sec}^T \bar{S}_{sec} = -I, \tag{3.66}$$

where $\bar{S}_{sec}$ is given implicitly as

$$S_{sec} = \frac{M}{L} \bar{S}_{sec}. \tag{3.67}$$

Eq. (3.67) expresses the solution S_{sec} of Eq. (3.65) in terms of the solution $\bar{S}_{sec}$ of Eq. (3.66). As Eq. (3.66) is independent of L/M, its solution $\bar{S}_{sec}$ is a constant matrix. Hence, we can write

$$\lambda_{\max}(S_{sec}) = \|S_{sec}\|_2 = \left\| \frac{M}{L} \bar{S}_{sec} \right\|_2 = \left| \frac{M}{L} \right| \left\| \bar{S}_{sec} \right\|_2 \propto \frac{M}{L}, \tag{3.68}$$

where $\left\| \bar{S}_{sec} \right\|_2$ is a proportionality constant. The sufficient condition for convergence given by Eq. (3.61) can be reformulated as

$$K_\alpha < K^{\text{ub}} = \frac{1}{2\lambda_{\max}(S_{sec})} = \frac{1}{2\left\| \bar{S}_{sec} \right\|_2} \frac{L}{M}, \tag{3.69}$$

i.e., K^{ub} is an upper bound for K_α dependent on L/M.

The spectral norm of the matrix B_{sec}, extracted from the matrix B in Eq. (2.59), corresponding to the column section of our interest is given by

$$\|B_{sec}\|_2 = \left\| \bar{B}_{sec} \right\|_2 \frac{V}{M}, \tag{3.70}$$

where

$$B_{sec} = \begin{bmatrix} -\frac{V}{M} & \frac{V}{M} & & \\ & -\frac{V}{M} & \ddots & \\ & & \ddots & \frac{V}{M} \\ & & & -\frac{V}{M} \end{bmatrix} = \frac{V}{M} \begin{bmatrix} -1 & 1 & & \\ & -1 & \ddots & \\ & & \ddots & 1 \\ & & & -1 \end{bmatrix} = \frac{V}{M} \bar{B}_{sec}. \tag{3.71}$$

Combining Eqs. (3.57), (3.69) and (3.70) , we obtain

$$K_1 \left\| \bar{B}_{sec} \right\|_2 \frac{V}{M} + CK_2K_3 \left\| \alpha \hat{D} \right\|_2 \|P\|_2 < \frac{1}{2\left\| \bar{S}_{sec} \right\|_2} \frac{L}{M}. \tag{3.72}$$

In Eq. (3.72), we need to separate α from the product with $\hat{D}$ within the norm for further derivations. As α can be assumed to be a diagonal matrix with equal positive values on its diagonal (see comments in Section 3.2.3), we can rewrite Eq. (3.72) as follows

$$K_1 \left\| \bar{B}_{sec} \right\|_2 \frac{V}{M} + CK_2K_3\alpha \left\| \hat{D} \right\|_2 \|P\|_2 < \frac{1}{2\left\| \bar{S}_{sec} \right\|_2} \frac{L}{M}, \tag{3.73}$$

where α can be assumed to be a scalar value. Thus, it follows from Eq. (3.73)

$$\alpha < \left(\frac{1}{2\left\| \bar{S}_{sec} \right\|_2} \frac{L}{M} - K_1 \left\| \bar{B}_{sec} \right\|_2 \frac{V}{M} \right) / \left(CK_2K_3 \left\| \hat{D} \right\|_2 \|P\|_2 \right). \tag{3.74}$$

Now we are left with the calculation of the constant C and estimation of constants K_1, K_2, and K_3. The constant C can be obtained from a well known inequality, see Golub and Van Loan (1996),

$$\frac{1}{\sqrt{n}} \|X\|_2 \leq \|X\|_1, \quad X \in \mathbb{R}^{m \times n}, \tag{3.75}$$

which we can use to extend Eq. (3.26) to

$$\frac{1}{\sqrt{m_{sec}q}}\left\|\alpha\hat{D}\delta\hat{y}^*\circ\left(P\,\bar{T}\right)\right\|_2 \overset{(3.75)}{\leq} \left\|\alpha\hat{D}\delta\hat{y}^*\circ\left(P\,\bar{T}\right)\right\|_1 \overset{CS}{\leq} \left\|\alpha\hat{D}\delta\hat{y}^*\right\|_2 \left\|P\,\bar{T}\right\|_2, \tag{3.76}$$

where m_{sec} is the number of trays in the column section and q the number of mixture components. Therefore (cf. derivation of Eq. (3.27), where C is the constant in the equivalence relation between two norms), it follows

$$C = \sqrt{m_{sec}\,q}. \tag{3.77}$$

The constants K_1 and K_2 can be approximated using the truncated Taylor polynomials of y and T for $\bar{x} = 0$ given as

$$\bar{y} \approx \dot{y}^T(\hat{x})\cdot\bar{x}, \quad \bar{T} \approx \dot{T}^T(\hat{x})\cdot\bar{x}. \tag{3.78}$$

Note that in Eq. (3.78), $\hat{x}$ should be the intended steady state of column operation. By the assumption $\exists K_1, K_2 \in \mathbb{R} : \|\bar{y}\|_2 \leq K_1\|\bar{x}\|_2, \left\|\bar{T}\right\|_2 \leq K_2\|\bar{x}\|_2$ of Theorem 3 and using the approximations in Eq. (3.78), it follows

$$K_1 = \|\dot{y}(\hat{x})\|_2, \quad K_2 = \left\|\dot{T}(\hat{x})\right\|_2. \tag{3.79}$$

In the proof of Theorem 3, we assumed $\exists K_3 \in \mathbb{R} : \ \|\delta\hat{y}^*\|_2 \leq K_3$. There are alternative ways to estimate K_3. The simplest way is to take the right-hand side of the well-known relation

$$\|x\|_2 \leq \sqrt{n}\,\|x\|_\infty, \quad x \in \mathbb{R}^n. \tag{3.80}$$

This results in an upper bound for $\|\delta\hat{y}^*\|_2$ in terms of the maximum value of the elements of vector $\delta\hat{y}^*$, denoted as $\overline{\delta y}$, as follows

$$K_3 := \sqrt{m_{seq}\,q}\,\|\delta\hat{y}^*\|_\infty = \overline{\delta y}\,\sqrt{m_{seq}\,q}. \tag{3.81}$$

The norms $\left\|\bar{S}_{sec}\right\|_2, \left\|\hat{D}\right\|_2$, and $\|P\|_2$ cannot be calculated symbolically and should be determined numerically for each particular plant. Finally, inserting Eqs. (3.77), (3.79), (3.81) into Eq. (3.74) results in

$$\alpha < \left(\frac{1}{2\left\|\bar{S}_{sec}\right\|_2}\frac{L}{M} - \|\dot{y}(\hat{x})\|_2\left\|\bar{B}_{sec}\right\|_2\frac{V}{M}\right) / \left(\overline{\delta y}\,m_{sec}\,q\left\|\dot{T}(\hat{x})\right\|_2\left\|\hat{D}\right\|_2\|P\|_2\right). \tag{3.82}$$

To use Eq. (3.82) for tuning, we first could set

$$\alpha_{coarse} := \left(\frac{1}{2\left\|\bar{S}_{sec}\right\|_2}\frac{L}{M} - \|\dot{y}(\hat{x})\|_2\left\|\bar{B}_{sec}\right\|_2\frac{V}{M}\right) / \left(\overline{\delta y}\,m_{sec}\,q\left\|\dot{T}(\hat{x})\right\|_2\left\|\hat{D}\right\|_2\|P\|_2\right) \tag{3.83}$$

and then, find an appropriate α_{fine} with $\alpha_{fine} \leq \alpha_{coarse}$ by improving α_{coarse} through repeated simulations (fine tuning). However, the numerator in Eq. (3.83) is required to be positive and a poor approximate $\|\dot{y}(\hat{x})\|_2$ of K_1 can prevent this. Since Eq. (3.82) and consequently Eq. (3.83) stem from sufficient and not necessary conditions for observer convergence, α_{fine} if at all obtainable from repeated simulations starting with α_{coarse} as given by Eq. (3.83) can turn out to be too small and not allow fast convergence. Therefore, a better alternative to Eq. (3.83) is the formula

$$\alpha_{coarse} := \left(\frac{1}{2 \left\| \bar{S}_{sec} \right\|_2} \frac{L}{M} \right) / \left(\overline{\delta y}\, m_{sec}\, q \left\| \dot{T}(\hat{x}) \right\|_2 \left\| \hat{D} \right\|_2 \|P\|_2 \right), \tag{3.84}$$

which provides a larger initial value for observer tuning. Eq. (3.84) depends obviously on L/M but not on V/M. A simulation example in the next section shows in agreement with Eq. (3.84) that larger values L/M increase and, in contrast to that, V/M has no noticeable effect on the convergence rate of the observer.

3.3.5 An effect of internal flows on the observer convergence time

The simulation study in Section 3.3.5 is based on the plant layout for the separation of an acetone-chloroform-benzene-toluene mixture shown in Fig. 1.1. Further details on the layout and model are given in Appendix C.5.

Simulation scenario

In the selected scenario, the feed flow rate $F2$, see Fig. 1.1, is varied to demonstrate that the internal column flows affect the observer convergence time. The initial state of the plant corresponds to a steady state reached for the feed flow rate $F2 = 10$ mol/s (this is the nominal condition given in Appendix C.5). The observer is started from a steady state corresponding to a feed flow rate $F2 = 10.1$ mol/s, i.e. with 1 %-bias. When the simulation approaches the time $t = 1$ h, the feed flow rate of the observer is decreased from 10.1 mol/s to 10 mol/s and the observer gain parameters α are (i) kept the same, or (ii) set to zero. In either case, the observer starts moving towards the steady state of the plant model and converges finally to this steady state. For non-zero gain parameters α a faster convergence can be expected. This is illustrated best by the convergence of the temperature differences included in the observer feedback. Figures 3.2 – 3.4 depict transients of the temperature differences between the plant and observer models with non-zero and zero gains respectively. The columns in the plant are labeled by C1, C2 and C3, while $\delta T_{j_1} = \hat{T}_{j_1} - T_{j_1}$, $\delta T_{j_2} = \hat{T}_{j_2} - T_{j_2}$ and $\delta T_{j_3} = \hat{T}_{j_3} - T_{j_3}$ denote the differences' transients on trays j_1, j_2, j_3, which relate to the three properly selected temperatures in each column constituting the differences. The simulation utilizes models of column sections

Table 3.1: Mean values of the factors $\frac{L}{2M}$ and $\frac{V}{M}$ in the columns C1, C2, and C3

column	$\varnothing\frac{L}{2M}$	$\varnothing\frac{V}{M}$
C1	0.027	0.03
C2	0.020	0.035
C3	0.012	0.022

with $L = L_j$, $M = M_j^L$, $V = V_j$, and $M_j^V = 0$. The observer gain parameters were tuned by a model-based approach in two steps, namely coarse and fine tuning. The overall tuning target was to make the observer as fast as possible and converge in at most half the time of the plant[2]. The tuning approach is as follows. First, we tuned the gain parameters of each observer column through repeated simulation together with the corresponding plant column apart from the other two columns. Subdividing the plant in individual columns in the first tuning step helps to reduce the number of trial-and-error iterations which are necessary to reach the overall tuning target. To further reduce the effort in the first tuning step, one could implement Eq. (3.84) and make the simulations with individual columns obsolete. Second, the gain parameters from the first part of the tuning routine were fine-tuned by repeated simulations of the plant and observer with all columns (the nominal data and observer tuning parameters are summarized in Appendix C.5). The second tuning step is necessary as the observer including the columns which were tuned separately may be unstable and we need to lower the gain parameters obtained in the first tuning step. As a result, the gain parameters should be close to their upper limits below which the observer convergence is retained. The gain parameters which are close to their upper limits will be necessary to draw conclusions from the simulation results.

Discussion

Deeper insights into the observer's qualitative behavior are delivered by analysis of Theorems 1 – 3 and their proofs. In the following, we discuss general observations with respect to these theorems. If using non-zero gains, the results for columns $C1$ and $C2$ depicted in Fig. 3.2 and 3.3 differ from those for column $C3$ in Fig. 3.4 in the time of convergence. The time which column $C3$ needs to converge ($C3$: $10h$, $10h$, $11h$) is nearly double compared to the former ones ($C1$: $8h$, $5h$, $5h$; $C2$: $6h$, $6h$, $4h$). Do our theorems indicate why this happens? Indeed they do, though there are undoubtedly other effects influencing observer convergence. However, we only focus on those which can be explained by the proved theorems. We remark that the longer convergence time of the observer in column $C3$ is not

[2] The ACBT process needs about 25 hours to reach a steady state, see Figures 3.3 and 3.4.

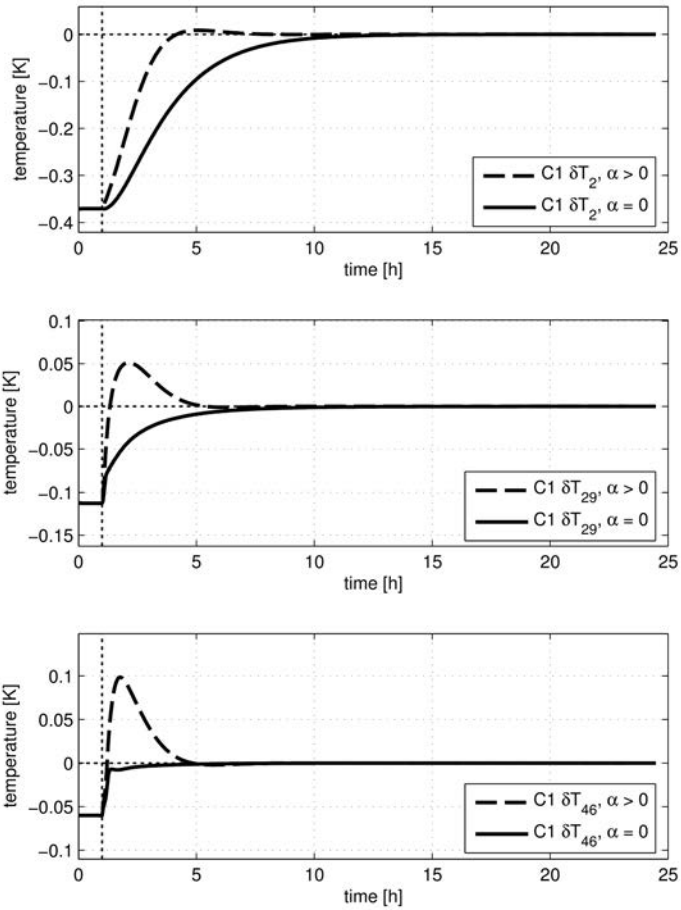

Figure 3.2: Step responses of $\delta T_2, \delta T_{29}$, and δT_{46} in column $C1$ with zero and non-zero gains after a 1%-step in feed flow rate $F2$; dotted vertical lines mark the time point of change in feed flow rate $F2$; dotted horizontal lines mark the zero lines.

caused by its small gains, the gains are rather too large due to the observed overshoots. The observer gain tuning parameters α for column $C2$ seem to be rather too small as there are no overshoots. However, these were the largest parameters obtained by our tuning.

Coming back to our simulation results, Table 3.1 lists mean values for both factors $L/2M$ and V/M in each column. We can use Eq. (3.82) to interpret these factors. As our tuning aimed at the largest possible gain parameters α, there should be a strong

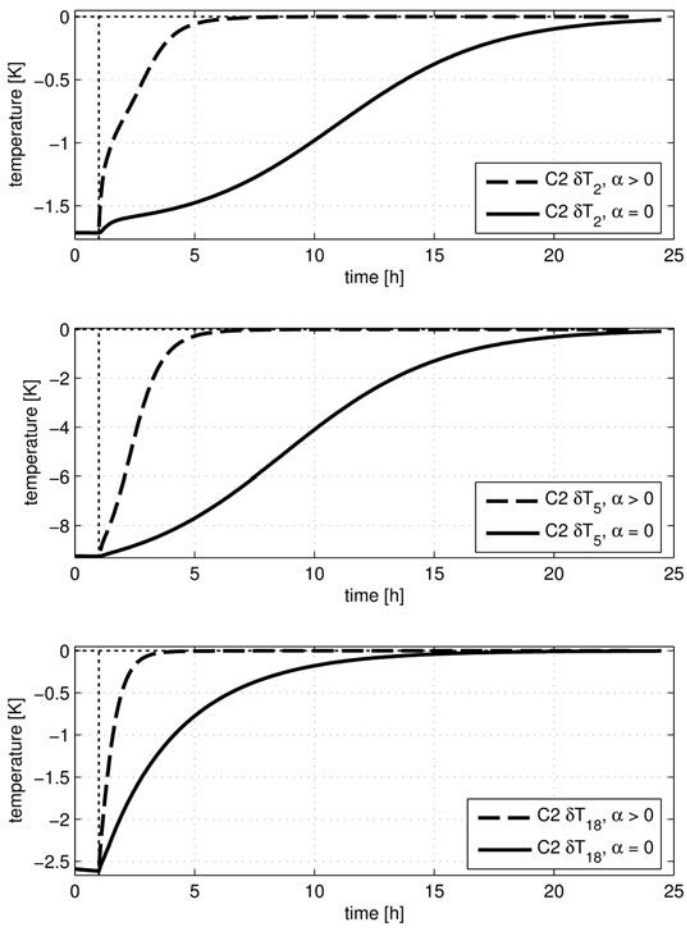

Figure 3.3: Step responses of $\delta T_2, \delta T_5$, and δT_{18} in column $C2$ with zero and non-zero gains after a 1%-step in feed flow rate $F2$; dotted vertical lines mark the time point of change in feed flow rate $F2$; dotted horizontal lines mark the zero lines.

relation between α and their upper bounds as given by Eq. (3.84). A change in the factors $L/2M$ and V/M, which are included in the upper bounds, should also affect the tuning of the gain parameters and consequently the convergence time. Note that a looser tuning would not allow such a conclusion. So, if the factors $L/2M$ and V/M affect somehow the convergence time then, due to Eq. (3.82), $L/2M$ should be inversely proportional and V/M

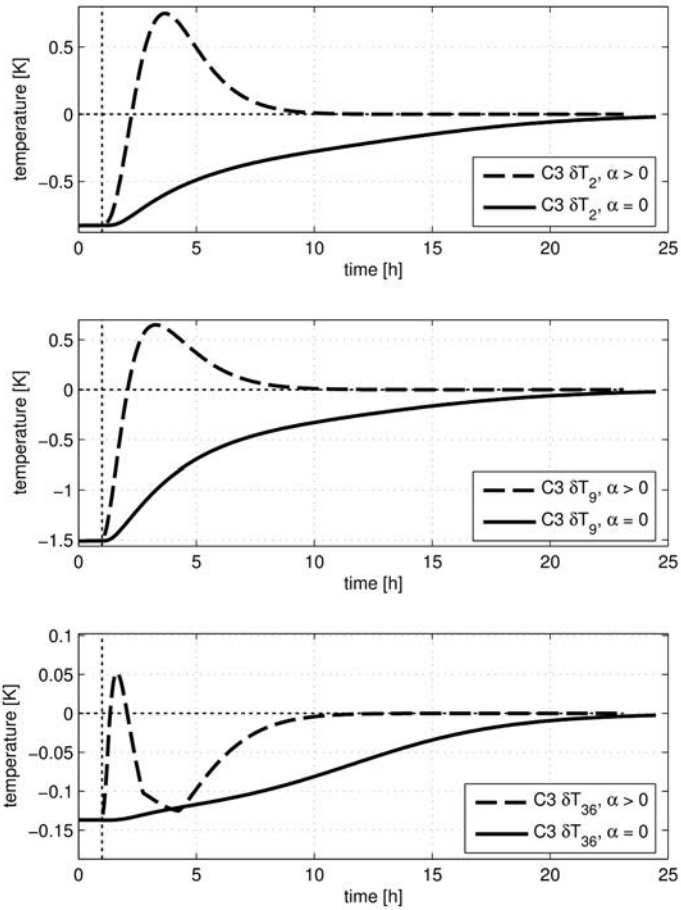

Figure 3.4: Step responses of $\delta T_2, \delta T_9$, and δT_{36} in column $C3$ with zero and non-zero gains after a 1%-step in feed flow rate $F2$; dotted vertical lines mark the time point of change in feed flow rate $F2$; dotted horizontal lines mark the zero lines.

be proportional to the convergence time. However, this argumentation is limited by the fact that in a well-operated column, changes in L may be followed by changes in V and vice versa. Hence, the particular effects of a change in one flow rate might be canceled by the effects of a change in the other flow rate. Consider again Table 3.1. We can observe that the factor $L/2M$ corresponds well with the observed convergence time when looking at the columns $C3$ and $C2$ or $C3$ and $C1$. The table values suggest that the temperature

differences in column $C3$ must converge about half as fast as those in columns $C1$ and $C2$. This conclusion is also confirmed by Figures 3.2 – 3.4. However, the picture is not so clear for columns $C1$ and $C2$ where we would expect $C1$ to converge faster than $C2$. If we then compare the convergence times in Figures 3.2 and 3.3, we cannot distinguish clearly between the columns as the temperature differences in column $C1$ converge within $8h, 5h$, and $5h$ and in column $C2$ within $6h, 6h$, and $4h$. Our suboptimal tuning could be one of the main reasons for this behavior. Some mutually canceling effects as those indicated above for liquid and vapor flow rates L and V are also possible.

In contrast to the factor $L/2M$, the values for V/M in Table 3.1 do not allow to draw a clear conclusion about the convergence times of the temperature differences. These values suggest that the temperature differences in column $C2$ converge slowest, those in column $C1$ somewhat faster, and those in column $C3$ fastest. This not only contradicts the conclusions drawn from the values for factor $L/2M$ in Table 3.1 but also the conclusions drawn from Figures 3.2 – 3.4. This supports our suggestion to consider the factor $L/2M$ and to drop V/M for observer tuning, i.e., to use Eq. (3.84) instead of Eq. (3.83).

3.4 Chapter summary

In this chapter, we examined the conditions for convergence of the Lang-Gilles observer for which no convergence results have been known. Three theorems with different assumptions implying observer convergence were presented and proved.

Theorem 1 claims observer convergence supposing a decomposition of matrix A into a lower triangular matrix G and a strictly upper triangular matrix E as $A = G + E$. Moreover constant observer gain parameters α and strict conditions on vapor compositions and temperatures are assumed. It is essential for the proof that the matrix G has negative eigenvalues under intended operating conditions, where the liquid flows down and the vapor up the distillation column. The matrix E includes the values which can be assigned to the particular flows between the distillation columns in the plant, where matrix E is a zero-matrix if there are no such flows between the columns. Applying Theorem D.1 to the decomposition of matrix A we can show that the eigenvalues of A also will be negative if $\|E\|_2$ is sufficiently small. However, the value $\|E\|_2$ could also be too large. This would not necessarily constrain the validity of the first theorem because we only need to show that the matrix A has negative eigenvalues what could be the case even if $\|E\|_2$ is not sufficiently small in the sense of Theorem D.1. Instead of relying on Theorem D.1, the eigenvalues of A can be calculated numerically for a particular plant. The conditions on

vapor compositions and temperatures expressed as

$$\exists K_1 \in \mathbb{R} : \|\bar{y}\|_\infty \leq K_1 \|\bar{x}\|_\infty^{1+\beta_1}, \tag{3.85}$$

$$\exists K_2 \in \mathbb{R} : \left\|\bar{T}\right\|_\infty \leq K_2 \|\bar{x}\|_\infty^{1+\beta_2}, \tag{3.86}$$

are difficult to fulfill in the practice, see Remark 1. They are required to be able to apply Theorem D.2, though. Their strictness arises from the exponents $1+\beta_1$ and $1+\beta_2$ and, as a consequence, the vapor concentrations and temperatures of the plant and observer must be very close to each other to agree with the strict conditions. The aim of the second theorem is, therefore, to replace one of these conditions with a milder one and reveal a condition which must be made stricter instead.

Theorem 2 substitutes the milder condition

$$\exists K_2 \in \mathbb{R} : \left\|\bar{T}\right\|_\infty \leq K_2 \|\bar{x}\|_\infty \tag{3.87}$$

for the condition given by Eq. (3.86). This new condition is equivalent to the requirement of the Lipschitz continuity for temperature T. It is well known that if T is assumed Lipschitz, then its derivative is bounded and it is differentiable almost everywhere. Thus, from the mathematical point of view, Lipschitz continuity is a very valuable theoretical property of a function. However, having a new milder condition we need to constrain the observer gain parameter α with a bound. This is a surprising result of the second theorem as α and temperature T seem to be independent. Looking closely, we recognize that α and T constitute the observer feedback term and in that sense they are not independent. The restriction on one of these variables can therefore be shifted to the other. On the other hand, if we could use milder conditions for "free", this would mean that the theorem is not stated well and should be improved. The question is also, can we replace both strict conditions given by Eqs. (3.85) and (3.86) to obtain Lipschitz continuity for vapor compositions and temperature and which compromise do we have to make? The answer on this question is given by the third theorem.

Theorem 3 replaces both strict conditions with the following ones

$$\exists K_1 \in \mathbb{R} : \|\bar{y}\|_2 \leq K_1 \|\bar{x}\|_2, \tag{3.88}$$

$$\exists K_2 \in \mathbb{R} : \left\|\bar{T}\right\|_2 \leq K_2 \|\bar{x}\|_2, \tag{3.89}$$

but requires the use of the Lyapunov theory for the proof. Also here we need to show that the matrix A has negative eigenvalues and, in contrast to Theorems 1 and 2, it is sufficient to derive a bound for f which is merely linear in $\|\bar{x}\|_2$. The proof of the theorem delivers a natural bound for the observer gain parameter α given in Eq. (3.74) which serves as a basis for the tuning method derived in Section 3.3.4. As pointed out in Section 3.3.4, this bound is not tight. However, the derived bound allows the identification of the fraction

term L/M as a limiting factor for α. In contrast to the term L/M, the fraction term V/M does not seem to affect α to the extent L/M does (cf. Section 3.3.5).

Future work might focus on completion of the observer theory. Especially the use of Theorem D.1 is a weak point in the proofs of the three convergence theorems. Nevertheless, this does not limit the usage of the theorems as the eigenvalues can be calculated numerically. Note that the three theorems provide only sufficient conditions for observer convergence. However, the necessary conditions are also desirable, and in the best case sufficient and necessary conditions for observer convergence should be identified. If sufficient and necessary conditions for observer convergence can be found, then probably a better bound for α and consequently a more efficient tuning method could be derived. On the other hand, an improvement of the proposed bound in Eq. (3.84), which reduces the number of the simulations required for fine tuning, might be easier and more relevant for the plant observers including several columns from the practical point of view.

4 Efficiency estimation in distillation columns

In the previous chapters, we have focused on distillation modelling and the theory of the Lang-Gilles observer. In the following, we will present two applications of this observer.

In the last chapter, the separation efficiency of a column was assumed to be known and constant. However, in practice, this parameter changes with operating conditions. In this chapter, we discuss available methods for tray efficiency estimation in distillation columns, and contribute in more detail to a new method for on-line efficiency estimation. The Lang-Gilles observer takes on an important role in this method as it allows inclusion of current measurements in the estimation procedure. Furthermore, we show effectiveness of the estimation method in a case study.

Parts of Sections 4.1, 4.2, and 4.3 have been published before (Stuckert et al., 2012). To better integrate published contents into this thesis, some modifications were necessary.

4.1 Introduction

Estimation of tray or column efficiencies in distillation columns is known to be highly relevant for the design and operation of distillation columns. There are several definitions of efficiency in the literature. An overview of the definitions is given by Klemola (1997). One of them, the Murphree tray efficiency, is used very often and was introduced in Section 2.3. It is known that the Murphree tray efficiency depends on the mixture properties, vapor and liquid flow conditions, and device geometry (Fair et al., 1983). Since this dependency is very complex and not completely understood, various correlations exist for the prediction of tray efficiency. According to Klemola (1997), the prediction methods include the following:

(a) Methods based on laboratory measurements: These methods require that the definition of an efficiency is used directly. For example, to obtain the Murphree tray efficiency, the inlet and outlet vapor and the liquid compositions are measured at certain points on a tray. Then, the vapor equilibrium composition is calculated from the liquid composition and the point efficiency is computed from all these values by applying Eq. (2.24). Since the point efficiency is only locally applicable, it is often converted

into the Murphree tray efficiency using Eq. (2.26a) or (2.26b). There are also other known equations to convert the point into the tray efficiency and the choice of the appropriate equation depends on the actual flow directions and mixing conditions in the column (Lewis Jr., 1936). A study applying this method is given by Young and Weber (1972).

(b) Empirical methods: These methods provide rough estimates of the overall column efficiency E_{OC}, defined as the ratio of the number of theoretical trays to the number of actual trays, based on very few variables, e.g., viscosity and relative volatility. One of the first empirical correlations for staged columns was derived by Drickamer and Bradford (1943) and is given as

$$E_{OC} = 17 - 61.1 \ \log \bar{\mu}_F, \tag{4.1}$$

where $\bar{\mu}_F$ is the viscosity evaluated at the arithmetic average between the column top and bottom temperatures. The correlation was derived empirically for data from 54 columns and recommended for use if the relative volatility is higher than 4. Eq. (4.1) was improved by O'Connell (1946). The new correlation also included the relative volatility α and reads as

$$E_{OC} = 0.492 \, (\bar{\mu}_F \alpha)^{-0.245}, \tag{4.2}$$

where α and $\bar{\mu}_F$ are again evaluated at the arithmetic average between the column top and bottom temperatures. Due to its simplicity, acceptable accuracy, and reliability, this correlation became a standard in industry (Kister, 1992).

(c) Theoretical methods which also partly incorporate empirical correlations: These methods are derived on the basis of the two-film theory (Lewis and Whitman, 1924). In particular, Eq. (2.30) in scalar form is taken to predict the overall number of transfer units on tray j, $NTU_{OV,j}$, in terms of the number of vapor phase transfer units $NTU_{V,j}$ and the number of liquid phase transfer units $NTU_{L,j}$. The variables $NTU_{V,j}$ and $NTU_{L,j}$ are estimated using empirical correlations. There is a number of correlations for computation of $NTU_{V,j}$ and $NTU_{L,j}$ (for an overview see Kooijman and Taylor, 2000), many of them are based on the first work on this topic presented by AIChE (1958). There, the correlations for estimating $NTU_{V,j}$ and $NTU_{L,j}$ on sieve trays were given as

$$NTU_{V,j} = \frac{0.776 + 4.57 h_w - 0.238 F_s + 104.8 Q_L / W}{\sqrt{Sc_V}}, \tag{4.3a}$$

$$NTU_{L,j} = 19.7 \sqrt{D^L} \, (0.4 F_s + 0.17) \, t_L, \tag{4.3b}$$

where F_S is the superficial factor, Sc_V is the vapor-phase Schmidt number, h_w is the exit weir height, W is the weir length, Q_L is the volumetric liquid flow rate, D^L is the Fick diffusivity in the liquid phase, and t_L is the liquid-phase residence time (Taylor and Krishna, 1993). The obtained estimate of $NTU_{OV,j}$ can be used to calculate the point efficiency by Eq. (2.29) and then, the Murphree tray efficiency by Eqs. (2.28a) or (2.28b).

(d) Estimation by comparison with similar operating columns: These methods aim at gathering efficiency data from labaratory, pilot, or industrial distillation columns and carrying the results over to other types of columns. The methods have been developed since late 1950s and peaked in the work of Fair et al. (1983), who showed that a scale-up of the Murphree point efficiency from their laboratory Oldershaw columns to industrial columns is possible. In this work, the authors converted the already acquired overall column efficiency of an industrial column to the Murphree point efficiency. They also gathered data from their Oldershaw columns with different tray specifications for several binary mixtures. For these specifications, the Murphree point efficiencies were determined by taking compositions at the top and bottom, computing the required numbers of theoretical trays by using the vapor-liquid equilibrium data, calculating the overall column efficiencies from the numbers of theoretical and actual trays, and finally, approximating the Murphree point efficiencies from the overall column efficiencies. They concluded that under certain conditions the Murphree point efficiencies of the Oldershaw columns were in good agreement with the industrial columns and proposed to augment the methods (a), (b), and (c) for efficiency prediction, already known at that time, with their method.

Note that the methods (a), (b), (c), and (d) have exclusively been used to support column design. The nominal tray efficiencies assumed during column design may deviate significantly from those in actual column operation for various reasons, including load changes and tray fouling. Hence, in a running distillation plant, all efficiency predictions based on these well-known methods are less applicable as also emphasized in the recent work of Sadeghifar (2015). Several indicators are currently available for monitoring of a possible loss of separation efficiency, including laboratory analyses of products or observation of the column temperature profile. Nevertheless, performance tests are vital for reliable estimation of tray efficiencies, although time-consuming tests are often undesirable. The importance of performance testing even for well-performing distillation units is emphasized by Kister (1990) as accurate estimates of tray efficiencies result in operating cost savings. These cost savings might result from

- reduced troubleshooting effort if unit malfunctions appear later,

- improved operating conditions from better insight into the process,
- suggestions for improving the process from exchange of data and ideas with plant designers,
- reliable test data allowing research engineers to improve proprietary procedures in their companies.

Again, considering Klemola's observation (Klemola, 1997) that performance degradation can be caused by small changes in the operating conditions, an estimation scheme should rely on actual plant measurement information and hence on measurement feedback. If tray efficiencies could be estimated by an on-line algorithm then the plant operator could use the information about actual tray efficiencies to run the plant more optimally.

To the best of our knowledge, there are no reports on adaptation of the efficiency-prediction methods outlined above for on-line efficiency estimation. However, there are other estimation techniques which are suitable for on-line estimation. In particular, the state observers introduced in Section 3.1, which have been used successfully for the estimation of compositions in distillation columns (Quintero-Marmol et al., 1991, Diehl et al., 2003, Grüner et al., 2004, Fortuna et al., 2005, Olanrewaju et al., 2012, etc.), could also be adopted for the estimation of tray efficiency when extending the observer state vector by the Murphree tray efficiency. Mejdell and Skogestad (1991a) developed principal-component-regression (PCR) and partial-least-squares (PLS) estimators to calculate distillate and bottom compositions in a column from the temperature measurements on different trays. These are linear estimators, whereas the relation between the compositions and the temperatures is highly nonlinear. Therefore, the authors use weighting functions and logarithmic transformations of compositions and temperatures to reduce model nonlinearity and report that their estimators perform well even for multi-component mixtures, pressure variations, and changes in operating conditions. Since the definition of the Murphree tray efficiency makes use of the vapor compositions, these estimators could presumably be modified to compute the Murphree efficiencies, too.

A different view on the estimation of the Murphree tray efficiencies is to think of it as a method for fault detection. A fault is defined as a departure from an acceptable range of an observed variable or a calculated parameter associated with a process (Himmelblau, 1978). So, fault detection is concerned with the detection of abnormal operating conditions. If we define some appropriate ranges for the Murphree efficiencies we can consider adopting a method for fault detection to detect the situations when the efficiencies leave the favorable ranges (e.g., due to a strong fouling). The importance of the methods aiming at prediction and prevention of operation troubles such as fouling, plugging, and so on, was emphasized by Kano and Ogawa (2010) who refer to the Aboshi plant that could

triple the productivity per plant employee after various methods have been implemented. A comprehensive overview over the diagnostic methods is given by Venkatasubramanian et al. (2003a,b,c). According to Venkatasubramanian et al. (2003c), the diagnostic methods can be subdivided into process history based, qualitative model-based, and quantitative model-based methods. The process history based methods include neural networks, PCR and PLS, and statistical (e.g. Bayes) classifiers (Venkatasubramanian et al., 2003b). These methods are developed using historical process data. Due to the lower modeling effort and simplicity, they have been widely used in the process industry. As Venkatasubramanian et al. (2003b) pointed out, the scope of the industrial applications is often restricted to sensor faults while the parametric faults, for which the model-based approaches might be more suitable since the processes are often strong nonlinear, have been less considered. As in our case the Murphree efficiencies leaving some desired ranges are considered parametric faults we focus on the quantitative model-based methods. So, the qualitative methods are left to the interested reader (Venkatasubramanian et al., 2003a). The quantitative model-based methods utilize, among others, the state observers, Kalman filters and least-squares parameter estimators similar to those presented above but focus more on decoupling the effects of faults from the effects of modeling errors. One of these methods, which is very similar to our method for efficiency estimation introduced later, was derived by Watanabe and Himmelblau (1983a). The authors proposed a two-level strategy for fault detection. The first level consists of estimation of the states of a process by a Luenberger observer. The second level consists of an estimation of the fault parameters by a least-squares procedure. This method was applied to a chemical reactor and shown to be faster than EKF as well as yielding unbiased and precise estimates (Watanabe and Himmelblau, 1983b).

The estimator proposed in Section 4.2 follows that idea to combine the state and parameter estimation into a two-level procedure. To this end, the state observer for distillation columns previously introduced in Section 3.2.2 is adopted and extended. Remember that it only relies on temperature measurements and requires VLE data for implementation. Efficiency estimates are periodically determined by means of nonlinear parameter estimation. The estimator is expected to monitor efficiency losses in columns as a result of fouling or foaming, for example.

The chapter is organized as follows. First, we state the estimation problem for the Murphree efficiency parameters. Then we discuss the new estimation algorithm first proposed by Stuckert et al. (2012). Next, a case study showing the effectiveness of this algorithm is presented. Finally, we discuss the results obtained and give an outlook for possible improvements of the algorithm.

4.2 Sequential state and parameter estimation

We propose to estimate the Murphree efficiency matrix in terms of estimating C_l, which may be defined as C_l^L or C_l^V in one of Eqs. (2.42c), (2.42d), (2.43c), and (2.43d) depending on the use case. The relations (2.42a), (2.42b), (2.43a), and (2.43b) could be in principle adopted, too. In this Chapter, Eq. (2.42d) is used, i.e., we assume that $C_l = C_l^L$. The suggested algorithm for C_l estimation incorporates the Lang-Gilles observer used in two ways: (i) for estimating the current state of the plant on the sampling grid, and (ii) for prediction of the observer temperatures when solving an optimization problem to obtain a new estimate for C_l. C_l is estimated periodically and it replaces the old value. Sirohi et al. (1996) compared a very similar algorithm (the old parameter value is especially not updated) for on-line parameter estimation in a continuous polymerization process with the common approach that extends the state vector in a state observer by adjoining it with the vector of unknown parameters (combined parameter and state estimation). They found that both approaches give identical results, however, the combined parameter and state estimation based on an EKF performed better for noisy measurements. Even so, we prefer not to use a combined parameter and state estimation. The main reason is that the estimation of the efficiency parameters, as proposed below, requires temperature differences measured between certain column trays, and our algorithm provides a natural way to exploit this particular information from the temperature measurements. Otherwise, the same information is difficult to incorporate in a combined parameter and state estimation, and without it, the extended state vector may suffer from low observability.

In the following, we formulate the estimation problems (i) and (ii) in Sections 4.2.1 and 4.2.2. Then, we introduce the entire algorithm in Section 4.2.3.

4.2.1 Estimation of the state variables

In order to estimate the state variables, the Lang-Gilles observer from Section 3.2.2 is used. The observer is initialized at time t_j with the state vector $\hat{x}(t_j)$ (liquid compositions on all trays) and efficiency parameter $\hat{C}_l$. The observer task is formulated as follows.

For a given initial state vector $\hat{x}(t_j)$, the efficiency parameter $\hat{C}_l$, and assuming that at least $q-1$ temperature measurements for the observer correction term $\tilde{T}_{j_1}, \ldots, \tilde{T}_{j_{q-1}}$ on trays $j_1, \ldots, j_{q-1}$ are available, estimate the state variables $\hat{x}(t)$ for $t > t_j$.

Recall that trays $j_1, \ldots, j_{q-1}$ are chosen from the trays located in the regions with high mass transfer. For properly designed columns, these regions should be in the middle parts of the column sections.

4.2.2 Estimation of the Murphree efficiency matrix

Estimation of the Murphree efficiency matrix is based on the observation that $E_{MV} \to 0$ if $C_l \to 0$ and $E_{MV} \to I$ if $C_l \to \infty$, i.e., larger C_l values increase and smaller C_l values reduce the mass transfer rate. The magnitude of the temperature difference $\Delta T_{k,m} = \tilde{T}_k - \tilde{T}_m$ between two trays k and m is also affected by C_l variations. Assume that measurements $\Delta T_{k,m}$ are available on a time interval $[t_{j-1}, t_j]$ for carefully selected trays k and m. Note that the trays k and m should be chosen as close as possible to the column (section) ends if one efficiency factor C_l per column (section) is assumed. Otherwise, the estimated factor $\hat{C}_l$ cannot represent the separation efficiency of that column (section). The trays k and m are in particular not the same as those used in the observer correction term. Using the observer model from Section 3.2.2, the temperature difference $\Delta \hat{T}_{k,m}^{pred}$ can also be predicted on time interval $[t_{j-1}, t_j]$ for any value of C_l by a simulation initialized with the observed state $\hat{x}(t_{j-1})$ at time t_{j-1}. In order to calculate $\hat{C}_l$, the parameter estimation problem, in which the difference between the predicted temperature difference and the corresponding measurements is minimized in the Euclidean norm, is formulated as

$$\min_{\hat{C}_l} \left\| \left\{ \Delta \hat{T}_{k,m}^{pred}(t, \hat{C}_l) - \Delta T_{k,m}(t) : t_{j-1} \leq t \leq t_j \right\} \right\|_2^2, \tag{4.4}$$

where t_j refers to the time at which the estimation is to be triggered. The minimization problem is solved by a trust-region algorithm (function *lsqnonlin*) delivered with Matlab (The MathWorks, Inc., 1994–2016).

4.2.3 Periodic estimation of the Murphree efficiency matrix and observer states

Our method for estimation of the Murphree efficiency matrix E_{MV} consists of a two-level procedure. Our main goal is to estimate C_l which is then used in Eq. (2.42d) to calculate E_{MV}. The observer task in level one of the method is defined in Section 4.2.1, namely, to continuously provide state estimates. The observer is initialized at time t_0 with the state vector $\hat{x}(t_0)$ and the efficiency parameter $\hat{C}_l$. In addition, for $j = 1, \ldots, \infty$ time intervals $[t_{j-1}, t_j]$ between two updates of $\hat{C}_l$ are chosen. For simplicity, the points in time $\{t_i : i = 0, \ldots, \infty\}$ can be distributed equidistantly, however, the interval lengths must be such that the observer can converge before $\hat{C}_l$ is re-estimated. This is done at time t_j when the method is switched from phase one (state estimation) to phase two (parameter estimation) which is defined in Section 4.2.2. Then, a new estimate for C_l, denoted by $\hat{C}_l^{new}$, is calculated using the state estimates $\hat{x}(t_{j-1})$ for initialization at time t_{j-1} and the temperature measurements on interval $[t_{j-1}, t_j]$ to obtain the temperature difference $\Delta T_{k,m}(t)$ between trays k and m for $t \in [t_{j-1}, t_j]$. Once there is an update for $\hat{C}_l$, the level

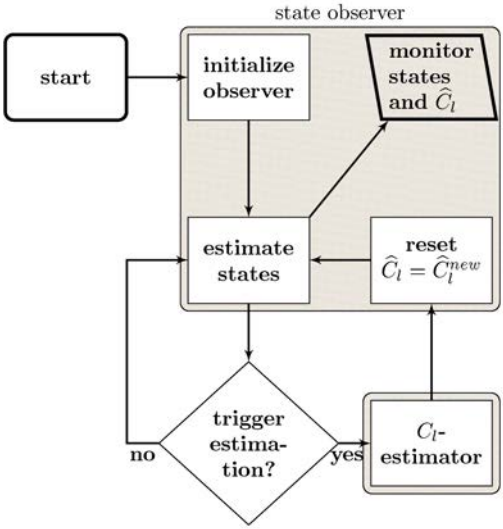

Figure 4.1: Periodic estimation of Murphree efficiency and observer states

two is switched to level one, i.e., $\hat{C}_l^{new}$ replaces the old value in the observer from level one that starts to estimate its state variables on interval $[t_j, t_{j+1}]$. The combined state and parameter estimation algorithm is summarized in Figure 4.1.

The convergence of this algorithm is expected if $\hat{C}_l$ stays identifiable and the states stay observable. Gerdin (2006) presented the criteria for the locally defined identifiability and observability of nonlinear DAEs supporting our expectation. In the next section, convergence of the algorithm is assessed in terms of a simulation study.

4.3 Case study: methanol-ethanol-water separation

The performance of the combined state and parameter estimation scheme is illustrated by means of the separation of pure methanol from a methanol-ethanol-water mixture (parameters for calculation of activity coefficients and vapor pressures are summarized in Appendix C.2). The plant replacement consists of one distillation column modeled by Eqs. (2.53a) – (2.57d) in Section 2.4.2. The applicability of the estimation scheme for plants including several columns was not in the focus of this study and must be examined in the future. Our column consists of a reboiler, a rectifying and stripping section, a feed tray, and a condenser. Every section has 20 trays, the feed flow rate and the molar

compositions are set to 1 kg/s and [0.4 0.2 0.2], the reflux and vapor boil-up rates are set to 1.56 kg/s and 1 kg/s (i.e., perfect reflux and boil-up rate control is assumed), and the column is operated at normal pressure, i.e., Eqs. (2.53d), (2.56e) are neglected and on each tray in the column, normal pressure is assumed. A state observer is implemented for the column as sketched in Section 3.2.2 without plant-model mismatch. The observer gain parameter α is set to 0.02 in the rectifying section and to 0.06 in the stripping section. This state observer is used in both levels of the estimation algorithm, i.e., for the state and C_l estimation. The temperatures used in the observer correction term are measured on trays 17 and 38. For C_l estimation, we use temperatures on trays 4 and 16 of each column section to calculate the temperature differences between them. We denote the efficiency factor in the plant-replacement model and in the observer by C_l^{true} and $\hat{C}_l$, respectively. The superscripts *rec* and *str* are used to refer to quantities in the rectifying or stripping sections. The estimation of C_l is triggered every 30 minutes.

In the following, we consider three different scenarios distinguished by the assumed number of C_l factors (one single factor for both column sections, i.e. $C_l^{true} := C_l^{true,rec} = C_l^{true,str}$, or multiple factors, i.e. $C_l^{true,rec} \neq C_l^{true,str}$) and by their time behavior (constant or drifting). The simulated time is 47 hours.

4.3.1 One single constant C_l^{true}

Both the plant model and the observer have uniform efficiency factors. We choose $C_l^{true} = 0.8$ and start the observer with $\hat{C}_l = 4$. These factors correspond to $E_{MV,j} = I - (I + 0.8 \cdot \Psi_j^{-1})^{-1}$ and $E_{MV,j} = I - (I + 4 \cdot \Psi_j^{-1})^{-1}$ on tray j by Eq. (2.42d). Figures 4.2 and 4.3 show the results which demonstrate that the algorithm converges to C_l^{true} after about 5 estimation cycles, i.e., 5 calls of Eq. (4.4), corresponding to 2.5 hours. However, since C_l^{true} stays constant during the simulation, the work is mainly done by level one of the algorithm, i.e., by the state observer used as a state estimator. This is the simplest situation for the algorithm. A more difficult situation, when a drifting efficiency factor must be estimated, is dealt with in Section 4.3.2.

4.3.2 One single drifting C_l^{true}

Both the plant-replacement model and the observer have uniform efficiency factors. The initial situation is the same as in Section 4.3.1 (see Figure 4.3), but C_l^{true} starts drifting with a rate of 0.2 per 24 h after about 11.5 h, see Figures 4.4 and 4.5. Handling of such drifts is necessary to monitor the occurrence of fouling in the column, for example. This case does not raise any difficulties for the algorithm either. The algorithm is capable to accurately estimate the parameter C_l^{true} even during the parameter drift. Note that the

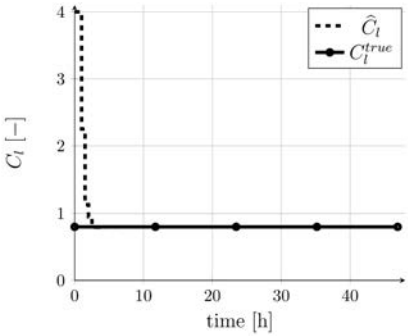

Figure 4.2: One single constant C_l^{true}

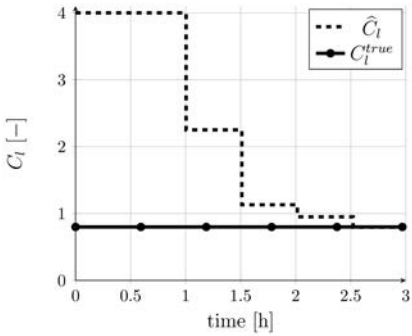

Figure 4.3: One single constant C_l^{true} within the time range $0 \ldots 3$ h

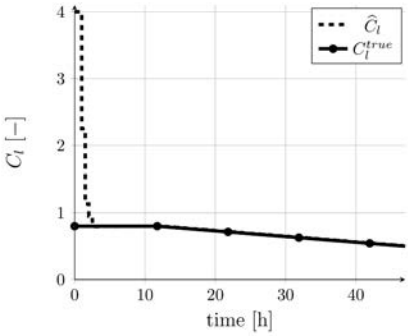

Figure 4.4: One single drifting C_l^{true}

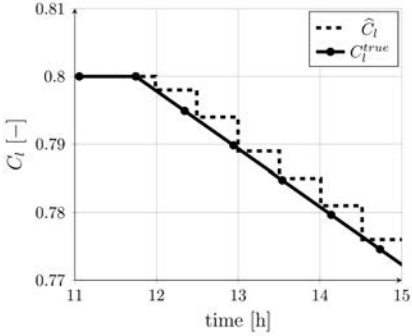

Figure 4.5: One single drifting C_l^{true} within the time range $11 \ldots 15$ h

situation becomes more challenging when one Murphree efficiency per column section is assumed as introduced in Section 4.3.3.

4.3.3 Multiple drifting C_l^{true}

In this more realistic scenario, we drop the assumption of uniform efficiency factors in favor of two factors $C_l^{true,rec}$ and $C_l^{true,str}$, i.e., introduce one uniform factor per section,

and allow their drifting. This choice is in agreement with Eq. (2.38b) affecting Eq. (2.42d) for Murphree tray efficiency in that the stripping factor $\frac{V_j}{L_j}\Psi_j$ being a part of Eq. (2.38b), and consequently our C_l factor taken from Eq. (2.37b), is significantly different in both column sections since the corresponding liquid and vapor flow rates are different. Using the same argument, Kister (1992) suggests assuming different values for Murphree efficiencies even in the subsections of a column section if the efficiencies vary significantly throughout this column section. A simultaneous estimation of both factors is now more difficult than in

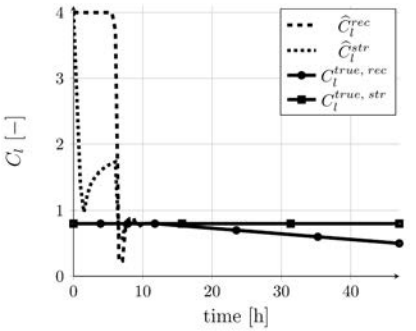

Figure 4.6: Multiple drifting C_l^{true}

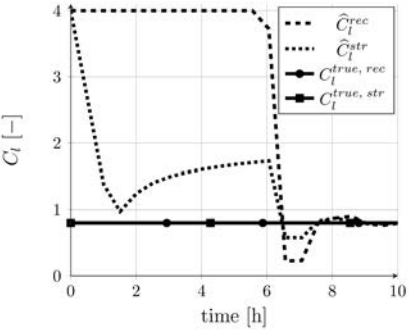

Figure 4.7: Multiple drifting C_l^{true} within the time range $0 \ldots 10$ h

the previous cases due to strong couplings of temperature differences and efficiency factors in both sections. Note that a sequential estimation of both factors, i.e., an estimation of $\hat{C}_l^{rec}$ and $\hat{C}_l^{str}$ alternating by time intervals, is disadvantageous since the parameters interfere more with each other. This interference appears because every change of the efficiency factor in one column section also affects the tray temperatures and consequently the estimation of the efficiency factor in the other column section.

During the first 6 hours, the estimation quality is not satisfactory, see Figures 4.6 and 4.7. While in the stripping section the estimate $\hat{C}_l^{str}$ is improved after two hours, in the rectifying section, $\hat{C}_l^{rec}$ stays unchanged during the first 5 hours or 10 estimation cycles. More accurate estimates for both efficiency factors are obtained not until 20 estimation cycles (10 hours) have been performed. The main reason for the poor estimation quality in the first 6 hours is that in level one of the algorithm the observer has not converged. For example, consider the top and bottom product concentrations shown in Figures 4.8 – 4.11 and for the time range $0 - 10$ h in Figures 4.12 – 4.15. We can observe that all these concentrations, and in particular the ethanol concentration in the reboiler, are

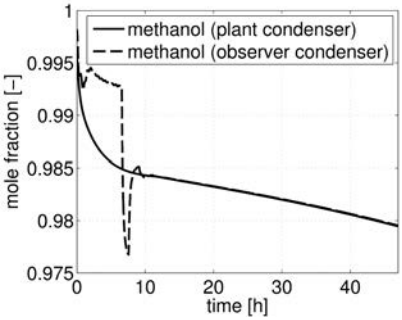

Figure 4.8: Methanol concentration in the condenser

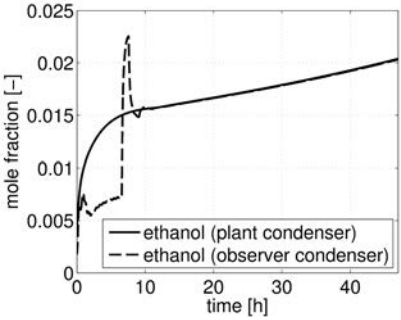

Figure 4.9: Ethanol concentration in the condenser

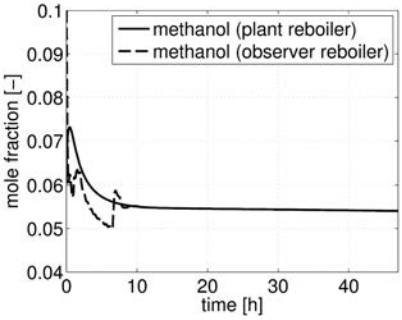

Figure 4.10: Methanol concentration in the reboiler

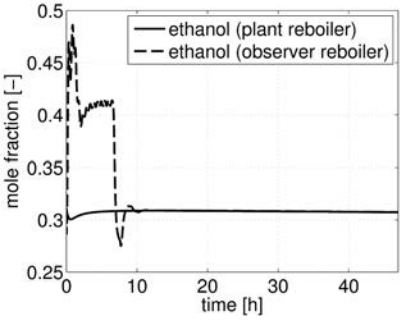

Figure 4.11: Ethanol concentration in the reboiler

estimated poorly. As parameter estimation in level two of the algorithm requires a good initial state estimate, these poor state estimates result in an insufficient quality of the parameter estimates. However, after the observer has converged, good estimates of the efficiency factors are obtained. Figure 4.6 depicts the results thereof.

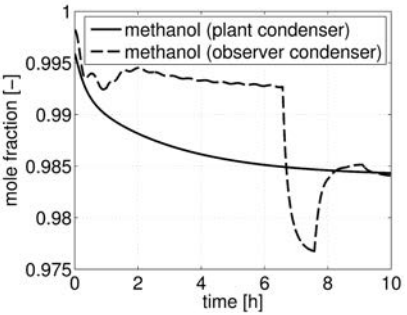

Figure 4.12: Methanol concentration in the condenser within the time range $0 \ldots 10$ h

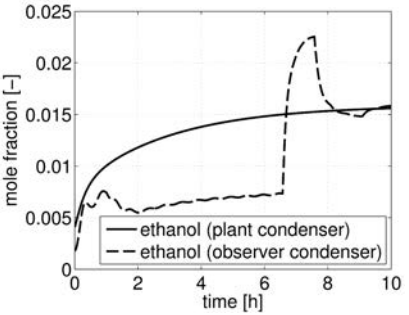

Figure 4.13: Ethanol concentration in the condenser within the time range $0 \ldots 10$ h

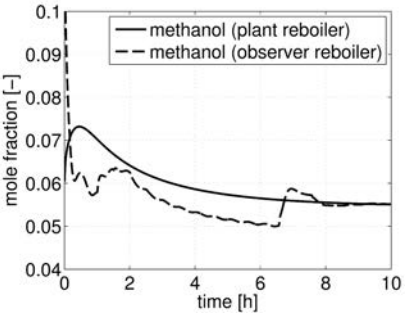

Figure 4.14: Methanol concentration in the reboiler within the time range $0 \ldots 10$ h

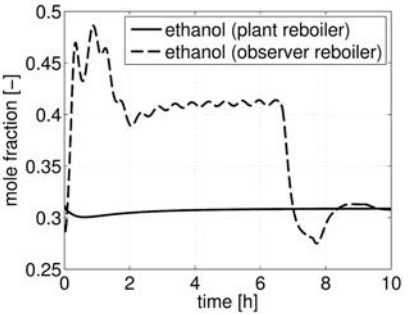

Figure 4.15: Ethanol concentration in the reboiler within the time range $0 \ldots 10$ h

4.4 Chapter summary

To estimate the efficiency factor C_l, defined by Eq. (2.37a) or (2.37b), on-line, we proposed a two-level algorithm which requires only a few temperature measurements apart from VLE data, namely, at least $q-1$ measurements to update the state observer and two measurements per column (section) to estimate the efficiency factor C_l in this column (section). The effectiveness of the estimation is demonstrated by a methanol-ethanol-water separation. Constant or drifting, a single efficiency factor for the whole column or specific efficiency factors for different column sections have been assumed. In all cases, the efficiency factors could be estimated with good quality by the proposed algorithm.

There are several points which may be addressed in further studies. First, as the case study takes as a basis no plant-model mismatch except for a mismatch in C_l, it should be verified how a plant-model mismatch would reduce the quality of efficiency estimates. This mismatch can be introduced through inaccuracy in parameters, e.g., thermodynamic parameters or column pressures (if assumed to be constant). This type of mismatch may be linked to the errors in VLE data which the parameters were derived from. According to Kister (2002), poor VLE data is one of the major sources for simulation problems. Inaccuracies in energy balances should also be investigated. Tray energy balances are particularly linked to the vapor flow rates in a column. For example, neglecting changes in tray energy balances caused by changing ambient conditions could introduce a significant plant-model mismatch due to the different vapor flow rates in the actual plant and its model. In this chapter, we did not use energy balances on column trays and the vapor flow rates throughout the column are determined by the energy input to the reboiler (CMO condition). So, one can introduce a plant-model mismatch for the vapor flow rate from the reboiler. The assumptions regarding tray geometry, tray hydraulics, and vapor flow rates affect the liquid flow rates in a column. Some relevant correlations for the liquid and vapor flow rates are summarized by Gani et al. (1986), where the interested reader can find further references. If the reflux flow rate sets the tray liquid flow rates as in the model used in this chapter, a plant-model mismatch for the reflux flow rate can be introduced. The case when the feed flow rate and composition are not exactly known can be handled by introducing a plant-model mismatch for these parameters.

Another point, outlined in the introduction to this chapter, is whether a PCR or PLS estimator similar to that developed by Mejdell and Skogestad (1991a) can be adopted for the estimation of the C_l parameter. A PCR/PLS estimator would have an advantage over the estimation with a state observer in that it is simpler to use. However, as PCR/PLS estimators are data-driven, it would probably be necessary to develop several estimators to cope with different operating conditions. In addition, it could be difficult to obtain all historical process data for the unfavorable operating conditions.

From the theoretical point of view, the convergence conditions and convergence rate of the proposed algorithm could be examined more thoroughly. One promising approach might be to separate this analysis into three steps. In a first step, the sufficient conditions for observer convergence need to be established. These were already given in Chapter 3. Next, the influence of the parameter estimation on convergence is studied. In a third step, the previous steps are combined and the convergence of the entire algorithm is shown.

Finally, more complicated plants including several distillation columns should be studied as such plants were not in the scope of this work. In addition, it is desirable to understand whether the simplifications of the efficiency model resulting in Eqs. (2.38a) and (2.38b) prove themselves in practice.

5 Application of the Lang-Gilles observer in distillation control

In Chapter 4, the Lang-Gilles observer was used to estimate tray compositions and Murphree efficiencies what could be used as a method for fault detection. In this chapter, we study another application of the Lang-Gilles observer in model-predictive control.

5.1 Introduction

Distillation control is an intensively studied field in process control. The current state of the art includes many different methods such as PID control, linear and nonlinear model-predictive control (MPC) or more generally model-based control (Skogestad, 1997, Kano and Ogawa, 2010). PID regulators play a dominant role in process control as they are easy to understand, require no time-consuming model development (except for simulation purposes), and make it possible to locally solve control problems in complex plants. In modern chemical plants, thousands of PID regulators may be installed while more advanced controllers such as MPC are used much less frequently (Kano and Ogawa, 2010). The main advantage of MPC is that it allows to efficiently maintain the operating constraints and that it can handle highly nonlinear interactions of process variables through the underlying model. The idea behind MPC is to turn a control into a finite-horizon optimization problem. At any time sampling point, this optimization problem is solved to obtain a sequence of future control actions. The first element of this sequence is then used to take the next control action and the remaining elements are dropped. At the following sampling time instants, the cycle consisting of stating and solving the optimization problem, taking a control action, and carrying on with the next time point is repeated on a moving time horizon. Besides PID and MPC, new or enhanced control methods appear, such as distributed model-predictive control (DMPC) (Scattolini, 2009). The term *distributed* refers to the fact that several local models instead of a single one for the entire plant are developed. The control problem with a common control target is then solved by coordinating several MPCs, where each of them has its own local model.

In model-based controllers, state observers are used for calculating state predictions

over a time horizon (e.g. in MPC) or estimating some state variables for state feedback. The quality of such predictions is essential to the performance of model-based controllers. Hence, various authors studied distillation state observers not only in a theoretical manner but also in the framework of model-based control. For instance, Wozny et al. (1989) design a Luenberger state observer for estimation of the vapor flow rate and the position of the temperature front in a distillation column from a few temperature measurements. Furthermore, the authors compare the performance of a linear state controller with that of a conventional PID controller. Quintero-Marmol et al. (1991) design two extended Luenberger observers (full- and reduced-order) for composition estimation in order to control batch distillation of a ternary mixture. The authors also give a thorough comparison of their observers. They report that their full-order observer was consistently better than the reduced-order observer and suggest using the latter if the computational load is an issue. Minimizing computational load and reducing modeling complexity were important for the work of other authors, too. Therefore, Brizuela et al. (1996) develop a model-predictive control based on neural nets and compare its performance with the performance of PI controllers. Shin et al. (2000b) and Roffel et al. (2003) use profile position observers to deliver estimates of profile positions. The former authors use their observer within the generic model controller while Roffel et al. (2003) provide a comparison of the profile position observer and partial least-squares estimators used together with a composition-temperature cascade controller.

To the best of our knowledge, there are no studies on the performance of the Lang-Gilles observer in a model-based control framework. Moreover, Lang and Gilles (1990) give an example for a plant with only one distillation column and so far, no results on design of the Lang-Gilles observer for distillation trains have been published. The observer is reported to be robust towards modeling errors, wrong parameters or uncertain inputs. However, the authors only mention an example where the mass transfer coefficient in the observer feedback term is not properly chosen and do not provide a larger study confirming their claim. To shed light on these issues, we will examine the observer for the ACBT process using a model-based controller and introducing a plant-model mismatch in the energy balances.

We proceed as follows. First of all, plantwide control is introduced which covers the concepts of control design for entire plants. In the context of plantwide control, we present a typical control scheme. Next, we formulate the control problem and describe the general control structure for our case study. The dynamics of the used process models were discussed in Section 2.5.1. According to this discussion, the linearized controller/observer model is capable of capturing the dominant nonlinear dynamics at the nominal state and may be used to reduce controller complexity and consequently computational load and

possible numerical obstacles. The regulatory control for the plant replacement and controller/observer was developed in Section 2.5.2 with respect to suggestions taken from Kister (1990). We will develop a second DMPC layer supervising the regulatory control. In order to find non-interacting sub-models for use in the model-predictive controller, we will study interactions between the plant-replacement sub-models using the relative gain array (RGA). Based on the conclusions resulting from the RGA study, the model of the plant including its decentralized base control system is decomposed into sub-models which are included in the supervisory DMPC. In particular, the sensitivity-driven distributed model-predictive control (S-DMPC) scheme is considered (Scheu and Marquardt, 2011). In this scheme, the distributed controllers cooperate in order to find the optimal solution for the full process. For this purpose, the controllers share sensitivity-based information about the local cost functions such that each controller can take the control objectives of other controllers into account. Finally, we present our large-scale simulation study, where we highlight the achievable control quality with the regulatory and supervisory controls, and draw conclusions at the end of the chapter.

5.2 Plantwide control

Many plantwide control schemes have been proposed over time and one can distinguish between the mathematical approach, where the main concepts are structural state controllability, observability and accessibility, and the process-oriented approach, where heuristic rules are developed based on experience and process understanding. A good review of both approaches is included in the paper of Larsson and Skogestad (2000).

The most comprehensive works on plantwide control are those of Larsson and Skogestad (2000) and Skogestad (2004), where the authors present a set of plantwide control guidelines that are based on the ideas of Foss (1973), Morari (1982), and Skogestad and Postlethwaite (1996). According to them, plantwide control is another term for control structure design for entire plants which requires selection of (a) manipulated variables, (b) controlled variables, (c) additional measurements, e.g., for plant stabilization, (d) control configuration, and (e) controller type. After completion of these five tasks, the control system is typically divided into control layers separated by time scale, where the upper layers calculate the setpoints (SP) of the lower layers, see Figure 5.1 (cf. Skogestad, 2004). Time-scale separation means that the scheduling layer runs once per week, the site-wide optimization is performed once per day and so forth. In this control scheme, the plant is assumed to run continuously, while the regulatory and supervisory control loops receive measurements from the plant at some suitable sampling rate.

Time-scale separation could be avoided by designing a single controller that stabilizes

the plant while the manipulated variables are calculated by on-line optimization. Due to the high modeling and tuning efforts, the development of such a controller would often be economically inefficient. That is to say that there are chemical plants controlled effectively by hierarchically designed control systems for which no modeling effort was necessary. So, one always has to take into account the cost of modeling a single controller and trade it off against the cost of developing a hierarchical control system. In practice, the latter control system would often be favored (Skogestad, 2004).

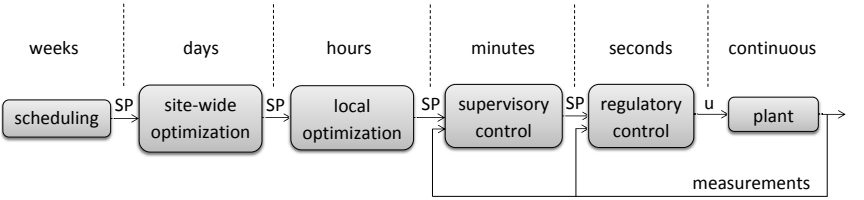

Figure 5.1: A typical hierarchically structured plantwide control scheme divided into different layers that can be associated with different time scales

5.3 Control design

In this section, we formulate the control problem for the ACBT process in the setting of plantwide control. After that we will recall the regulatory layer and discuss the design of the supervisory layer. The remaining control layers including scheduling, site-wide and local optimizations are not in the scope of this work.

5.3.1 Control problem statement

First we recall the layout of the ACBT process in Figure 1.1. There, an acetone-chloroform-benzene-toluene mixture is separated by a distillation train consisting of three distillation columns. The regulatory control layer for this process was already introduced in Section 2.5.2. The control objective for the complete plant is as follows: when disturbances in the feed appear (changes in composition or flow rate), maintain the product concentrations (acetone, chloroform, benzene, toluene) as close as possible to the given setpoints. Achieve this by regulating (i) temperatures on two trays (yet to be chosen) of the first and third distillation column, (ii) one temperature in the second column, and (iii) the flow rate of the recycle loop.

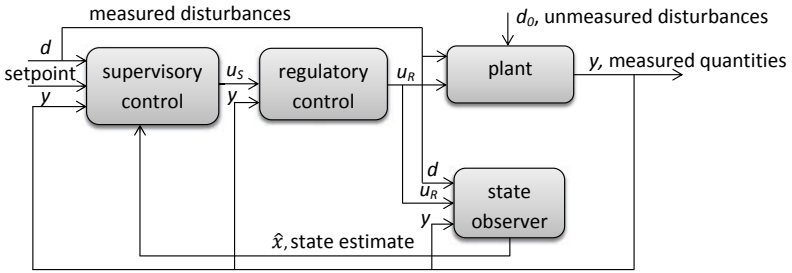

Figure 5.2: The control system structure

In the second distillation column, only a temperature in the stripping section is regulated since temperature measurements in the rectifying section are not suitable for control due to a different type of condenser which requires a different control scheme.

In our case study, we will assume that no on-line measurements of product qualities are available as it is often the case for distillation columns. A basic control scheme without such information can hardly achieve the above control objective for the complete plant properly. Our control problem therefore consists in utilizing the regulatory layer, which is able to stabilize the plant for varying flow rate or composition of the feed, and in designing a supervisory layer (a model-based controller) that obtains the state observer predictions of the tray concentrations and especially product qualities to keep the latter close to the setpoints. In particular, we want to investigate for our plant the advantages of a two-layer over a single-layer control architecture for the distillation plant in Figure 1.1.

The selected two-layer control structure is depicted in Figure 5.2 (cf. Figure 5.1). The supervisory controller, which may be realized by either an MPC, or a DMPC, sets the setpoints of some certain regulatory controllers which manipulate the plant. The state observer passes the estimate of the current plant state on to the supervisory controller. The supervisory controller, as well as the regulatory controllers and state observer, receives the measurements from the plant. The measured disturbances are taken into consideration in the supervisory controller and state observer while the unmeasured disturbances act directly on the plant.

5.3.2 Design of regulatory and supervisory controllers

The regulatory control layer and its partitioning

The regulatory control layer for the ACBT process was already introduced in Section 2.5.2. For better readability, the regulatory controllers whose setpoints are manipulated by the supervisory controller are tagged as rn, where n is the controller number, and the controllers in Figure 1.1 are renumbered to those in Figure 5.3 as tabulated in Table 5.1.

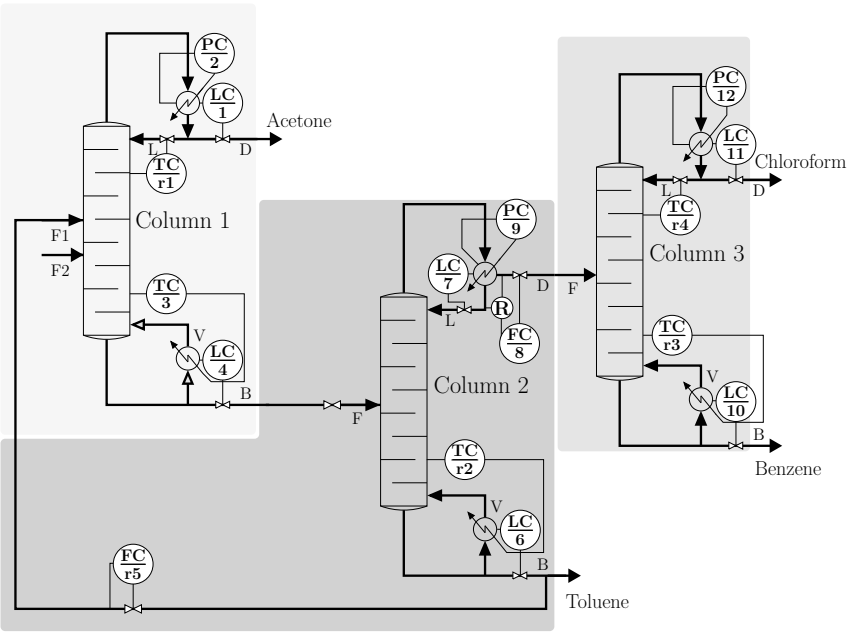

Figure 5.3: The ACBT process including regulatory control layer and its partitioning

The choice of rn regulators is explained in the next section.

Input-output pairings on the supervisory control layer

According to Wang et al. (2008), decentralized control remains dominant in industry applications because of its simplicity in design and ease of implementation, tuning, and low cost maintenance. Decentralized controllers have few parameters reducing tuning time and

Table 5.1: Renumbering of regulatory controllers

Figure 1.1	Figure 5.3	Figure 1.1	Figure 5.3
1	1	10	7
2	2	11	8
3	r1	12	9
4	3	13	10
5	4	14	r3
7	r5	15	r4
8	6	16	11
9	r2	17	12

a decentralized structure allows restructuring the control system by bringing subsystems in and out of service individually, which allows the system to handle changing control objectives during different operating conditions. However, a possible disadvantage, when using this control structure, is the degraded closed-loop performance caused by interactions among loops stemming from nonzero off-diagonal elements in the transfer function matrix of the multi-variable system. Therefore, the main task in the design of decentralized control systems is to determine loop pairings with negligible cross interactions among individual loops, i.e., choosing potential pairs of manipulated and controlled variables which interact most with each other while other variables are less affected by the chosen ones. To find appropriate loop pairings Bristol (1966) suggested the so-called relative gain array (RGA) matrix with entries defined as the ratios of two gains representing first, the process gain in an isolated control loop and, second, the process gain in the same control loop when all other control loops are closed. The RGA matrix is calculated using the steady-state gain matrix $G(0)$ as

$$RGA = G(0) \circ G(0)^{-T}, \tag{5.1}$$

where $\circ$ is the Hadamard product. The choice of loop pairings based on RGA suggests that input-output pairings associated with RGA elements close to 1 should be preferred. Negative or large RGA elements are disadvantageous as they correspond to loops which may be nominally stable, but which become unstable if saturation occurs (Goodwin et al., 2005).

In our case study, there are three models involved, the rigorous plant-replacement model, the controller and the observer models, the latter of which are the same (except for feedback term in the observer). A DMPC approach suggests dividing the plant model into non-interacting sub-models and developing an MPC for each sub-model. To find non-interacting

sub-models, we will use the RGA analysis. In practice, it is only possible to compute the RGA of the controller model, but not of the plant-replacement model. Hence, we restrict the RGA calculation to the controller model only. In our case study, we want to separate the mixture into almost pure components. Hence, we restrict ourselves to the RGA calculation for the transfer function, mapping the outputs of the controllers $r1$, $r2$, $r3$, $r4$, and $r5$ to the measurements they receive, see Figure 5.3. We justify our choice by the educated guess that with these five controllers, each of the components purities can be affected appropriately. For the nominal operating condition adopted from Kraemer et al. (2009) (see Appendix C.6, Table C.8), the following steady-state RGA matrix is obtained:

$$RGA = \begin{pmatrix} 0.99 & 0.01 & -0.00 & 0.00 & 0.00 \\ 0.01 & 0.99 & -0.00 & 0.00 & 0.00 \\ 0.00 & 0.00 & 11.15 & -10.15 & 0.00 \\ -0.00 & -0.00 & -10.15 & 11.15 & 0.00 \\ 0.00 & 0.00 & 0.00 & 0.00 & 1.00 \end{pmatrix}. \tag{5.2}$$

This RGA matrix has positive diagonal values which are close to 1 except for two values. Furthermore, there are couplings between the controllers (i) $r1$, $r2$ (see first two columns of the RGA matrix), and (ii) $r3$, $r4$ (see the third and forth columns of the RGA matrix), whereas the controller $r5$ is completely decoupled from the influence of all the former (see the fifth column of the RGA matrix). As there is only a minor coupling between controllers $r1$ and $r2$, we adopt the partitioning of the model into three sub-models disregarding this coupling. The first model includes the controller $r1$, the second model includes controllers $r2$ and $r5$, and the third model includes the coupled controllers $r3$, $r4$. Note that the controllers $r2$ and $r5$ are included in one and not in separate models due to a strong interaction between the setpoint of $r2$ and the output of $r5$ which occurred during the normal operation. This still agrees with the calculated steady-state RGA which cannot reliably predict input-output interactions at non-steady states by definition (Jensen et al., 1986). The strong interaction between controllers $r2$ and $r5$ can also be explained by analyzing the cause-effect chain from $r2$ to $r5$ which is as follows. $r2$ controls a temperature in the stripping section near the reboiler of column $C2$ by manipulating the vapor boil-up rate. The reboiler level is set by the controller 6 which manipulates the flow rate of the bottom product in column $C2$. The bottom product is also partly recycled and the recycled flow rate is set by the controller $r5$. It is clear that the controller $r5$ cannot arbitrarily set the recycle flow rate as it conflicts with the controller 6.

Our final model partitioning is highlighted in Figure 5.3 by differently colored areas. The setpoints of controllers $r1 - r5$ constitute the set of variables to be manipulated by the supervisory control layer.

Supervisory control layer

On the supervisory control layer, the DMPC algorithm of Scheu and Marquardt (2011) is implemented. In order to minimize the on-line computational effort, the regulator control problem is transferred off-line into a standard QP formulation. The plant model that is considered here is given by Eqs. (2.61a) and (2.61b). For further usage as a state space model in the DMPC framework, it is convenient to rename the variables in these equations and add the output equation as follows. The matrices A, B, C are renamed into A_1, A_2, B and the vectors y and z into v and u. Then, the renamed equations read as

$$\dot{x} = A_1\, x + A_2\, v + B\, u, \quad x(0) = x^{init}, \tag{5.3a}$$

$$v = f(x, v, p, T, C_l), \tag{5.3b}$$

$$y = C\, x + D\, u, \tag{5.3c}$$

where Eq. (5.3c) is the output equation, C is the output matrix, and D is the feedthrough matrix. For the ACBT process, y is the vector of product concentrations acetone, chloroform, benzene, and toluene. The state space Eqs. (5.3a) – (5.3c) can be further generalized by introducing disturbances in state and output equations as

$$\dot{x} = A_1\, x + A_2\, v + B\, u + B^d\, d, \quad x(0) = x^{init}, \tag{5.4a}$$

$$v = f(x, v, p, T, C_l), \tag{5.4b}$$

$$y = C\, x + D\, u + D^d\, d, \tag{5.4c}$$

where B^d and D^d are disturbance matrices and d is the disturbance vector. Linearizing Eqs. (5.4a) – (5.4c) at a nominal state x^{nom}, we obtain a linearized continuous-time state space model which, in contrast to the one in Scheu and Marquardt (2011), explicitly incorporates disturbances, i.e.,

$$\Delta\dot{x} = A_c\, \Delta x + B_c\, \Delta u + B_c^d\, \Delta d, \quad \Delta x(0) = 0, \tag{5.5a}$$

$$\Delta y = C_c\, \Delta x + D_c\, \Delta u + D_c^d\, \Delta d, \tag{5.5b}$$

where the new variables

$$\Delta x = x - x^{nom}, \tag{5.6a}$$

$$\Delta u = u - u^{nom}, \tag{5.6b}$$

$$\Delta d = d - d^{nom}, \tag{5.6c}$$

$$\Delta y = y - y^{nom} = y - C_c\, x^{nom} - D_c\, u^{nom} - D_c^d\, d^{nom} \tag{5.6d}$$

indicate the deviations of the differential state, the input vector, the disturbance vector, and the output vector from the nominal values indicated by index *nom*. A_c, B_c, B_c^d, C_c,

D_c, and D_c^d are the continuous-time system matrices defined as

$$A_c = A_1 - A_2 \left(\frac{\partial F}{\partial v}\right)\Big|^{-1}_{x^{nom},p^{nom},T^{nom},C_l^{nom}} \frac{\partial F}{\partial x}\Big|_{x^{nom},p^{nom},T^{nom},C_l^{nom}}, \tag{5.7a}$$

$$B_c = B, \tag{5.7b}$$

$$B_c^d = B^d, \tag{5.7c}$$

$$C_c = C, \tag{5.7d}$$

$$D_c = D, \tag{5.7e}$$

$$D_c^d = D^d. \tag{5.7f}$$

Note that the partial derivative factors in Eq. (5.7a) are obtained by the implicit function Theorem D.5 from Appendix D applied to Eq. (5.4b). In order to do so, Eq. (5.4b) needs to be reformulated as

$$F(x, v) := v - f(x, v, p, T, C_l) = 0, \tag{5.8}$$

where the pressure p, the temperature T, and the separation efficiency factor C_l are fixed to the values corresponding to the nominal state x^{nom}. Then, the partial derivative of the vapor-equilibrium is given by

$$\frac{\partial v}{\partial x} = -\left(\frac{\partial F}{\partial v}\right)^{-1} \frac{\partial F}{\partial x}, \tag{5.9}$$

and is consequently used in Eq. (5.7a).

Then, the continuous-time system (5.5) is discretized using an equidistant time sampling $t_0, t_1, \ldots$, i.e., $\Delta t = t_k - t_{k-1}$ for $k \in \mathbb{N}$. Hence, the system (5.5) is transformed to the discrete-time system

$$\Delta x_{k+1} = A_d \, \Delta x_k + B_d \, \Delta u_k + B_d^d \, \Delta d_k, \quad \Delta x_0 = 0, \tag{5.10a}$$

$$\Delta y_k = C_d \, \Delta x_k + D_d \, \Delta u_k + D_d^d \, \Delta d_k, \tag{5.10b}$$

where $\Delta x_k = \Delta x(t_k)$ is the deviation of the initial state at sample k from the nominal value and the input and disturbance vectors are assumed constant between the sampling instants, i.e.,

$$\Delta u(t) = \Delta u_k = \Delta u(t_k), \quad t_k \le t < t_{k+1}, \tag{5.11a}$$

$$\Delta d(t) = \Delta d_k = \Delta d(t_k), \quad t_k \le t < t_{k+1}. \tag{5.11b}$$

The discrete matrices $A_d, B_d, B_d^d, C_d, D_d, D_d^d$, indicated by index d, are defined as

$$A_d = \exp(A_c\,\Delta t), \tag{5.12a}$$

$$B_d = \int_0^{\Delta t} \exp(A_c\,\tau)\; B_c\; d\tau, \tag{5.12b}$$

$$B_d^d = \int_0^{\Delta t} \exp(A_c\,\tau)\; B_c^d\; d\tau, \tag{5.12c}$$

$$C_d = C_c, \tag{5.12d}$$

$$D_d = D_c, \tag{5.12e}$$

$$D_d^d = D_c^d. \tag{5.12f}$$

Notice that the time-discrete system (5.10) gives the exact value of the state vector at the sampling instants (e.g. Åström and Wittenmark, 2011).

The discrete system (5.10) is used to derive the prediction model

$$\Delta\mathbf{y}_k = \mathcal{T}_x\,\Delta x_k + \mathcal{T}_d\,\Delta\mathbf{d}_k + \mathcal{T}_u\,\Delta\mathbf{u}_k, \tag{5.13}$$

where $\Delta\mathbf{y}_k$ is the predicted output trajectory which contains n_{pr} predicted samples of output

$$\Delta\mathbf{y}_k = \left(\Delta y_k^T,\, \Delta y_{k+1}^T,\, \ldots,\, \Delta y_{k+n_{\mathrm{pr}}-1}^T\right)^T, \tag{5.14}$$

$\Delta\mathbf{d}_k$ is the predicted disturbance trajectory which contains n_{pr} predicted samples of disturbance

$$\Delta\mathbf{d}_k = \left(\Delta d_k^T,\, \Delta d_{k+1}^T,\, \ldots,\, \Delta d_{k+n_{\mathrm{pr}}-1}^T\right)^T, \tag{5.15}$$

and $\Delta\mathbf{u}_k$ is the control trajectory which contains n_{co} control samples

$$\Delta\mathbf{u}_k = \left(\Delta u_k^T,\, \Delta u_{k+1}^T,\, \ldots,\, \Delta u_{k+n_{\mathrm{co}}-1}^T\right)^T. \tag{5.16}$$

The matrices $\mathcal{T}_x$, $\mathcal{T}_d$, and $\mathcal{T}_u$ depend on the system matrices as follows

$$\mathcal{T}_x = \begin{pmatrix} C_d \\ C_d A_d \\ \vdots \\ C_d A_d^{n_{\mathrm{pr}}-1} \end{pmatrix}, \tag{5.17a}$$

$$\mathcal{T}_d = \begin{pmatrix} D_d^d & 0 & \dots & \dots & 0 \\ C_d B_d^d & D_d^d & \ddots & & \vdots \\ C_d A_d B_d^d & C_d B_d^d & D_d^d & \ddots & \vdots \\ \vdots & \vdots & \ddots & \ddots & 0 \\ C_d A_d^{k+n_{\mathrm{pr}}-1} B_d^d & C_d A_d^{k+n_{\mathrm{pr}}-2} B_d^d & \dots & C_d B_d^d & D_d^d \end{pmatrix}, \tag{5.17b}$$

$$\mathcal{T}_u = \begin{pmatrix} D_d & 0 & \dots & \dots & 0 \\ C_d B_d & D_d & \ddots & & \vdots \\ C_d A_d B_d & C_d B_d & D_d & \ddots & \vdots \\ \vdots & \vdots & \ddots & \ddots & 0 \\ C_d A_d^{k+n_{\mathrm{co}}-1} B_d & C_d A_d^{k+n_{\mathrm{co}}-2} B_d & \dots & C_d B_d & D_d \end{pmatrix}. \tag{5.17c}$$

We also define the nominal output and input trajectories as

$$\mathbf{y}^{nom} = \left((y^{nom})^T, (y^{nom})^T, \dots, (y^{nom})^T \right)^T, \tag{5.18}$$

$$\mathbf{u}^{nom} = \left((u^{nom})^T, (u^{nom})^T, \dots, (u^{nom})^T \right)^T, \tag{5.19}$$

where $\mathbf{y}^{nom}$ and $\mathbf{u}^{nom}$ have the same dimensions as $\Delta\mathbf{y}_k$ and $\Delta\mathbf{u}_k$ defined in Eqs. (5.14) and (5.16).

To derive a standard parametric QP, a quadratic cost function J, which reflects deviations of the system's output and input trajectories from given reference trajectories and the change of the inputs,

$$\begin{aligned} J = {} & \frac{1}{2} \left(\Delta\mathbf{y}_k - (\mathbf{y}^{ref} - \mathbf{y}^{nom}) \right)^T Q_y \left(\Delta\mathbf{y}_k - (\mathbf{y}^{ref} - \mathbf{y}^{nom}) \right) + \\ & \frac{1}{2} \left(\Delta\mathbf{u}_k - (\mathbf{u}^{ref} - \mathbf{u}^{nom}) \right)^T Q_u \left(\Delta\mathbf{u}_k - (\mathbf{u}^{ref} - \mathbf{u}^{nom}) \right) + \\ & \frac{1}{2} \left(\Delta\mathbf{u}_k - \Delta\mathbf{u}_{k-1} \right)^T Q_{du} \left(\Delta\mathbf{u}_k - \Delta\mathbf{u}_{k-1} \right) \end{aligned} \tag{5.20a}$$

as well as constraints on the system's output, input, and on the slope of the input,

$$\Delta\mathbf{y}^{lb} \leq \Delta\mathbf{y}_k \leq \Delta\mathbf{y}^{ub}, \quad \Delta\mathbf{y}^{lb} := \mathbf{y}^{lb} - \mathbf{y}^{nom}, \quad \Delta\mathbf{y}^{ub} := \mathbf{y}^{ub} - \mathbf{y}^{nom}, \tag{5.20b}$$

$$\Delta\mathbf{u}^{lb} \leq \Delta\mathbf{u}_k \leq \Delta\mathbf{u}^{ub}, \quad \Delta\mathbf{u}^{lb} := \mathbf{u}^{lb} - \mathbf{u}^{nom}, \quad \Delta\mathbf{u}^{ub} := \mathbf{u}^{ub} - \mathbf{u}^{nom}, \tag{5.20c}$$

$$\mathbf{du}^{lb} \leq \Delta\mathbf{u}_k - \Delta\mathbf{u}_{k-1} \leq \mathbf{du}^{ub}, \tag{5.20d}$$

have to be formulated, where Q_y, Q_u, and Q_{du} are the weighting matrices for the output, input, and the change of the input variables. $\mathbf{y}^{ref}$ and $\mathbf{u}^{ref}$ are the output and input reference trajectories. $\mathbf{y}^{lb}, \mathbf{y}^{ub}, \mathbf{u}^{lb}, \mathbf{u}^{ub}, \mathbf{du}^{lb}, \mathbf{du}^{ub}$ are the sample-wise defined lower and upper bounds for the output and input trajectories and the change of the input trajectory indicated by the superscripts lb and ub. Casting Eqs. (5.13) – (5.17c) and (5.20a) – (5.20d) into the standard QP form results in

$$\min_{\Delta \mathbf{u}_k} \frac{1}{2} \Delta \mathbf{u}_k^T \mathcal{H} \Delta \mathbf{u}_k + \mathcal{F}^T(\Delta \mathbf{p}_k) \Delta \mathbf{u}_k \tag{5.21a}$$

$$\text{s.t. } \mathcal{A} \Delta \mathbf{u}_k + \mathcal{B}(\Delta \mathbf{p}_k) \geq 0, \tag{5.21b}$$

with the matrices defined as

$$\mathcal{H} = Q_\Delta^T Q_{du} Q_\Delta + Q_u + \mathcal{T}_u^T Q_y \mathcal{T}_u, \tag{5.22a}$$

$$\mathcal{F} = \left(\Delta \mathbf{p}_k^T \mathcal{T}_p^T Q_y \mathcal{T}_u - (\mathbf{u}^{ref} - \mathbf{u}^{nom})^T Q_u - (\mathbf{y}^{ref} - \mathbf{y}^{nom})^T Q_y \mathcal{T}_u\right)^T, \tag{5.22b}$$

$$\mathcal{A} = \left(\mathcal{T}_u, -\mathcal{T}_u, I, -I, Q_\Delta, -Q_\Delta\right)^T, \tag{5.22c}$$

$$\mathcal{B} = \left(\mathcal{T}_p \Delta \mathbf{p}_k - \Delta \mathbf{y}^{lb}, \Delta \mathbf{y}^{ub} - \mathcal{T}_p \Delta \mathbf{p}_k, -\Delta \mathbf{u}^{lb}, \Delta \mathbf{u}^{ub}, -\mathbf{du}^{lb}, \mathbf{du}^{ub}\right)^T, \tag{5.22d}$$

where

$$\Delta \mathbf{p}_k := [\Delta x_k^T, \Delta \mathbf{d}_k^T]^T, \tag{5.23a}$$

$$\mathcal{T}_p := (\mathcal{T}_x, \mathcal{T}_d), \tag{5.23b}$$

and the matrix Q_Δ is defined as

$$Q_\Delta = \begin{pmatrix} I & 0 & \cdots & \cdots & 0 \\ -I & I & \ddots & & \vdots \\ 0 & \ddots & \ddots & \ddots & \vdots \\ \vdots & \ddots & \ddots & \ddots & 0 \\ 0 & \cdots & 0 & -I & I \end{pmatrix}. \tag{5.23c}$$

I in Eq. (5.23c) is an identity matrix of the size $n_u \times n_u$ with n_u being the length of Δu_k, while in Eq. (5.22c), I is an identity matrix of the size of Q_Δ. Again, QP (5.21) is based on the controller/observer model given by Eqs. (2.61a) and (2.61b) in Section 2.4.4.

For the on-line algorithm, the supervisory control task is decomposed into three smaller problems resulting in three distributed controllers for the three subsystems (see the highlighted subsystems in Figure 5.3). Each distributed controller considers only a part of the QP, namely the control parameters related to the corresponding subsystem, as well as the constraints related to that subsystem. Consequently the matrices and vectors are partitioned as follows: $\mathcal{H} = (\mathcal{H}_{i,j})_{i,j \in \mathbb{I}}$, $\mathcal{A} = (\mathcal{A}_{i,j})_{i,j \in \mathbb{I}}$, $\mathcal{F} = (\mathcal{F}_i)_{i \in \mathbb{I}}$, $\mathcal{B} = (\mathcal{B}_i)_{i \in \mathbb{I}}$, and

$\Delta\mathbf{u}_k = (\Delta\mathbf{u}_{k,i})_{i\in\mathbb{I}}$, where the set $\mathbb{I} = \{1, 2, 3\}$ indicates the set of subsystems. Then, each of the controllers iteratively solves the following smaller QP, involving only local decision variables and constraints:

$$\min_{\Delta\mathbf{u}_{k,i}} \frac{1}{2}\Delta\mathbf{u}_{k,i}^T\,\mathcal{H}_{i,i}\,\Delta\mathbf{u}_{k,i} + \mathcal{F}_i^T(\Delta\mathbf{p}_k)\,\Delta\mathbf{u}_{k,i} + \left(\sum_{j\in\mathbb{I}\setminus i}\Delta\mathbf{u}_{k,j}^{T\,[q]}\,\mathcal{H}_{j,i} + \mathcal{F}_j^T(\Delta\mathbf{p}_k) - \lambda_j^{T[q]}\,\mathcal{A}_{j,i}\right)\Delta\mathbf{u}_{k,i}, \tag{5.24a}$$

$$\text{s.t. } \mathcal{A}_{i,i}\,\Delta\mathbf{u}_{k,i} + \sum_{j\in\mathbb{I}\setminus i}\mathcal{A}_{i,j}\,\Delta\mathbf{u}_{k,j}^{[q]} + \mathcal{B}_i(\Delta\mathbf{p}_k) \geq 0. \tag{5.24b}$$

In these expressions the superscript $[q]$ indicates the Lagrange multipliers λ_i and the optimal control parameters $\Delta\mathbf{u}_{k,i}$ of the q-th iteration. In Eq. (5.24a), the term in the round brackets is derived from necessary conditions of optimality for subsystems $j \neq i$. The term Δx_k included in the vector $\Delta\mathbf{p}_k$ in Eq. (5.23a) is obtained from the deviation of the state estimate $\hat{x}_k$ from the nominal state. The state estimate $\hat{x}_k$ is calculated by the Lang-Gilles observer at every sample k, and, as a consequence of using state estimates instead of measurements, the output prediction by Eq. (5.13) and solution of the QP would be inaccurate if the observer provides inaccurate state estimates. However, since our controller/observer model is high-dimensional (cf. Eq. (2.64a)), it is not practicable to use measurements.

5.4 Case study: output feedback control of ACBT separation

For the simulation study, the plant replacement and the DMPC controller/state observer models are implemented in gPROMS (Process Systems Enterprise, 1997-2013), see Appendix B. This results in about 500 differential and 5000 algebraic variables for the plant-replacement model, and about 350 differential and 3500 algebraic variables for each of both, the controller and the state observer. The models are connected to a generic environment for the simulation of dynamical systems and for advanced process control, which is realized in Matlab, using the IPCOS OPC server for data storage and communication (IPCOS NV, 2013), as depicted in Figure 5.4 (Elixmann et al., 2014). In the selected scenario, the molar fractions of the feed $F2$, see Figure 5.3, are changed from $[0.25, 0.25, 0.25, 0.25]$ mol/mol to $[0.25, 0.2, 0.3, 0.25]$ mol/mol at $t = 10$ h, where the values in the brackets correspond to the compositions ordered as [acetone, chloroform, benzene, toluene], i.e., we simulate an abrupt changeover of the feed quality.

The simulation is started in the nominal steady state of the plant (plant replacement model). The nominal condition data for the plant columns are summarized in Ap-

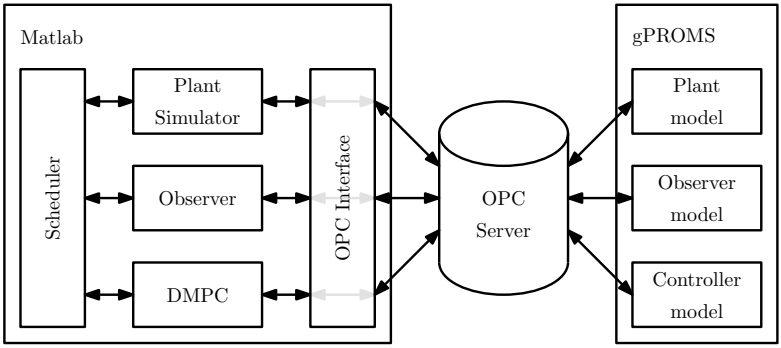

Figure 5.4: Generic software architecture for simulation and advanced process control

pendix C.6. To illustrate the step response behavior of the plant, we consider three different situations: (i) there is no supervisory control and the PID regulatory layer is turned off (open-loop behavior), (ii) there is no supervisory control and the PID regulatory layer is turned on, and (iii) the complete control environment, including the supervisory and regulatory control layers, is turned on. Here, the supervisory control layer is comprised of the DMPC described in Section 5.3.2.

5.4.1 The PID regulatory layer is turned off (open-loop process)

In this case, there is no supervisory control and the regulatory controllers $r1$, $r5$, $r2$, $r3$, and $r4$ are in manual mode. Figure 5.5 depicts the open-loop step response of the plant. This response to the feed change shows that no satisfactory behavior of product concentrations can be achieved if the above controllers are in manual mode, i.e., if the flow rates of the valves they operate are constant at their nominal values. Notice that the chloroform concentration deviates most from its nominal value. This component proved to amplify the feed disturbances and to influence negatively the stability of a simulation in the majority of cases.

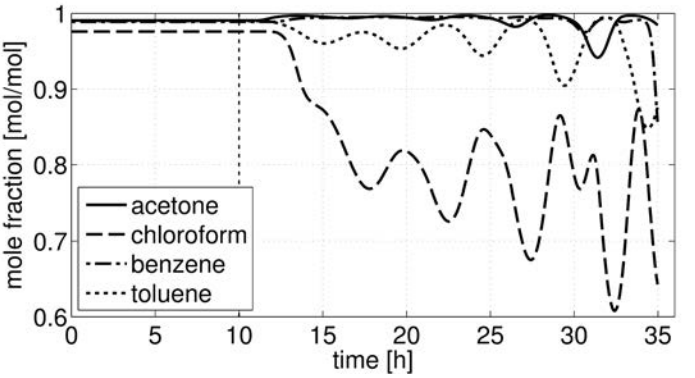

Figure 5.5: Open-loop response of the plant-product concentrations to the feed disturbance with regulatory layer turned off; product concentrations: acetone concentration in the top stream of column 1, toluene concentration in the bottom stream of column 2, chloroform concentration in the top and benzene concentration in the bottom streams of column 3; dashed vertical line marks the time point of change in feed flow rate $F2$.

5.4.2 The PID regulatory layer is turned on

Contrary to the first case, all PI controllers of the base control layer are activated. The regulated temperatures and consequently product concentrations can be stabilized. Note that no concentration measurements or estimates are used in this control scheme. In this way a satisfactory control of products qualities is possible. However, it takes about 10 hours to reject the feed disturbances to the chloroform and benzene concentrations in the top and bottom streams of column 3 as shown in Figure 5.6. To improve disturbance rejection, we either could search for a better controller tuning or investigate other control schemes such as a two-layer control approach. Here, we focus on the second alternative in the following Section 5.4.3.

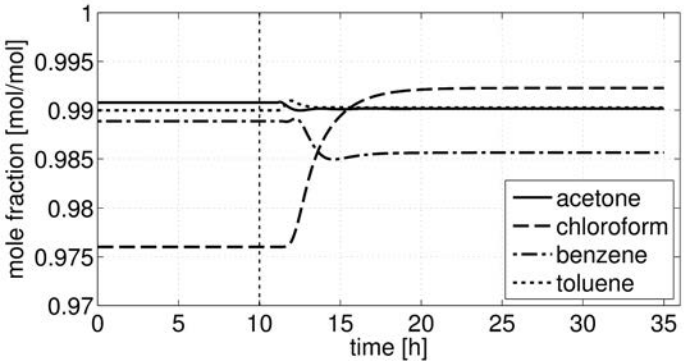

Figure 5.6: Response of the plant-product concentrations to the feed disturbance with regulatory layer turned on; product concentrations: acetone concentration in the top stream of column 1, toluene concentration in the bottom stream of column 2, chloroform concentration in the top and benzene concentration in the bottom streams of column 3; dashed vertical line marks the time point of change in feed flow rate $F2$.

5.4.3 The supervisory and regulatory control layers are turned on

In this case, both, the supervisory and regulatory control layers are turned on. The DMPC incorporates the control model which obtains state estimates from the Lang-Gilles state observer to calculate optimal setpoints for the regulatory layer of the plant (replacement) resulting in a cascade control system (Skogestad, 2004, Scattolini, 2009). Note that our control model requires a full state estimate and alternative approaches such as Kalman Filter (Kalman, 1960) or Luenberger observer (Luenberger, 1964) could be adopted for this task, too. Simpler estimators such as PLS/PCR are maybe the best for state estimation from the practical point of view. However, these estimators rely on more than few temperature measurements and have been shown to estimate well only the column-product compositions using temperature measurements on a large number of or all column trays (Mejdell and Skogestad, 1991a,b, 1993, Mejdell and Andersson, 1994). Therefore, it could be practically infeasible to design a full state PLS/PCR estimator and our choice of the Lang-Gilles observer is based on the fact that the Lang-Gilles observer requires only a few temperature measurements, calculates the full state, and is also robust against some parameter uncertainties.

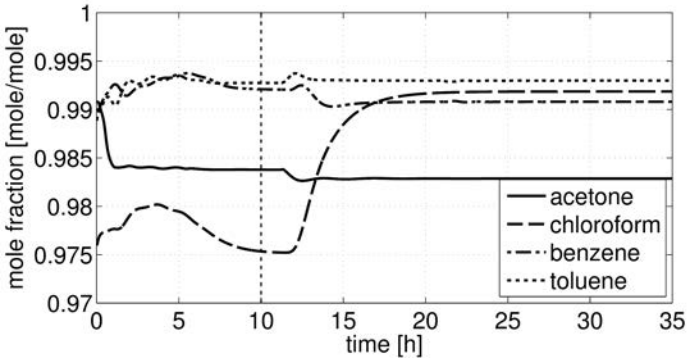

Figure 5.7: Response of the plant-product concentrations to the feed disturbance with controllers of both layers including the state observer turned on; product concentrations: acetone concentration in the top stream of column 1, toluene concentration in the bottom stream of column 2, chloroform concentration in the top and benzene concentration in the bottom streams of column 3; dashed vertical line marks the time point of change in feed flow rate $F2$.

The objective of the DMPC is to minimize the deviations in the product qualities (acetone, chloroform, benzene, and toluene) from their setpoints in the least-squares sense. These setpoints are set as follows: acetone 0.988 mol/mol, chloroform 0.98 mol/mol, benzene 0.992 mol/mol, and toluene 0.99 mol/mol. The lower bounds for qualities of all products are set to 0.97 mol/mol. For further DMPC parameters see Appendix C.4. The simulation scenario is as follows. First, the DMPC is switched off and the simulation runs until a steady state of the plant-replacement model. Then, the simulation is restarted from this steady state and runs, with the DMPC switched on. 10 h after restart the disturbance to the feed composition occurs. This scenario results in Figure 5.7 which shows the trajectories of product concentrations and Figure 5.8 which depicts the three most strongly manipulated SPs of the regulatory controllers calculated by the DMPC. In general, we can observe that the DMPC essentially sets the PID setpoints to their limits before the feed disturbance occurs. This can be interpreted based on process insight. By setting the SPs of PID $r1$ and $r2$ to their upper limits, the DMPC tries to lower the acetone purity in the distillate of the first column and increase the toluene purity in the second column. On the other hand, by setting the SP of PID $r5$ to the lower limit, the DMPC reduces the liquid flow rate to the reboiler of the first column and this increases the acetone purity in the distillate of the first column. Nevertheless, the manipulation of the SP of $r2$ has a stronger effect than that of $r5$ as seen in Figure 5.7. This means that in the first few hours the response of the product concentrations agrees with the reference values for concentra-

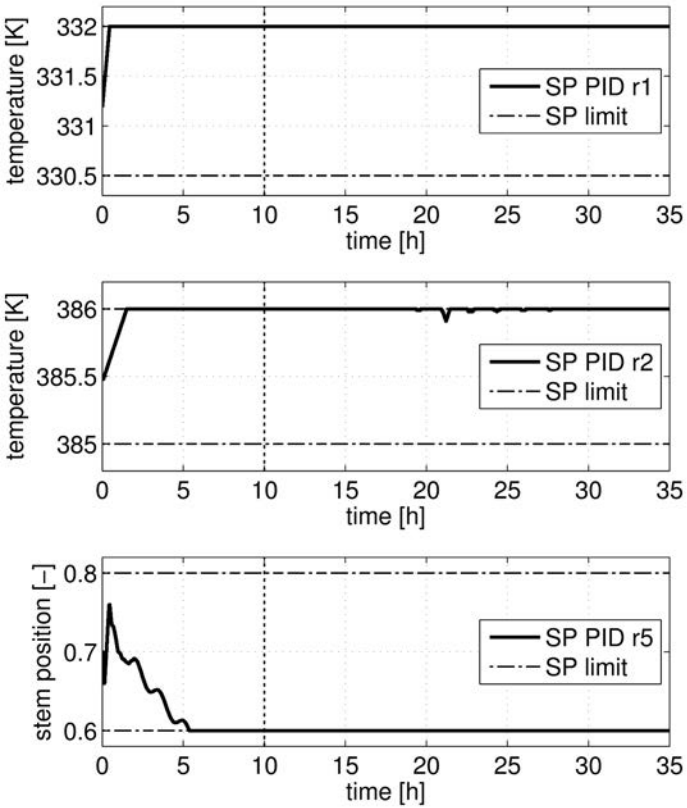

Figure 5.8: Setpoints of the regulatory layer; dashed vertical lines mark the time point of change in feed flow rate $F2$.

tions. The situation changes when the feed disturbance occurs after 10 h of simulation time (dashed vertical lines in Figures 5.7 – 5.9). Then, no DMPC action to reject this disturbance can be observed, cf. Figure 5.8. The stationary acetone and benzene qualities in Figure 5.7 are lower/higher than those in Figure 5.6. The setpoints for acetone and chloroform in particular are not met (offsets about -0.005 mol/mol and $+0.012$ mol/mol are present at the steady state), i.e., for different operating conditions, no crucial advantage in setpoint tracking of the two-layer approach compared to the one-layer approach in Section 5.4.2 could be demonstrated. Disturbance rejection of both approaches is also very similar, cf. Figures 5.7 and 5.6 after 10 h of simulation time. This is not surprising,

since we did not improve the control structure by using the two-layer approach. Moreover, the plant-model mismatch is not the reason for missing control improvement. To

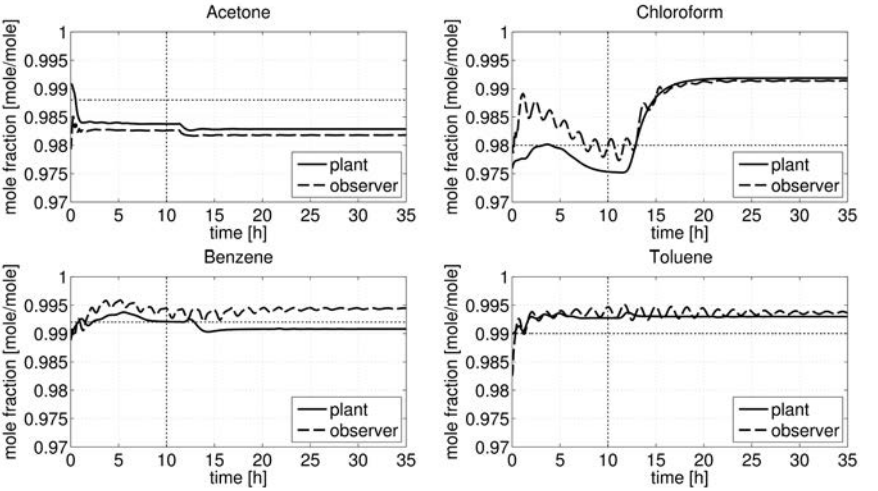

Figure 5.9: Plant replacement and observer product concentrations; dashed vertical line marks the time point of change in feed flow rate $F2$; dashed horizontal lines mark the setpoints for the product concentrations.

realize this, consider Figure 5.9 which shows the product concentrations in the plant and the observer models. The deviations between individual concentrations in the plant and observer are comparable with those reported for other state observers as outlined in Section 3.1. The largest deviation in Figure 5.9 is about 0.01 mol/mol and the deviations for acetone and chloroform concentrations at the end of simulation are much smaller (less than 0.002 mol/mol) than the deviations between the actual plant-replacement concentrations and their setpoints (about 0.012 mol/mol). This shows that the Lang-Gilles observer is well suitable for the use as a state estimator in model-predictive control.

There is another point about the observer which is worth noting. The oscillations in product concentrations occur most likely because of the plant-model mismatch and a tight observer tuning and could be reduced with looser tuning.

Note also that in this case study, the observer simulation time dominated with 60.6% of the total time, the simulation time for the plant-replacement model was 34.6% and the calculation time for the DMPC was 4.8%.

5.5 Chapter summary

For a complex distillation column sequence, we developed a two-layer control system consisting of a decentralized base control layer involving only single-loop PID controllers and a supervisory control layer realized by a DMPC which relies on a linearized model of the plant. The Lang-Gilles state observer is used to provide state information to the DMPC. The different control strategies are illustrated by means of a case study.

With first-principles models, rich nonlinear dynamics can be observed. This complicates control design and evaluation in closed-loop process simulation. In particular, despite the use of state-of-the-art technology, the numerical solutions suffer from instability if aggressive controller tunings are chosen. Hence, besides making the simulations more robust, effective tuning routines for the distillation observer and the DMPC controller are desirable to avoid time-consuming simulation studies and allow the roll-out of this technology to industry.

The utilization of first-principles models allows us to avoid a laborious identification task. The unknown parameters in these models are estimated from the plant data or taken from literature (see Section 2.4.5). This approach, though it seems complicated at first glance, is straightforward. Moreover, if numerically robust models are required, the nonlinear models could be linearized and reduced. We think that for large plants with complex dynamics such an approach could be more appropriate than the one using simpler transfer functions which must be identified (Hammarström et al., 1982). However, in the case of linearized models, reduction seems to be inevitable. The reason is the poorly damped pair of eigenvalues we identified in our plant in Section 2.5.1. The system is therefore almost unstable. For unstable systems, the optimization performed by an MPC to minimize the objective function becomes ill-conditioned for a sufficiently large prediction horizon, and for a sufficiently short prediction horizon, the optimization is ill posed, as pointed out by Rossiter (2004). Unfortunately, our plant is high-dimensional and has large time constants (some hours), i.e., the DMPC requires a large prediction horizon. This greatly limits the achievable control quality. The additional research needed to overcome this problem, e.g. by reducing the model or using suggestions for algorithm reformulation in Rossiter (2004), is beyond the scope of this thesis and is left for the future.

We experienced no substantial improvement in control performance (disturbance rejection and setpoint tracking) when using a model-predictive controller on top of the base-control layer. There are several reasons for that which come into consideration, e.g., the poorly damped pair of eigenvalues in the controller model shown in Figure 2.8 from Section 2.5.1 that can impair model predictions or a poor tuning of the DMPC parameters. It is not clear how the DMPC parameters should be tuned to achieve best control results. The accuracy of the controller model is also known to be crucial to the performance of the

model predictive controller (e.g. Hammarström et al., 1982). The general recommendation to keep the flow rates of the model and the actual plant within a 5% margin (Luyben, 1992) is helpful for modeling the steady-state behavior, however this is difficult to achieve in a transient. On the other hand, the accuracy of the observer state predictions was sufficiently good to believe that other points should be investigated first. The Lang-Gilles observer robustness might be an issue for plants comprising several distillation columns. In this case, linearized observer models could be considered to reduce numerical problems. The use of PLS/PCR estimators is also possible. However, if a full state of a large plant is required as in our case, these estimators require too many temperature measurements and are of little use.

6 Summary and conclusions

Distillation has played a major role for centuries, being used for manufacturing distilled water, perfume oils, alcohol, and various chemical products. Its use and development in the ancient world until the 19th century is extensively illustrated by Forbes (1970). Among other things, Forbes mentions that the discovery of alcohol and mineral acids "had a profound influence on the evolution of the art of distilling" in the Middle Ages. In the same way, progress in the natural sciences, mathematics, and later emerging computer technology paved the way for the first distillation models and their further enhancements; since the earliest attempts, distillation modeling has expanded considerably, especially in recent decades.

In the early days of distillation modeling, models were based upon physical principles and assumed equilibrium stages. However, the equilibrium-stage concept requires an accurate VLE model and significant improvements in modeling VLE were not achieved before the equations of state for VLE prediction were introduced. By this time, empirical models based on neural nets, transfer functions etc., as well as hybrid models, had also been developed. These empirical and hybrid models have been popular because of the considerably lower modeling effort they promise. However, they are also vulnerable to poor data and that is their substantial drawback when compared with the fundamental models.

Along with modeling, control and state estimation have attracted much interest. In the modern chemical process industry PID control, conventional advanced control, and linear/nonlinear model-predictive control are widely used. PID control often dominates control applications in chemical plants due to its simplicity and lower investment costs. For instance, in the Japanese plant MCC Mizushima, the ratio of applications of PID, advanced control, and model-predictive control is 100:10:1 (Kano and Ogawa, 2010). On the other hand, the flexible constraint handling in model-predictive control is sometimes favored over simplicity, and a more complex MPC is chosen. For that to work well, accurate models and state estimates are essential. If the process is observable then in theory state estimates can be determined. However, in practice, it is more difficult to obtain good state estimates for nonlinear systems such as distillation. Many researchers have therefore addressed state observers in their works, e.g., Lang and Gilles (1990) developed a distillation observer taking into account mass and heat transfer between the liquid and vapor phases on trays.

Another relevant research topic is the estimation of distillation efficiency. Different efficiency definitions have been proposed for distillation – the Muphree efficiency is probably the best-known efficiency among chemical engineers (Murphree, 1925). An accurate efficiency *prediction* is typically desired to improve the design of trays or packings and construct energy-efficient distillation columns. In case of column malfunctions, an efficiency can be *estimated* after laborious preparations and is used to locate problem areas in the distillation column under inspection. An on-line efficiency estimation to improve control or to monitor the column operation poses a challenge and is therefore rather uncommon.

The approach of this work is to test and prepare the Lang-Gilles observer for practical use in the spirit of Foss (1973) criticizing the gap between control theory and application which admittedly still exists. Therefore, case studies with more complex distillation models, including state-of-the-art VLE models and a plant-model mismatch, are considered inevitable. This apparently contradicts the preferred approach in theoretical literature, which avoids any plant-model mismatch. For methods developed without considering a plant-model mismatch, we principally need the assumption that the underlying models can be made arbitrarily accurate (unless the methods turn out to be very robust). However, such an assumption is rarely validated, and nor can it be; since not all physical mechanisms are perfectly understood yet, one can by no means improve a physical distillation model up to any required degree of accuracy, nor is it well investigated which effect each of the different physical mechanisms has on the overall model accuracy. Unfortunately, our approach enormously complicates our case studies because one has to cope with several models deviating from each other, and numerical difficulties, which arise from the complicated setting and particular complexity of every model. Besides, we have to forgo some analysis since there is no adequate methodology for large-scale nonlinear systems yet. Nonetheless, to bridge the gaps noted by Foss it might help to diverge from the beaten track.

To provide a flexible modeling framework for our case studies, we implemented several libraries in gPROMS. gPROMS is very attractive as it supports physical modeling and has one of the best DAE solvers on the market. Our libraries include standard distillation column parts such as reboiler, condenser, and tray section, of which the columns may be composed. Complicated plants consisting of several columns are built by combining and properly connecting single columns. Distillation models are interfaced with different mixture components and VLE functions to investigate non-ideal mixtures too. An additionally implemented interface enables reading external data to automatically initialize models. This is especially important for large models as this feature is not available in gPROMS. To stabilize distillation models PID controllers should be utilized for base control.

In terms of practical use of the complex distillation models, more research on robust

reinitialization of DAE systems must be done. Though the reinitialization algorithm in gPROMS usually performs well, there is no guarantee of this and in our ACBT control study, the simulation crashes due to a failed reinitialization occurred about once per 100 reinitializations. Therefore, for advanced control with more complex distillation models a robustified algorithm for reinitialization would be crucial.

There are no theoretical studies on the convergence behavior of the Lang-Gilles observer either for single distillation columns or for complete plants comprising several coupled distillation columns. To close this gap, we examined the conditions for convergence of the Lang-Gilles observer for plants of arbitrary size. Three theorems with different assumptions implying observer convergence were proved. The first theorem claims observer convergence supposing constant observer gains and strict conditions on vapor compositions and temperatures while in the second theorem only Lipschitz continuous temperatures are assumed and the role of gain tuning for observer convergence is shown. The third theorem is based on Lyapunov theory and assumes Lipschitz continuity with respect to the liquid compositions of both the vapor compositions and boiling temperatures.

Moreover, a model-based tuning method was proposed which gives initial gain values for further fine-tuning of the observer gains in simulations. The method calculates a quantity that is an approximation of the upper bound for an observer gain. This bound is derived based on the proof of Theorem 3. It was found to be proportional to the ratio of the liquid flow rate to the liquid holdup in a column section.

The convergence results presented are still incomplete; the theorems given provide only sufficient conditions for observer convergence. In fact one should identify sufficient and necessary conditions for observer convergence. However, in our opinion this is a very difficult task due to nonlinearities of the observer feedback term. Further analysis of the Lang-Gilles observer, which is very fast but vulnerable to loss of accuracy in the presence of a structural plant-model mismatch (as the Luenberger observer), will also help to develop a more accurate, fast, and numerically robust observer.

Since a separation efficiency factor is integrated in the Lang-Gilles observer as a parameter, this observer can be used to estimate the efficiency. Therefore, based on the Lang-Gilles observer we proposed an algorithm for efficiency estimation which requires only a few temperature measurements apart from VLE data. The case study conducted offers insights on how the algorithm performs if no plant-model mismatch is assumed. From the practical point of view, the effects of a plant-model mismatch should be explored, too. Another point concerns a possible linearization of the state observer to fulfill the requirements of robust operation. When the observer is linearized, additional inaccuracy is introduced in estimation and needs to be analyzed. In addition, we need to learn whether the lumped parameter describing efficiency can prove itself in practice. From the theoretical point of

view, the convergence conditions and convergence rate of the proposed algorithm could be examined more thoroughly. One promising approach might be to separate this analysis into three steps. In a first step, the sufficient conditions for observer convergence are established as done in this thesis. Then, the influence of the parameter estimation on convergence is studied. In a third step, the previous steps should be combined to show the convergence of the complete algorithm.

To study the advantages of a two-layer over a single-layer control architecture for operation of a complex distillation train, we developed a two-layer control system consisting of a decentralized base control layer involving single-loop PID controllers and a supervisory control layer realized by a DMPC which relies on a linearized model of the plant. During operation the DMPC receives estimates of the concentrations from the Lang-Gilles observer to calculate predictions for the plant outputs. The Lang-Gilles observer also provides product concentrations to the DMPC what enables us to specify setpoints for very important, but often not available on-line, product concentrations instead of setpoints for less important, but usually measured on-line, temperatures. The different control strategies are illustrated by means of a case study based on our exemplary distillation train. Unfortunately, our plant is high-dimensional and has large time constants, i.e., the DMPC requires a large prediction horizon. This greatly limits achievable control quality. The additional research needed to cope with this problem, e.g. by reducing the model or using a reformulated control algorithm (Rossiter, 2004), is beyond the scope of this thesis and is left for the future.

We experienced no substantial improvement in control performance when using a model-predictive controller on top of the base-control layer. This is probably the case because of a poorly damped pair of eigenvalues in the controller model and/or a poor tuning of the DMPC parameters. The accuracy of the controller model is known to be crucial to the performance of the model-predictive controller, too. The general recommendation to keep the flow rates of the model and the actual plant within a 5% margin (Luyben, 1992) is helpful for modeling the steady-state behavior; this is however difficult to achieve in a transient. On the other hand, the Lang-Gilles observer was found to give sufficiently accurate state predictions for DMPC reinitializations. Thus, no controller/observer model refinement is recommended at the moment. Nevertheless, a better understanding of the necessary modeling accuracy in combination with controller tuning will further help to improve our results.

Appendix

A Derivation of particular column assumptions

Common simplifications of the energy balance described in Section 2.2.1 require further assumptions. In the following Sections A.1 and A.2, these assumptions are derived from conditions given by Skogestad (1997). We also derive a simplified energy balance equation for total and partial condensers in Section A.3; a shortened derivation thereof was given by Häggblom (1991).

A.1 Derivation of the constant enthalpy assumption

The constant enthalpy assumption, i.e., $dh_{L,j}/dt = 0$, is deduced from the following conditions:

1. The column pressure equals the reference pressure p which is constant.
2. Pure components are saturated liquids at the reference pressure.
3. Heat of mixing is negligible such that the liquid enthalpy on stage j is $h_{L,j} = \sum_i x_{i,j} c^L_{p,i} (T_j - T_{b,i})$, where $c^L_{p,i}$ is the liquid molar heat capacity of component i at pressure p, T_j is the temperature in tray j, and $T_{b,i}$ is the boiling temperature of component i at the reference pressure.
4. Tray temperature T_j is the average of the component boiling points, i.e., $T_j = \sum_i x_{i,j} T_{b,i}$.
5. Heat capacities for all components are the same, i.e., $c_p = c^L_{p,1} = \ldots = c^L_{p,q}$.

Then, from conditions 1 to 4, we obtain

$$\begin{aligned} h_{L,j} &= \sum_i x_{i,j} c^L_{p,i} (T_j - T_{b,i}) \\ &= x_{1,j} c^L_{p,1} \left((x_{1,j} - 1) T_{b,1} + x_{2,j} T_{b,2} + \ldots + x_{q,j} T_{b,q} \right) + \\ &\quad x_{2,j} c^L_{p,2} \left(x_{1,j} T_{b,1} + (x_{2,j} - 1) T_{b,2} + \ldots + x_{q,j} T_{b,q} \right) + \\ &\quad \ldots \\ &\quad x_{q,j} c^L_{p,q} \left(x_{1,j} T_{b,1} + \ldots + x_{q-1,j} T_{b,q-1} + (x_{q,j} - 1) T_{b,q} \right). \end{aligned} \tag{A.1.1}$$

Since $(x_{i,j} - 1) = -\sum_{k \neq i} x_{k,j}$, Eq. (A.1.1) becomes

$$\begin{aligned} h_{L,j} = x_{1,j}c^L_{p,1}\left(\left(-\sum_{k\neq 1} x_{k,j}\right)T_{b,1} + x_{2,j}T_{b,2} + \ldots + x_{q,j}T_{b,q}\right) + \\ x_{2,j}c^L_{p,2}\left(x_{1,j}T_{b,1} + \left(-\sum_{k\neq 2} x_{k,j}\right)T_{b,2} + \ldots + x_{q,j}T_{b,q}\right) + \\ \ldots \\ x_{q,j}c^L_{p,q}\left(x_{1,j}T_{b,1} + \ldots + x_{q-1,j}T_{b,q-1} + \left(-\sum_{k\neq q} x_{k,j}\right)T_{b,q}\right). \end{aligned} \tag{A.1.2}$$

Finally, expanding Eq. (A.1.2) and using the condition 5, we obtain

$$h_{L,j} = 0, \tag{A.1.3}$$

and thus

$$\frac{dh_{L,j}}{dt} = 0. \qquad \square \tag{A.1.4}$$

A.2 Derivation of the constant molar overflow condition (CMO)

We assume conditions 1 to 5 from Section A.1. This implies Eq. (A.1.3) which justifies the assumption $h_{L,j} = h_{F,j} = 0$ for all trays j and the feed flow. So, the energy balance Eq. (2.5) becomes

$$\frac{dU_j}{dt} = V_{j+1}h_{V,j+1} - \left(V_j + S^V_j\right)h_{V,j}. \tag{A.2.1}$$

With negligible vapor holdups, i.e., $M^V_j = 0$, and using the approximation $h_{L,j} \approx u_j$ reasonable for liquids, where $u_j = U_j/M_j$ is the specific internal energy, the left hand side of Eq. (A.2.1) becomes

$$\frac{dU_j}{dt} = \frac{d(M_j u_j)}{dt} = \frac{d((M^L_j + M^V_j)u_j)}{dt} = \frac{d(M^L_j h_{L,j})}{dt} = M^L_j\frac{dh_{L,j}}{dt} + h_{L,j}\frac{dM^L_j}{dt} = 0. \tag{A.2.2}$$

Then, neglecting side streams, i.e., setting $S^V_j = 0$, and combining Eqs. (A.2.1) and (A.2.2), we obtain

$$0 = V_{j+1}h_{V,j+1} - V_j h_{V,j}. \tag{A.2.3}$$

Assume in addition to the conditions 1 to 5 from Section A.1:

1. The vapor phase is ideal and all components have equal heats of vaporization $h^{vap} = h^{vap}_1 = \ldots = h^{vap}_q$ at the column pressure such that $h_{V,j} = h^{vap} + \sum_i x_{i,j}c^V_{p,i}\left(T_i - T_{b,i}\right)$, where $c^V_{p,i}$ is the vapor molar heat capacity.

2. Vapor heat capacity $c_{p,i}^V$ is equal for all components.

Then, similar to the derivation in Section A.1, the term $\sum_i x_{i,j} c_{p,i}^V (T_i - T_{b,i})$ is zero and thus $h_{V,j} = h^{vap}$. Therefore, Eq. (A.2.3) reduces to

$$0 = V_{j+1} - V_j. \tag{A.2.4}$$

Finally, Eq. (A.2.4) inserted in overall material balance Eq. (2.3) for a tray j with zero side and feed streams and negligible holdup change, i.e. $S_j^L = S_j^V = F_j = \frac{dM_j}{dt} = 0$, implies

$$0 = L_{j-1} - L_j. \qquad \square \tag{A.2.5}$$

A.3 Derivation of a simplified energy balance equation for condensers

The simplified energy balance equation for the condenser is derived from the energy balance Eq. (2.5) adopted as

$$\frac{dM_0 u_0}{dt} = V_1 h_{V,1} - L_0 h_{L,0} - F_0 h_{F,0} + Q_0, \tag{A.3.1}$$

where $u_0 = U_0/M_0$ is the specific internal energy in the condenser, V_1 is the vapor flow rate to the condenser, L_0 is the reflux flow rate, F_0 is the distillate flow rate, $h_{V,1}$, $h_{L,0}$, $h_{F,0}$ are the specific enthalpies of the streams V_1, L_0, F_0, and $-Q_0$ is the heat flow removed from the condenser.

In order to proceed, the following assumptions and definitions are made (cf. Häggblom (1991)). We assume that the internal energy in the condenser equals the liquid enthalpy as

$$u_0 = h_{L,0}. \tag{A.3.2}$$

The specific enthalpy $h_{L,0}$ may be expressed as

$$h_{L,0} = \sum_{i=1}^{q} h_{L,0,i} x_{i,0}, \tag{A.3.3}$$

where $h_{L,0,i}$ is the partial specific enthalpy of component i and q is the number of components. Note that $h_{L,0,i}$ is independent of composition or time. $x_{i,0}$ is the mole fraction of component i in the condenser. In general, we may express the specific enthalpy $h_{S,j}$ of stream S by additionaly introducing the thermal condition $q_{S,j}$ of stream S on tray j as follows:

$$h_{S,j} = h_{S,j}^L + q_{S,j} \left(h_{S,j}^V - h_{S,j}^L \right) = h_{S,j}^L + q_{S,j} \Delta h_{S,j}, \tag{A.3.4}$$

where the superscripts L and V indicate saturated liquid and vapor enthalpies of stream S. The thermal condition $q_{S,j}$ has the following ranges:

$$
\begin{aligned}
&q_{S,j} < 0 : \text{stream } S \text{ is subcooled liquid} \\
&q_{S,j} = 0 : \text{stream } S \text{ is saturated liquid} \\
&0 < q_{S,j} < 1 : \text{stream } S \text{ is partially flashed} \\
&q_{S,j} = 1 : \text{stream } S \text{ is saturated vapor} \\
&q_{S,j} > 1 : \text{stream } S \text{ is superheated vapor}
\end{aligned}
$$

The left-hand side of Eq. (A.3.1) can be expanded as follows

$$
\begin{aligned}
\frac{dM_0 u_0}{dt} &\overset{\text{(A.3.2)}}{=} \frac{dM_0 h_{L,0}}{dt} \\
&\overset{\text{(A.3.4)}}{=} \frac{dM_0 h_{L,0}^L}{dt} + \frac{dM_0 q_{L,0} \Delta h_{L,0}}{dt} \\
&\overset{\text{(A.3.3)}}{=} \sum_{i=1}^{q} h_{L,0,i}^L \frac{dM_0 x_{i,0}}{dt} + \frac{dM_0 q_{L,0} \Delta h_{L,0}}{dt} \\
&= \sum_{i=1}^{q} h_{L,0,i}^L \frac{dM_0 x_{i,0}}{dt} + M_0 \Delta h_{L,0} \frac{dq_{L,0}}{dt} + q_{L,0} \Delta h_{L,0} \frac{dM_0}{dt}.
\end{aligned} \tag{A.3.5}
$$

Combining Eqs. (A.3.5) and (A.3.1) we obtain

$$
\sum_{i=1}^{q} h_{L,0,i}^L \frac{dM_0 x_{i,0}}{dt} + M_0 \Delta h_{L,0} \frac{dq_{L,0}}{dt} + q_{L,0} \Delta h_{L,0} \frac{dM_0}{dt} = V_1 h_{V,1} - L_0 h_{L,0} - F_0 h_{F,0} + Q_0, \tag{A.3.6}
$$

which is equivalent to

$$
M_0 \frac{dq_{L,0}}{dt} = -\sum_{i=1}^{q} \frac{h_{L,0,i}^L}{\Delta h_{L,0}} \frac{dM_0 x_{i,0}}{dt} - q_{L,0} \frac{dM_0}{dt} + \frac{V_1 h_{V,1} - L_0 h_{L,0} - F_0 h_{F,0} + Q_0}{\Delta h_{L,0}}. \tag{A.3.7}
$$

Inserting the mass balance Eqs. (2.53a) and (2.53b) or Eqs. (2.54a) and (2.54b) in

Eq. (A.3.7) we obtain

$$\begin{aligned}
M_0\frac{dq_{L,0}}{dt} &= -\sum_{i=1}^{q}\frac{h^L_{L,0,i}}{\Delta h_{L,0}}\left(V_1 y_{i,1} - L_0 x_{i,0} - F_0 y_{i,0}\right) - q_{L,0}\left(V_1 - L_0 - F_0\right) + \\
&\quad \frac{V_1 h_{V,1} - L_0 h_{L,0} - F_0 h_{F,0} + Q_0}{\Delta h_{L,0}} \\
&\overset{(A.3.4)}{=} -\sum_{i=1}^{q}\frac{h^L_{L,0,i}}{\Delta h_{L,0}}\left(V_1 y_{i,1} - L_0 x_{i,0} - F_0 y_{i,0}\right) - q_{L,0}\left(V_1 - L_0 - F_0\right) + \\
&\quad \frac{V_1 h^V_{V,1}}{\Delta h_{L,0}} - \frac{L_0\left(h^L_{L,0} + q_{L,0}\Delta h_{L,0}\right)}{\Delta h_{L,0}} - \frac{F_0\left(h^L_{F,0} + q_{F,0}\Delta h_{F,0}\right)}{\Delta h_{L,0}} + \frac{Q_0}{\Delta h_{L,0}} \\
&= -q_{L,0}V_1 + q_{L,0}F_0 + \frac{V_1\Delta h_{L,0}}{\Delta h_{L,0}} - \frac{F_0 q_{F,0}\Delta h_{F,0}}{\Delta h_{L,0}} + \frac{Q_0}{\Delta h_{L,0}} \\
&\overset{\Delta h_{F,0}=\Delta h_{L,0}}{=} \left(1 - q_{L,0}\right)V_1 + \left(q_{L,0} - q_{F,0}\right)F_0 + \frac{Q_0}{\Delta h_{L,0}}. \qquad \text{(A.3.8)}
\end{aligned}$$

In a total condenser, the thermal conditions of the reflux and distillate flows are equal, i.e. $q_{L,0} = q_{F,0}$. So, the energy balance in Eq. (A.3.8) becomes

$$M_0\frac{dq_{L,0}}{dt} = \left(1 - q_{L,0}\right)V_1 + \frac{Q_0}{\Delta h_{L,0}}. \qquad \text{(A.3.9)}$$

In a partial condenser, the reflux flow is a saturated liquid and the distillate flow a saturated vapor, i.e. $q_{L,0} = 0$, $q_{F,0} = 1$. Therefore, the energy balance in Eq. (A.3.8) reduces to an algebraic equation

$$0 = V_1 - F_0 + \frac{Q_0}{\Delta h_{L,0}}. \qquad \text{(A.3.10)}$$

B Implementation of distillation libraries

B.1 Modeling environment

In order to manage the model equations in Sections 2.4.1, 2.4.2, and 3.2.2 each set of equations was implemented in gPROMS (Process Systems Enterprise, 1997-2013) and packaged for reuse. From our experience, using gPROMS accelerates implementation of the models by up to 5 times over an implementation in a high-level programming language, unfortunately at the price of flexibility. However, including external software allows us to partly overcome modeling obstacles resulting from the lack of flexibility. In what follows, we briefly describe the structure of two such external software programs, also termed as Foreign Objects, which are essential for complex distillation simulations. In addition, we comment on some implementational issues such as the model libraries and main numerical obstacles.

B.2 External software

Thermodynamic properties

Appropriate thermodynamic models are a prerequisite for distillation calculations with non-ideal mixtures (mainly required for calculations of enthalpies, boiling/dew temperatures, and vapor compositions). It is also desirable to have a large mixture database and be able to easily configure the mixtures in different simulation scenarios. gPROMS does not offer these possibilities, but the problem can be resolved through a Foreign Object with necessary features linked to the gPROMS models. The Foreign Object providing all thermodynamic calculations (PropsFO) was therefore implemented. Its principal schematic is shown in Fig. B.1.

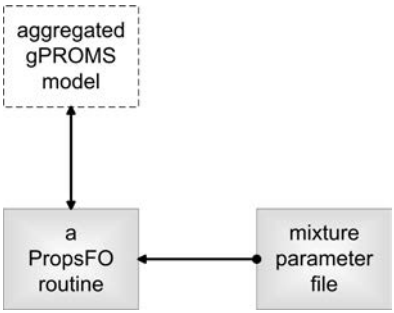

Figure B.1: Schematic of the PropsFO module calculating thermodynamic properties

Prior to the simulation, the mixture-defining parameters are stored in a file. This file is loaded during the model initialization and stored in main memory afterwards. Every function call initiated by the gPROMS model is then processed within the PropsFO while the corresponding function has access to the mixture parameters located in memory. The result is finally returned to the calling gPROMS model and gPROMS continues with the simulation.

It is worth noting that outsourcing functionality to the PropsFO is a very sophisticated way to perform rather complex thermodynamic calculations outside the gPROMS environment which simplifies the model code, introduces flexibility with regard to the mixture, and also helps to make simulations faster and more robust.

Data input

In gPROMS, models are initialized for simulation by explicitly setting each of the model's variables before the simulation starts. Explicit setting of the variables is appropriate for small models. In contrast, models of larger processes may have hundreds or even thousands of variables (cf. the ACBT process in Section 5.4). In these models, the (initial) values for variables might be listed in a file, e.g., as a result of a process design study, and have to be manually transferred from that file to the gPROMS model. It is, unfortunately, a laborious task which is prone to errors and results in a confusing list of variables in the gPROMS model, once the transfer of all variables is completed.

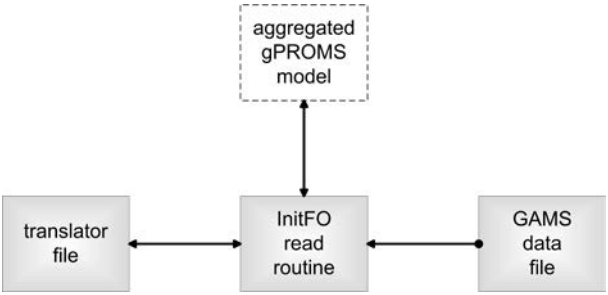

Figure B.2: Schematic of the initialization module InitFO

The initial values for our simulation studies in Sections 3.3.5 and 5.4 were stored in a large GAMS file (GAMS Development Corporation, 2013) which was created by Kraemer et al. (2009) in their process design study. To make model initialization easier to handle, the Foreign Object InitFO was implemented (Fig. B.2). InitFO has two important features. First, it loads a GAMS file with variables assumed to be in the GAMS output format and

stores it in main memory. Afterwards, InitFO can retrieve the value of any variable that has a string-identifier. Secondly, since gPROMS only allows passing numerical arguments to the functions, a one-to-one mapping from numerical values to string-identifiers is necessary to mediate between gPROMS and the variables in the GAMS file. This mapping is implemented in a so-called translator file. The whole workflow is then straightforward: during initialization, the gPROMS model passes the numerical identifier of a variable in the GAMS file to the "read"-function of the InitFO module. The "read"-function loads the GAMS file to the memory, "translates" the numerical identifier into its string-identifier by consulting the translator file, finds the identified variable by its name-string in the stored GAMS file, reads and returns the value of this variable to the gPROMS model.

Summing up, InitFO helps to write, structure and simplify the gPROMS code for model initialization. It allows FOR-loops, thus reducing code size and error rate. Furthermore, InitFO is very fast and therefore allows the reading of large data files.

B.3 Implementational issues

In order to conduct demanding case studies, well-implemented models are essential. These models rely on external software as outlined in the previous section, but beyond that, model libraries and numerical obstacles are especially worthy of consideration.

Distillation libraries

Consider Table B.1 showing the assignment of the equations to the different distillation-column parts which are partitioned into different libraries. These column parts are typically abstracted during the modeling process from a distillation column. That enables us to create libraries which form a basis for modeling variously arranged distillation columns, including the basic structure with one condenser, two sections, one feed tray, and one reboiler. Notice that distillation column parts for the plant replacement and the controller in our implementation are contained in different libraries to account for plant-model mismatch.

Remarks on numerics

In the past, working with complex simulations required a profound knowledge of both the simulated process and the numerical algorithms. Nowadays, process knowledge grows with one's experience in process simulation, and today's state-of-the-art simulation environments such as gPROMS hide major numerical problems from the user provided that he builds relatively simple, numerically well-behaved models. As soon as larger plants with a

Table B.1: Created libraries and corresponding equations

library unit	plant replacement	controller	observer
condenser	(2.45a) – (2.45d)	(2.53a) – (2.53c)	(2.53a) – (2.53c)
partial condenser	(2.46a) – (2.46e)	(2.54a) – (2.54e)	(2.54a) – (2.54e)
column section	(2.49a) – (2.49f)	(2.56a) – (2.56e)	(3.1a) – (3.1g)
feed tray	(2.47a) – (2.47f)	(2.55a) – (2.55d)	(2.55a) – (2.55d)
reboiler	(2.50a) – (2.50d)	(2.57a) – (2.57d)	(2.57a) – (2.57d)

large number of parameters and state variables are to be simulated, however, the situation might completely change.

One main reason for difficulties with numerics is that rigorous distillation models tend to be highly nonlinear. The principal sources of the nonlinearities according to Perry and Green (2008) are

- nonlinearity of the VLE,
- more than one liquid phase (not relevant for our case studies),
- a large number of stages,
- a high operating pressure,
- a very steep compositions/temperature profile, or
- various combinations of the above.

Another cause of numeric obstacles is a less transparent interaction between the model and solver parameters. Distillation column models comprising models in Sections 2.4.1 – 2.4.2 are differential algebraic equations (DAEs). It is well known that these require consistent initial values to start a simulation and may become stiff (Cameron et al., 1986). Besides, they often exhibit very nonlinear behavior. gPROMS offers a general purpose DAE solver (DASOLV) based on Backward Differentiation Formulas (BDF) capable of solving such highly nonlinear, stiff DAE-systems. If discontinuities appear, e.g., when the user applies a control action to any of the assigned variables, a nonlinear solver (in our case the Block Decomposition nonlinear Solver (BDNLSOL)) initiates the reinitialization of the DAE system (Process Systems Enterprise, 2009). However, the case study in Section 5.4 takes the reinitialization solver to the limit of what it can do.

We identified two typical situations in which the simulation can crash. The first very uncommon situation occurs if the DAE solver cannot fulfill the integration tolerances at

a certain point. This problem can usually be solved by changing the threshold values for the absolute and relative tolerances of the solver. The second situation is related to the reinitialization solver and concerns, from our experience, up to one per hundred reinitializations. In this case, changing the range of the relevant model variables or solver parameters sometimes solved the problem for the required simulation horizon but could provoke a crash during reinitialization at a later point. A very helpful technique for solving reinitialization problems is to avoid the usage of (some) selected algebraic variables, e.g. by filtering them (Kröner et al., 1997).

Models which possess a large number of differential variables and parameters are especially prone to the above numerical problems. This shows that linearized and, if necessary, reduced models should still be used in on-line applications to avoid most of the numerical problems.

C Simulation data

C.1 Parameters for prediction of activity coefficients and vapor pressures in ACBT mixture

The Wilson parameters $\lambda_{i,j}$ and liquid-phase molar volumes ν_i^L required in Eq. (2.14) for prediction of activity coefficients in an ACBT mixture were taken from Aspen Plus (Aspen Technology, Inc., 1981-2010). They are summarized in Table C.1. The corresponding

Table C.1: Wilson parameters for ACBT mixture: acetone ($i = 1$), chloroform ($i = 2$), benzene ($i = 3$), and toluene ($i = 4$).

$\lambda_{i,1}$	[-]	$\lambda_{i,2}$	[-]	$\lambda_{i,3}$	[-]	$\lambda_{i,4}$	[-]	ν_i^L	$[\mathrm{cm^3/mol}]$
$\lambda_{1,1}$:	0.0	$\lambda_{1,2}$:	28.8819	$\lambda_{1,3}$:	543.9352	$\lambda_{1,4}$:	356.0129	ν_1^L:	74.05
$\lambda_{2,1}$:	-484.3856	$\lambda_{2,2}$:	0.0	$\lambda_{2,3}$:	-161.8065	$\lambda_{2,4}$:	-365.8311	ν_2^L:	80.67
$\lambda_{3,1}$:	-182.5230	$\lambda_{3,2}$:	49.6010	$\lambda_{3,3}$:	0.0	$\lambda_{3,4}$:	377.9760	ν_3^L:	89.41
$\lambda_{4,1}$:	13.6840	$\lambda_{4,2}$:	552.1459	$\lambda_{4,3}$:	-354.9859	$\lambda_{4,4}$:	0.0	ν_4^L:	106.85

gas constant is $R = 1.98721\,\mathrm{cal/K\cdot mol}$, where $1\,\mathrm{cal} = 4.182\,\mathrm{J}$. The vapor pressure p_i^{sat} in Eq. (2.11) is calculated by Eq. (2.12); the required parameters $C_{i,1}, \ldots, C_{i,9}$ are summarized in Table C.2.

Table C.2: Parameters of the Extended Antoine equation for calculation of the vapor pressures in $[Pa]$ of acetone ($i = 1$), chloroform ($i = 2$), benzene ($i = 3$), and toluene ($i = 4$); the temperature bounds $C_{i,8}$ and $C_{i,9}$ are in $[K]$.

i	$C_{i,1}$	$C_{i,2}$	$C_{i,3}$	$C_{i,4}$	$C_{i,5}$	$C_{i,6}$	$C_{i,7}$	$C_{i,8}$	$C_{i,9}$
1	0.732391e2	-0.562684e4	0.0	0.625888e-2	-0.805705e1	0.127440e-16	6.0	274.597	508.1
2	0.494950e2	-0.490924e4	0.0	0.697118e-3	-0.404868e1	0.102370e-16	6.0	277.794	536.4
3	0.738624e2	-0.597044e4	0.0	0.553760e-2	-0.807976e1	0.661298e-17	6.0	293.361	562.1
4	0.712775e2	-0.641329e4	0.0	0.416630e-2	-0.750535e1	0.541998e-17	6.0	318.725	591.7

C.2 Parameters for prediction of activity coefficients and vapor pressures in MEW mixture

The Wilson parameters $\lambda_{i,j}$ and liquid-phase molar volumes ν_i^L required in Eq. (2.14) for prediction of activity coefficients in a methanol-ethanol-water (MEW) mixture are summarized in Table C.3. The corresponding gas constant is $R = 1.98721\,\mathrm{cal/K\cdot mol}$, where

Table C.3: Wilson parameters for MEW mixture: methanol ($i = 1$), ethanol ($i = 2$), and water ($i = 3$).

$\lambda_{i,1}$	[-]	$\lambda_{i,2}$	[-]	$\lambda_{i,3}$	[-]	ν_i^L	$[\mathrm{cm}^3/\mathrm{mol}]$
$\lambda_{1,1}$:	0.0	$\lambda_{1,2}$:	-148.2382	$\lambda_{1,3}$:	90.7566	ν_1^L:	40.46
$\lambda_{2,1}$:	342.6344	$\lambda_{2,2}$:	0.0	$\lambda_{2,3}$:	330.6937	ν_2^L:	58.36
$\lambda_{3,1}$:	440.0672	$\lambda_{3,2}$:	912.3767	$\lambda_{3,3}$:	0.0	ν_3^L:	18.05

$1\,\mathrm{cal} = 4.182\,\mathrm{J}$. The vapor pressure p_i^{sat} in Eq. (2.11) is calculated by Eq. (2.12); the required parameters $C_{i,1}, \ldots, C_{i,9}$ are summarized in Table C.4.

Table C.4: Parameters of the Extended Antoine equation for calculation of the vapor pressures in $[atm]$ of methanol ($i = 1$), ethanol ($i = 2$), and water ($i = 3$); the temperature bounds $C_{i,8}$ and $C_{i,9}$ are in $[K]$.

i	$C_{i,1}$	$C_{i,2}$	$C_{i,3}$	$C_{i,4}$	$C_{i,5}$	$C_{i,6}$	$C_{i,7}$	$C_{i,8}$	$C_{i,9}$
1	11.7190	-3482.6359	-40.1783	0.0	0.0	0.0	0.0	320.7613	384.6678
2	11.5907	-3405.2832	-57.3186	0.0	0.0	0.0	0.0	334.5338	398.4844
3	11.6281	-3783.5446	-47.4183	0.0	0.0	0.0	0.0	354.4922	425.0666

C.3 Regulatory control parameters

The regulatory control of the ACBT process depicted in Figure 1.1 (and of the same process with a different regulator numbering in Figure 5.3) includes several PI regulators. These PI regulators are specified by Eqs. (2.52a) – (2.52d). An anti-windup for the integral term was also implemented. The tuning parameters of the regulators in Figure 1.1 are given in Table C.5. Note that the correspondence between the regulator numberings in Figures 1.1 and 5.3 is shown in Table 5.1. The regulator inputs and outputs are restricted to lie within the given minimum and maximum values. Note that the pressure controllers PI 2 in column $C1$ and PI 17 in column $C3$ are not available in the models based on equations from Section 2.4.2 where the corresponding pressures are set constant. All PI controllers were tuned manually, where the setpoints were chosen to obtain as pure products as possible.

Table C.5: PI controller parameters

PID No.	Mode	Input min	Input max	Output min	Output max	Bias	Gain [-]	Reset time [s]	Setpoint
1	PI	0 mol	20 kmol	0 %	100 %	50 %	1	2000	10.5 kmol
2[1]	PI	0.95 bar	1.2 bar	-50 MJ/s	-40 MJ/s	-46.15916 MJ/s	10	5000	1.013 bar
3	PI	330 K	340 K	0 %	100 %	66 %	2	1000	331.1 K
4	PI	363.5 K	370 K	41 MJ/s	50 MJ/s	41 MJ/s	0.01	1000	364.2 K
5	PI	0 mol	20 kmol	0 %	100 %	50 %	0.1	2000	10.5 kmol
7	PI	0 mol/s	20 mol/s	0 %	100 %	70 %	1	100	70 %
8	PI	0 mol	20 kmol	0 %	100 %	54 %	2	1000	9 kmol
9	PI	385 K	395 K	45 MJ/s	60 MJ/s	51 MJ/s	0.5	100	385.5 K
10	PI	0 mol	50 kmol	0 %	100 %	55 %	3	100	9 kmol
11	PI	0 %	100 %	0 %	100 %	45 %	0.1	1000	50.5 %
12	PI	0.95 bar	1.1 bar	-60 MJ/s	-10 MJ/s	-33.9 MJ/s	10	100	1.013 bar
13	PI	0 mol	10 kmol	0 %	100 %	50 %	1	1000	3 kmol
14	PI	350 K	360 K	20 MJ/s	35 MJ/s	26.6 MJ/s	10	1000	357.9 K
15	PI	335 K	350 K	65 %	100 %	76 %	0.1	550	338.4 K
16	PI	0 mol	10 kmol	0 %	100 %	50 %	1	1000	3 kmol
17[1]	PI	0.9 bar	1.1 bar	-50 MJ/s	-30 MJ/s	-40 MJ/s	50	100	1.013 bar
R	ratio								

[1] available only in the plant replacement based on equations from Section 2.4.1;
in controller/observer models based on equations from Section 2.4.2, constant pressures are assumed.

C.4 Supervisory control parameters

The supervisory control layer consists of a DMPC outlined in Section 5.3.2. The DMPC tuning parameters were introduced in Eqs. (5.20a) – (5.20d). They are summarized in Table C.6 for the ACBT case study in Section 5.4. Note that the weighting matrices Q_y and Q_u are diagonal. Their elements scale with respect to the chosen input and output variables. The 4-tuples in $\mathbf{y}^{ref}$ (also in $\mathbf{y}^{lb}$ and $\mathbf{y}^{ub}$) refer to the concentrations of acetone, chloroform, benzene, and toluene given in mol/mol. The 5-tuples in $\mathbf{u}^{ref}$ (also in $\mathbf{u}^{lb}$, $\mathbf{u}^{ub}$,$\mathbf{du}^{lb}$, and $\mathbf{du}^{ub}$) refer to the setpoints of the PIDs $r1 - r5$ numbered as $3, 9, 14, 15,$ and 7 in Table C.5. The setpoint of PID 7 ($r5$), which regulates the recycle valve (see Figure 5.3), is specified as the fraction of the maximum flow rate. The DMPC sampling time is set to 100 s. Finally, the number of predicted and controlled samples is 100 and 3, respectively.

Table C.6: DMPC tuning parameters

parameter	value
weighting matrices	
Q_y	$1000 \cdot \mathrm{diag}([\left(\frac{1}{0.01}\right)^2, \left(\frac{1}{0.01}\right)^2, \left(\frac{1}{0.01}\right)^2, \left(\frac{1}{0.01}\right)^2], \ldots, [\left(\frac{1}{0.01}\right)^2, \left(\frac{1}{0.01}\right)^2, \left(\frac{1}{0.01}\right)^2, \left(\frac{1}{0.01}\right)^2]) \in \mathbb{R}^{4n_{\mathrm{pr}} \times 4n_{\mathrm{pr}}}$
Q_u	$\mathrm{diag}([\left(\frac{1}{0.05}\right)^2, \left(\frac{1}{0.05}\right)^2, \left(\frac{1}{0.01}\right)^2, \left(\frac{1}{0.01}\right)^2, \left(\frac{1}{0.002}\right)^2], \ldots, [\left(\frac{1}{0.05}\right)^2, \left(\frac{1}{0.05}\right)^2, \left(\frac{1}{0.01}\right)^2, \left(\frac{1}{0.01}\right)^2, \left(\frac{1}{0.002}\right)^2]) \in \mathbb{R}^{5n_{\mathrm{co}} \times 5n_{\mathrm{co}}}$
Q_{du}	$0 \in \mathbb{R}^{5n_{\mathrm{co}} \times 5n_{\mathrm{co}}}$
reference trajectories	
$\mathbf{y}^{ref}$	$([0.988, 0.98, 0.992, 0.99], \ldots, [0.988, 0.98, 0.992, 0.99])^T \in \mathbb{R}^{4n_{\mathrm{pr}}}$
$\mathbf{u}^{ref}$	$([331.2, 385.5, 357.5, 338.4, 0.7], \ldots, [331.2, 385.5, 357.5, 338.4, 0.7])^T \in \mathbb{R}^{5n_{\mathrm{co}}}$
bound trajectories	
$\mathbf{y}^{lb}$	$([0.97, 0.97, 0.97, 0.97], \ldots, [0.97, 0.97, 0.97, 0.97])^T \in \mathbb{R}^{4n_{\mathrm{pr}}}$
$\mathbf{y}^{ub}$	$([1, 1, 1, 1], \ldots, [1, 1, 1, 1])^T \in \mathbb{R}^{4n_{\mathrm{pr}}}$
$\mathbf{u}^{lb}$	$([330.5, 385, 350, 335, 0.6], \ldots, [330.5, 385, 350, 335, 0.6])^T \in \mathbb{R}^{5n_{\mathrm{co}}}$
$\mathbf{u}^{ub}$	$([332, 386, 359, 350, 0.8], \ldots, [332, 386, 359, 350, 0.8])^T \in \mathbb{R}^{5n_{\mathrm{co}}}$
$\mathbf{du}^{lb}$	$-0.01 \cdot ([5, 1, 5, 5, 1], \ldots, [5, 1, 5, 5, 1])^T \in \mathbb{R}^{5n_{\mathrm{co}}}$
$\mathbf{du}^{ub}$	$0.01 \cdot ([5, 1, 5, 5, 1], \ldots, [5, 1, 5, 5, 1])^T \in \mathbb{R}^{5n_{\mathrm{co}}}$
predicted, controlled samples and DMPC sampling time	
n_{pr}	100
n_{co}	3
Δt	100 s

C.5 Nominal design condition used in Section 3.3.5

The simulation study in Section 3.3.5 is based on the plant layout for the separation of an acetone-chloroform-benzene-toluene mixture shown in Fig. 1.1. The nominal condition for the distillation columns used in the study is specified in Table C.7. The column models are those from Section 2.4.2 and the choice of model parameters and specific flow rates is discussed in Section 2.4.5. The mixture parameters are summarized in Section C.1 and tuning parameters of the regulatory controllers are tabulated in Table C.5.

Note that the column $C1$ in the plant replacement has three sections and two feed trays; in Table C.7, section 1 refers to the column section between the feed $F1$ and condenser, section 2 refers to the section between the feeds $F2$ and $F1$, and section 3 refers to the section between the reboiler and feed $F2$. The columns $C2$ and $C3$ are basic columns each having two sections and a feed tray; section 1 refers to the rectifying section and section 2 refers to the stripping section. The observer models are also based on the models from Section 2.4.2. The observer correction term was introduced in Eq. (3.1a) from Section 3.2.2. The observer gain parameters α_i are given in the next to last row of Table C.7, while the last row of the table lists the tray numbers used to calculate temperature differences in the observer correction term. These parameters were tuned manually to make the observer as fast as possible and retain its convergence.

The parameters in Table C.7 are related to the model equations from Section 2.4.2 as follows. The number of theoretical stages in each column section gives the number of different values the variable j in Eqs. (2.56a) – (2.56e) may take. The distillate composition refers to the state variables $x_{1,0}$ (acetone), $x_{2,0}$ (chloroform), $x_{3,0}$ (benzene), and $x_{4,0}$ (toluene) in Eq. (2.53a) (total condenser) or Eq. (2.54a) (partial condenser), while the bottom composition refers to the reboiler state variables $x_{1,m+1}$ (acetone), $x_{2,m+1}$ (chloroform), $x_{3,m+1}$ (benzene), and $x_{4,m+1}$ (toluene) in Eq. (2.57a). Note that the concentration of toluene on stage j can be calculated by $x_{4,j} = 1 - x_{1,j} - x_{2,j} - x_{3,j}$. Similarly, the feed composition is related to the feed variables $z_{1,j}, z_{2,j}, z_{3,j}$, and $z_{4,j}$, while the feed flow rate is denoted by F_j in Eq. (2.55a). L_0 in Eq. (2.53a) is the reflux flow rate, while the boilup flow rate is V_{m+1} in Eq. (2.57c). The liquid holdup per stage refers to M_j^L in Eq. (2.56a), whereas the liquid holdups in condenser, reboiler and feed tray M_0^L, M_{m+1}^L, M_j^L are those in Eqs. (2.53a) – (2.53c), (2.57a) – (2.57b), and (2.55a). The condenser pressure p_0 is calculated by Eq. (2.53d), while the reboiler pressure p_{m+1} is calculated by Eq. (2.56e) in which the reboiler is assumed to be the $(m_{sec}+1)$-th stage of the column section above.

Table C.7: Plant replacement/observer data (nominal condition)

column	C1	C2	C3
number of theoretical stages [-]	section 1: 6 section 2: 5 section 3: 37	section 1: 11 section 2: 12	section 1: 15 section 2: 23
distillate composition [mol/mol] (acetone, chloroform, benzene, toluene)	(0.990, 0.006, 0.003, 0.001)	(0.005, 0.499, 0.496, 0.000)	(0.011, 0.982, 0.007, 0.000)
bottom composition [mol/mol] (acetone, chloroform, benzene, toluene)	(0.002, 0.171, 0.175, 0.652)	(0.000, 0.000, 0.009, 0.991)	(0.000, 0.016, 0.984, 0.000)
feed composition [mol/mol] (acetone, chloroform, benzene, toluene)	F1: (0.000, 0.000, 0.009, 0.991) F2: (0.25, 0.25, 0.25, 0.25)	(0.002, 0.171, 0.175, 0.652)	(0.005, 0.499, 0.496, 0.000)
feed flow rate [mol/s]	F1: 7 F2: 10	14.43	4.93
reflux flow rate [mol/s]	12.29	10.96	10.33
boilup flow rate [mol/s]	14.76	15.89	7.87
liquid holdup per stage [mol]	525	450	150
liquid holdup in condenser [kmol]	10.5	9	3
liquid holdup in reboiler [kmol]	10.5	9	3
liquid holdup in feed tray [mol]	525	450	150
pressure [bar]	condenser: 1.013 reboiler: 1.309	condenser: 1.013 reboiler: 1.171	condenser: 1.013 reboiler: 1.195
observer gain [-] $(\alpha_1, \alpha_2, \alpha_3)$	(0.0003, 0.0003, 0.0003)	(0.0, 0.0002, 0.0002)	(0.0, 0.0005, 0.0005)
stage number j_1, j_2, j_3 in Eq. (3.1a) [-]	2, 29, 46	2, 5, 18	2, 9, 36

C.6 Nominal design condition used in Section 5.4

The simulation study in Section 5.4 is based on the plant layout for the separation of an acetone-chloroform-benzene-toluene mixture shown in Fig. 5.3 (also in Fig. 1.1 without the layout partitioning). The study includes a plant-replacement model, a DMPC controller and a Lang-Gilles observer. The nominal condition for the distillation columns used in the study is summarized in Tables C.8 (controller/observer model) and C.9 (plant-replacement model). The parametrization of the distillation models and the specific flow rates in the columns are discussed in Section 2.4.5. The mixture parameters are summarized in Section C.1. The tuning parameters of the regulatory controllers are described in Appendix C.3 and those of the supervisory DMPC in Appendix C.4.

The controller/observer model equations are given in Section 2.4.2. The parameters in Table C.8 are related to these equations as explained in Section C.5. Note that the column $C1$ in the plant replacement has three sections and two feed trays; in Tables C.8 and C.9, section 1 refers to the column section between the feed $F1$ and condenser, section 2 to the section between the feeds $F2$ and $F1$, and section 3 to the section between the reboiler and the feed $F2$. The columns $C2$ and $C3$ are basic columns each having two sections and a feed tray; section 1 refers to the rectifying section and section 2 to the stripping section. The observer models are also based on the models from Section 2.4.2. The observer correction term was introduced in Eq. (3.1a) from Section 3.2.2. The observer gain parameters α_i are given in the next to last row of Table C.8, while the last row of the table lists the tray numbers used to calculate temperature differences in the observer correction term.

The plant-replacement model is based on equations from Section 2.4.1. The parameters in Table C.9 are related to the model equations as follows. The number of theoretical stages in each column section gives the number of different values the variable j in Eqs. (2.49a) – (2.49f) may take. The distillate composition refers to the state variables $x_{1,0}$ (acetone), $x_{2,0}$ (chloroform), $x_{3,0}$ (benzene), and $x_{4,0}$ (toluene) in Eq. (2.45a) (total condenser) or Eq. (2.46a) (partial condenser), while the bottom composition refers to the reboiler state variables $x_{1,m+1}$ (acetone), $x_{2,m+1}$ (chloroform), $x_{3,m+1}$ (benzene), and $x_{4,m+1}$ (toluene) in Eq. (2.50a). Note that the concentration of toluene on stage j can be calculated by $x_{4,j} = 1 - x_{1,j} - x_{2,j} - x_{3,j}$. Similarly, the feed composition is related to the feed variables $z_{1,j}, z_{2,j}, z_{3,j}$, and $z_{4,j}$, while the feed flow rate is denoted by F_j in Eq. (2.47a). L_0 in Eq. (2.45a) is the reflux flow rate, while the boilup flow rate is V_{m+1} in Eq. (2.50c). The liquid holdup per stage refers to $\breve{M}_j^L$ in Eq. (2.49d), whereas the holdups in condenser, reboiler and feed tray M_0^L, M_{m+1}^L, M_j^L are those in Eqs. (2.45a) – (2.45b), (2.50a) – (2.50b), and (2.47a) at the nominal condition. The condenser pressure p_0 is calculated by Eq. (2.45d), while the reboiler pressure p_{m+1} is calculated by Eq. (2.49f) in which the reboiler is assumed to be the $(m_{sec}+1)$-th stage of the column section above. The model parameters were determined according to Section 2.4.5.

Table C.8: Controller/observer data (nominal condition)

column	C1	C2	C3
number of theoretical stages [-]	section 1: 6 section 2: 5 section 3: 37	section 1: 11 section 2: 12	section 1: 15 section 2: 23
distillate composition [mol/mol] (acetone, chloroform, benzene, toluene)	(0.990, 0.006, 0.003, 0.001)	(0.005, 0.499, 0.496, 0.000)	(0.010, 0.983, 0.007, 0.000)
bottom composition [mol/mol] (acetone, chloroform, benzene, toluene)	(0.002, 0.171, 0.176, 0.651)	(0.000, 0.000, 0.009, 0.991)	(0.000, 0.016, 0.984, 0.000)
feed composition [mol/mol] (acetone, chloroform, benzene, toluene)	F1: (0.000, 0.000, 0.009, 0.991) F2: (0.25, 0.25, 0.25, 0.25)	(0.002, 0.171, 0.176, 0.651)	(0.005, 0.499, 0.496, 0.000)
feed flow rate [mol/s]	F1: 7 F2: 10	14.50	4.98
reflux flow rate [mol/s]	12.57	11.07	10.44
boilup flow rate [mol/s]	15.06	16.05	7.95
liquid holdup per stage [mol]	525	450	150
liquid holdup in condenser [kmol]	10.5	9	3
liquid holdup in reboiler [kmol]	10.5	9	3
liquid holdup in feed tray [mol]	525	450	150
pressure [bar]	condenser: 1.013 reboiler: 1.309	condenser: 1.013 reboiler: 1.171	condenser: 1.013 reboiler: 1.195
observer gain [-] $(\alpha_1, \alpha_2, \alpha_3)$	(0.0003, 0.0003, 0.0003)	(0.0, 0.0002, 0.0002)	(0.0, 0.0005, 0.0005)
stage number j_1, j_2, j_3 in Eq. (3.1a) [-]	2, 29, 46	2, 5, 18	2, 9, 36

Table C.9: Plant replacement data (nominal condition)

column	C1	C2	C3
number of theoretical stages [-]	section 1: 6 section 2: 5 section 3: 37	section 1: 11 section 2: 12	section 1: 15 section 2: 23
distillate composition [mol/mol] **(acetone, chloroform, benzene, toluene)**	(0.992, 0.005, 0.003, 0.000)	(0.008, 0.498, 0.494, 0.000)	(0.016, 0.979, 0.005, 0.000)
bottom composition [mol/mol] **(acetone, chloroform, benzene, toluene)**	(0.003, 0.171, 0.176, 0.650)	(0.000, 0.000, 0.010, 0.990)	(0.000, 0.006, 0.993, 0.001)
feed composition [mol/mol] **(acetone, chloroform, benzene, toluene)**	F1: (0.000, 0.000, 0.010, 0.990) F2: (0.25, 0.25, 0.25, 0.25)	(0.003, 0.171, 0.176, 0.650)	(0.008, 0.498, 0.494, 0.000)
feed flow rate [mol/s]	F1: 7 F2: 10	14.50	5.00
reflux flow rate [mol/s]	12.57	11.07	10.44
boilup flow rate [mol/s]	14.11	15.12	9.62
liquid holdup per stage [mol]	525	450	150
liquid holdup in condenser [kmol]	10.5	9	3
liquid holdup in reboiler [kmol]	10.5	9	3
liquid holdup in feed tray [mol]	525	450	150
pressure [bar]	condenser: 1.013 reboiler: 1.309	condenser: 1.013 reboiler: 1.171	condenser: 1.013 reboiler: 1.195

D Auxiliary theorems

In this section we recall results from other authors.

Theorem D.1 (cf. Golub and Van Loan (1996)). *Let $Q^H AQ = D + R$ be a Schur decomposition of $A \in \mathbb{C}^{n,n}$ with a diagonal matrix D and a strictly upper triangular matrix R. Moreover, let E be an arbitrary matrix. If $\mu \in \sigma(A+E)$ and p is the smallest positive integer such that $|R|^p = 0$, then*

$$\min_{\lambda \in \sigma(A)} |\lambda - \mu| \leq \max(\theta, \theta^{1/p})$$

where

$$\theta = \|E\|_2 \sum_{k=0}^{p-1} \|R\|_2^k ,$$

$\sigma(A+E)$ denotes the spectrum of $A+E$, and $\|\cdot\|_2$ the spectral norm.

Our convergence analysis, summarized in Theorems 1 and 2, is based upon a theorem derived by Perron (1929) which follows below. We use a slightly different notation for convenience. Note that the specific norms are not essential due to the equivalence of norms in finite dimensional spaces.

Theorem D.2 (cf. Perron (1929)). *Let the system be given as*

$$\dot{y} = Ay + f(y,t), \quad y(0) = y_0,$$

where f is continuous in $\|y\|_\infty \leq \delta$, $t \geq 0$ for a real $\delta > 0$. If (i) all eigenvalues of A have negative real parts and (ii)

$$\|f(y,t)\|_\infty \leq K \|y\|_1 ,$$

for some constant $K > 0$, all $\|y\|_\infty \leq \delta$, all t, and (iii)

$$\forall \varepsilon > 0 \exists \delta > 0, t_e > 0 \colon \ \|f(y,t)\|_\infty \leq \varepsilon \|y\|_1 , \forall \|y\|_\infty \leq \delta, t \geq t_e$$

then every solution y with sufficiently small $\|y_0\|_\infty$ exists in $[0,\infty)$ and the solution $y = 0$ is asymptotically stable.

The stability concept in Lyapunov's sense for autonomous systems is not directly applicable to non-autonomous systems. However, $\mathcal{K}$-class functions allow us to overcome this obstacle.

Definition D.1 (cf. Liao et al. (2007)). *If a continuous function $\phi : [0,a) \subseteq \mathbb{R}^+ \to \mathbb{R}^+$, where $\mathbb{R}^+ = \{x \in \mathbb{R} \mid x \geq 0\}$ is the set of non-negative real numbers, is monotonically strictly increasing, and $\phi(0) = 0$, we call ϕ a $\mathcal{K}$-class function, denoted by $\phi \in \mathcal{K}$.*

Theorem D.3 (cf. Chen (2005)). *If there exist functions $V : \mathcal{D} \times [t_0, \infty) \to \mathbb{R},\ (x,t) \mapsto V(x,t)$ and $\beta(\cdot), \gamma(\cdot), \delta(\cdot) \in \mathcal{K}$ ($\mathcal{K}$ as in Definition D.1), such that*

1. *$V(0, t_0) = 0$,*
2. *$V(x,t) > 0$ for all $x \neq 0$ in $\mathcal{D}$ and all $t \geq t_0$,*
3. *$\beta(\|x\|) \leq V(x,t) \leq \gamma(\|x\|)$ for all $t \geq t_0$,*
4. *$\dfrac{dV(x,t)}{dt} \leq -\delta(\|x\|) \leq 0$ for all $t \geq t_0$.*

Then, the system

$$\dot{x} = f(x,t),\ x(t_0) = x_0 \in \mathbb{R}^n,$$

where $f : \mathcal{D} \times [0, \infty) \to \mathbb{R}^n$ is continuously differentiable in a neighborhood of the origin, $\mathcal{D} \subseteq \mathbb{R}^n$, with a given initial state $x_0 \in \mathcal{D}$, is asymptotically stable about its zero equilibrium.

In the proof of Theorem 3 we exploit Theorem D.3 whose item 3 is shown using the following well-known result.

Theorem D.4 (cf. Courant-Fischer Minimax Theorem, Golub and Van Loan (1996)). *If $A \in \mathbb{R}^{n \times n}$ is symmetric, then*

$$\lambda_k(A) = \max_{\dim(S)=k} \min_{0 \neq y \in S} \frac{y^T A y}{y^T y},$$

where S with $dim(S) = k$ refers to any k-dimensional subspace of $\mathbb{R}^{n \times n}$, $\lambda_k(A)$ are the eigenvalues of A sorted as $\lambda_n(A) \leq \cdots \leq \lambda_2(A) \leq \lambda_1(A)$ and $k = 1, \ldots, n$.

The following implicit function theorem is a standard tool in analysis which we use to derive the system matrix A_e in Eqs. (5.5) from Section 5.3.2.

Theorem D.5 (cf. Walter (1995)). *Let $G \subset \mathbb{R}^{n+m}$ be an open set and $f : G \to \mathbb{R}^m$ be an implicit continuously differentiable function with the coordinates $x \in \mathbb{R}^n$ and $y \in \mathbb{R}^m$. Suppose for a point $(\xi, \eta) \in G$ that*

$$f(\xi, \eta) = 0 \text{ and } \det \frac{\partial f}{\partial y}(\xi, \eta) \neq 0.$$

Then there exist open sets $U = U(\xi) \subset \mathbb{R}^n$, $V = V(\eta) \subset \mathbb{R}^m$ and a unique continuously differentiable function $g : U \to V$ such that

$$f(x, g(x)) = 0 \text{ and } f(x,y) \neq 0 \text{ for } y \neq g(x),\ (x,y) \in U \times V \subset G.$$

Furthermore, the partial derivative of g is given by

$$\frac{\partial g}{\partial x} = -\left(\frac{\partial f}{\partial y}\right)^{-1} \frac{\partial f}{\partial x}.$$

Bibliography

Z. Abdullah, N. Aziz, and Z. Ahmad. Nonlinear modelling application in distillation column. *Chemical Product and Process Modeling*, 2(3):Article 12, 2007.

D. S. Abrams and J. M. Prausnitz. Statistical thermodynamics of liquid mixtures: A new expression for the excess Gibbs energy of partly or completely miscible systems. *AIChE Journal*, 21(1):116–128, 1975.

AIChE. *Bubble-Tray: Design Manual Prediction of Fractionation Efficiency.* A.I.Ch.E. Manual. American Institute of Chemical Engineers, 1958.

J. Álvarez and C. Fernández. Geometric estimation of nonlinear process systems. *Journal of Process Control*, 19(2):247–260, 2009.

M. Amrhein, F. Allgöwer, and W. Marquardt. Validation and analysis of linear distillation models for controller design. In *European Control Conference, ECC'93*, pages 221–232, 1993.

Aspen Technology, Inc. *Aspen Physical Property System, Physical Property Models.* www.aspentech.com, 1981-2010. V7.2.

Aspen Technology, Inc. *Aspen Plus®*. www.aspentech.com, 1981-2011. V7.3.

K. Åström and B. Wittenmark. *Computer-Controlled Systems: Theory and Design, Third Edition.* Dover Books on Electrical Engineering. Dover Publications, 2011.

P. T. Atteridg, E. J. Lemieux, W. C. Schreiner, and R. A. Sundback. Entrainment from bubble-cap trays. *AIChE Journal*, 2(1):3–12, 1956.

R. Baratti, A. Bertucco, A. D. Rold, and M. Morbidelli. Development of a composition estimator for binary distillation columns. application to a pilot plant. *Chemical Engineering Science*, 50(10):1541–1550, 1995.

R. Baratti, S. Corti, and A. Servida. A feedforward control strategy for distillation columns. *Artificial Intelligence in Engineering*, 11(4):405–412, 1997.

R. Baratti, A. Bertucco, A. D. Rold, and M. Morbidelli. A composition estimator for multicomponent distillation columns – development and experimental test on ternary mixtures. *Chemical Engineering Science*, 53(20):3601–3612, 1998.

M. Barolo and F. Berto. Composition control in batch distillation: Binary and multicomponent mixtures. *Industrial & Engineering Chemistry Research*, 37(12):4689–4698, 1998.

A. Benallou, D. E. Seborg, and D. A. Mellichamp. Dynamic compartmental models for separation processes. *AIChE Journal*, 32(7):1067–1078, 1986.

M. Benedict, G. B. Webb, and L. C. Rubin. An empirical equation for thermodynamic properties of light hydrocarbons and their mixtures I. Methane, ethane, propane and n-butane. *The Journal of Chemical Physics*, 8:334–345, 1940.

A. Bettoni, M. Bravi, and A. Chianese. Inferential control of a sidestream distillation column. *Computers & Chemical Engineering*, 23(11–12):1737–1744, 2000.

J. Birk. *Rechnergestützte Analyse und Lösung nichtlinearer Beobachtungsaufgaben*. Number 294 in Fortschritt-Berichte VDI / 8. VDI-Verlag, Düsseldorf, 1992.

P. P. Biswas, S. Ray, and A. N. Samanta. Nonlinear control of high purity distillation column under input saturation and parametric uncertainty. *Journal of Process Control*, 19(1):75–84, 2009.

U. Block and B. Hegner. Development and application of a simulation model for three-phase distillation. *AIChE Journal*, 22(3):582–589, 1976.

H. H. J. Bloemen, C. T. Chou, T. J. J. van den Boom, V. Verdult, M. Verhaegen, and T. C. Backx. Wiener model identification and predictive control for dual composition control of a distillation column. *Journal of Process Control*, 11(6):601–620, 2001.

E. Bristol. On a new measure of interaction for multivariable process control. *IEEE Transactions on Automatic Control*, 11(1):133–134, 1966.

E. Brizuela, M. Uria, and R. Lamanna. Predictive control of a multi-component distillation column based on neural networks. In *Proceedings of the 1996 International Workshop on Neural Networks for Identification, Control, Robotics, and Signal/Image Processing*, NICROSP '96, pages 270–278, Washington, DC, USA, 1996. IEEE Computer Society.

P. S. Buckley. *Techniques of process control*. Wiley & Sons, 1964.

P. S. Buckley, W. L. Luyben, and J. P. Shunta. *Design of Distillation Column Control Systems*. Edward Arnold, London, 1985.

I. T. Cameron, C. A. Ruiz, and R. Gani. A generalized model for distillation columns – II: Numerical and computational aspects. *Computers & Chemical Engineering*, 10(3): 199–211, 1986.

E. Castellanos-Sahagún and J. Alvarez. Decentralized cascade control of binary distillation columns. *Proceedings of the 2004 American Control Conference*, 4:3556–3561, 2004.

G. Chen. Stability of nonlinear systems. In *Encyclopedia of RF and Microwave Engineering*, pages 4881–4896. John Wiley & Sons, Inc., 2005.

Y. S. Cho and B. Joseph. Reduced-order steady-state and dynamic models for separation processes. Part I. Development of the model reduction procedure. *AIChE Journal*, 29 (2):261–269, 1983.

Y. S. Choe and W. L. Luyben. Rigorous dynamic models of distillation columns. *Industrial & Engineering Chemistry Research*, 26(10):2158–2161, 1987.

T. Damartzis and P. Seferlis. Optimal design of staged three-phase reactive distillation columns using nonequilibrium and orthogonal collocation models. *Industrial & Engineering Chemistry Research*, 49(7):3275–3285, 2010.

F. Deza and J. Gauthier. Nonlinear observers for distillation columns. In *Proceedings of the 30th IEEE Conference on Decision and Control*, volume 2, pages 1492–1493, 1991.

M. Diehl, R. Findeisen, S. Schwarzkopf, I. Uslu, F. Allgöwer, H. G. Bock, E. D. Gilles, and J. P. Schlöder. An efficient algorithm for nonlinear model predictive control of large-scale systems. Part II: Experimental evaluation for a distillation column. *at - Automatisierungstechnik*, 51(1):22–29, 2003.

J. J. Downs and S. Skogestad. An industrial and academic perspective on plantwide control. *Annual Reviews in Control*, 35(1):99–110, 2011.

H. G. Drickamer and J. R. Bradford. Overall plate efficiency of commercial hydrocarbon fractionating columns as a function of viscosity. *Transactions of American Institute of Chemical Engineers*, 39:319–360, 1943.

D. Elixmann, J. Puschke, H. Scheu, R. Schneider, I. Wolf, and W. Marquardt. A software environment for economic NMPC and dynamic real-time optimization of chemical processes. *Automatisierungstechnik : at*, 62(2, SI):150–161, 2014.

J. R. Fair, H. R. Null, and W. L. Bolles. Scale-up of plate efficiency from laboratory Oldershaw data. *Industrial & Engineering Chemistry Process Design and Development*, 22(1):53–58, 1983.

R. J. Forbes. *A short history of the art of distillation*. E. J. Brill, Leiden, Netherlands, 1970.

L. Fortuna, S. Graziani, and M. G. Xibilia. Soft sensors for product quality monitoring in debutanizer distillation columns. *Control Engineering Practice*, 13(4):499–508, 2005.

A. S. Foss. Critique of chemical process control theory. *AIChE Journal*, 19(2):209–214, 1973.

B. A. Foss, B. Lohmann, and W. Marquardt. A field study of the industrial modeling process. *Journal of Process Control*, 8(5-6):325–338, 1998.

A. Fredenslund, R. L. Jones, and J. M. Prausnitz. Group-contribution estimation of activity coefficients in nonideal liquid mixtures. *AIChE Journal*, 21(6):1086–1099, 1975.

GAMS Development Corporation. *GAMS*. www.gams.com, 2013.

R. Gani, C. A. Ruiz, and I. T. Cameron. A generalized model for distillation columns – I. Model description and applications. *Computers & Chemical Engineering*, 10 (3): 181–198, 1986.

R. Gani, T. S. Jepsen, and E. S. Pérez-Cisneros. A generalized reactive separation unit model. Modelling and simulation aspects. *Computers & Chemical Engineering*, 22, Supplement 1(0):363–370, 1998. European Symposium on Computer Aided Process Engineering 8.

M. Gerdin. Local identifiability and observability of nonlinear differential-algebraic equations. In *14th IFAC Symposium on System Identification, 2006*. Elsevier Science Ltd, 2006.

E. Gilles and B. Retzbach. Reduced models and control of distillation columns with sharp temperature profiles. *IEEE Transactions on Automatic Control*, 28(5):628–630, 1983.

G. H. Golub and C. F. Van Loan. *Matrix computations (3rd ed.)*. Johns Hopkins University Press, Baltimore, MD, USA, 1996.

J. C. Gómez and E. Baeyens. Identification of block-oriented nonlinear systems using orthonormal bases. *Journal of Process Control*, 14(6):685–697, 2004.

G. C. Goodwin, M. E. Salgado, and E. I. Silva. Time-domain performance limitations arising from decentralized architectures and their relationship to the RGA. *International Journal of Control*, 78(13):1045–1062, 2005.

S. Grüner, S. Schwarzkopf, I. Uslu, A. Kienle, and E. D. Gilles. Nonlinear model predictive control of multicomponent distillation columns using wave models. *International Symposium on Advanced Control of Chemical Processes (ADCHEM), Hong Kong*, 2004.

T. Guo, J. Lu, W. Xiang, Y. Guo, and K. Wu. Dynamic modeling and control of the air separation unit in an IGCC power plant. *2009 International Conference on Sustainable Power Generation and Supply*, pages 1–7, 2009.

K. E. Häggblom. Modeling of flow dynamics for control of distillation columns. In *American Control Conference*, pages 785–790, 1991.

J. Hahn and T. F. Edgar. An improved method for nonlinear model reduction using balancing of empirical gramians. *Computers & Chemical Engineering*, 26(10):1379–1397, 2002.

C. Hall. *Laws and Models: Science, Engineering, and Technology*. CRC Press, 1999.

L. Hammarström, K. Waller, and K. Fagervik. On modeling accuracy for multivariable distillation control. *Chemical Engineering Communications*, 19(1-3):77–90, 1982.

M. Han and S. Park. Control of high-purity distillation column using a nonlinear wave theory. *AIChE Journal*, 39(5):787–796, 1993.

M. Headley. Guidelines for selecting the proper valve characteristic. *Valve Magazine*, Spring, 2003.

A. Higler, R. Chande, R. Taylor, R. Baur, and R. Krishna. Nonequilibrium modeling of three-phase distillation. *Computers & Chemical Engineering*, 28(10):2021 – 2036, 2004.

D. Himmelblau. *Fault detection and diagnosis in chemical and petrochemical processes*. Chemical engineering monographs. Elsevier Scientific Pub. Co., 1978.

G. M. Howard. Unsteady state behavior of multicomponent distillation columns: Part I: Simulation. *AIChE Journal*, 16(6):1022–1029, 1970.

IPCOS NV. *IPCOS OPC Server*. www.ipcos.com, 2013.

A. H. Jazwinski. *Stochastic Processes and Filtering Theory*. Academic Press, New York, 1970.

N. Jensen, D. G. Fisher, and S. L. Shah. Interaction analysis in multivariable control systems. *AIChE Journal*, 32(6):959–970, 1986.

B. Joseph and C. Brosilow. Inferential control of processes: Part III. Construction of optimal and suboptimal dynamic estimators. *AIChE Journal*, 24(3):500–509, 1978.

R. E. Kalman. A new approach to linear filtering and prediction problems. *Transactions of the ASME–Journal of Basic Engineering*, 82(Series D):35–45, 1960.

M. Kano and M. Ogawa. The state of the art in chemical process control in Japan: good practice and questionnaire survey. *Journal of Process Control*, 20(9):969 – 982, 2010.

M. Kano, K. Miyazaki, S. Hasebe, and I. Hashimoto. Inferential control system of distillation compositions using dynamic partial least squares regression. *Journal of Process Control*, 10(2-3):157–166, 2000.

M. Kano, N. Showchaiya, S. Hasebe, and I. Hashimoto. Inferential control of distillation compositions: selection of model and control configuration. *Control Engineering Practice*, 11(8):927–933, 2003.

A. Kienle. Low-order dynamic models for ideal multicomponent distillation processes using nonlinear wave propagation theory. *Chemical Engineering Science*, 55(10):1817–1828, 2000.

H. Z. Kister. *Distillation Operation*. McGraw-Hill, 1990.

H. Z. Kister. *Distillation Design*. McGraw-Hill, 1992.

H. Z. Kister. Can we believe the simulation results? *Chemical Engineering Progress*, 98 (10):52–58, 2002.

K. T. Klemola. *Tray Efficiency Prediction of an Industrial Distillation Column*. Acta Polytechnica Scandinavica. Finnish Academy of Technology, 1997.

H. A. Kooijman and R. Taylor. *The ChemSep Book*. H.A. Kooijman and R. Taylor, 2000.

K. Kraemer, S. Kossack, and W. Marquardt. Efficient optimization-based design of distillation processes for homogeneous azeotropic mixtures. *Industrial & Engineering Chemistry Research*, 48(14):6749–6764, 2009.

R. Krishnamurthy and R. Taylor. A nonequilibrium stage model of multicomponent separation processes. Part I: Model description and method of solution. *AIChE Journal*, 31 (3):449–456, 1985.

A. Kröner, W. Marquardt, and E. D. Gilles. Getting around consistent initialization of DAE systems? *Computers & Chemical Engineering*, 21(2):145–158, 1997.

A. Kumar and P. Daoutidis. Nonlinear model reduction and control for high-purity distillation columns. *Industrial & Engineering Chemistry Research*, 42(20):4495–4505, 2003.

L. Lang and E. D. Gilles. Nonlinear observers for distillation columns. *Computers & Chemical Engineering*, 14(11):1297–1301, 1990.

T. Larsson and S. Skogestad. Plantwide control - a review and a new design procedure. *Modelling, Identification and Control*, 21(4):209–240, 2000.

R. Levy, A. Foss, and E. Green. Response modes of a binary distillation column. *Industrial & Engineering Chemistry Fundamentals*, 8:765–776, 1969.

W. K. Lewis and G. L. Matheson. Studies in distillation. *Industrial & Engineering Chemistry*, 24(5):494–498, 1932.

W. K. Lewis and W. G. Whitman. Principles of gas absorption. *Industrial & Engineering Chemistry*, 16(12):1215–1220, 1924.

W. K. Lewis Jr. Rectification of binary mixtures. *Industrial & Engineering Chemistry*, 28 (4):399–402, 1936.

X. Liao, L. Wang, and P. Yu. *Stability of Dynamical Systems*, volume 5 of *Monograph Series on Nonlinear Science and Complexity*. Elsevier Science, 2007.

A. Linhart and S. Skogestad. Computational performance of aggregated distillation models. *Computers & Chemical Engineering*, 33(1):296–308, 2009.

D. G. Luenberger. Observing the state of a linear system. *IEEE Transactions on Military Electronics*, 8(2):74–80, 1964.

M. L. Luyben, B. D. Tyreus, and W. L. Luyben. Plantwide control design procedure. *AIChE Journal*, 43(12):3161–3174, 1997.

W. L. Luyben. Derivation of transfer functions for highly nonlinear distillation columns. *Industrial & Engineering Chemistry Research*, 26(12):2490–2495, 1987.

W. L. Luyben, editor. *Practical Distillation Control*. Van Nostrand Reinhold, 1992.

W. Marquardt. *Nichtlineare Wellenausbreitung – Ein Weg zu reduzierten dynamischen Modellen von Stofftrennprozessen*. Number 161 in Fortschritt-Berichte VDI / 8. VDI-Verlag, Düsseldorf, 1988.

W. Marquardt. Nonlinear model reduction for optimization based control of transient chemical processes. In *Proceedings of CPC 6 (pp. 30–60), Tucson, Arizona*, 2001.

W. Marquardt and M. Amrhein. Development of a linear distillation model from design data for process control. *Computers & Chemical Engineering*, 18:349–353, 1994.

T. J. McAvoy and Y. H. Wang. Survey of recent distillation control results. *ISA Transactions*, 25:5–21, 1986.

W. L. McCabe and E. W. Thiele. Graphical design of fractionating columns. *Industrial & Engineering Chemistry*, 17(6):605–611, 1925.

T. Mejdell and B.-O. Andersson. Using temperature profile for product quality estimation on a distillation column. *ISA Transactions*, 33(1):27 – 34, 1994.

T. Mejdell and S. Skogestad. Estimation of distillation compositions from multiple temperature measurements using partial-least-squares regression. *Industrial & Engineering Chemistry Research*, 30(12):2543–2555, 1991a.

T. Mejdell and S. Skogestad. Composition estimator in a pilot-plant distillation column using multiple temperatures. *Industrial & Engineering Chemistry Research*, 30(12): 2555–2564, 1991b.

T. Mejdell and S. Skogestad. Output estimation using multiple secondary measurements: High-purity distillation. *AIChE Journal*, 39(10):1641–1653, 1993.

M. Morari. Integrated plant control: a solution at hand or a research topic for the next decade? In *Proc. of Second international conference on chemical process control (CPC-2)*, 1982.

N. P. Müller and H. Segura. An overall rate-based stage model for cross flow distillation columns. *Chemical Engineering Science*, 55(13):2515–2528, 2000.

E. V. Murphree. Rectifying column calculations with particular reference to N component mixtures. *Industrial and Engineering Chemistry*, 17:747–750, 1925.

S. Nugroho, Y. Y. Nazaruddin, and H. A. Tjokronegoro. Non-linear identification of aqueous ammonia binary distillation column based on simple Hammerstein model. In *5th Asian Control Conference*, volume 1, pages 118–123, 2004.

H. E. O'Connell. Plate efficiency of fractionating columns and absorbers. *Transactions of American Institute of Chemical Engineers*, 42:741–755, 1946.

R. M. Oisiovici and S. L. Cruz. State estimation of batch distillation columns using an extended Kalman filter. *Chemical Engineering Science*, 55(20):4667–4680, 2000.

R. M. Oisiovici and S. L. Cruz. Inferential control of high-purity multicomponent batch distillation columns using an extended Kalman filter. *Industrial & Engineering Chemistry Research*, 40(12):2628–2639, 2001.

M. J. Olanrewaju and M. A. Al-Arfaj. Estimator-based control of reactive distillation system: Application of an extended Kalman filtering. *Chemical Engineering Science*, 61 (10):3386–3399, 2006.

M. J. Olanrewaju, B. Huang, and A. Afacan. Development of a simultaneous continuum and noncontinuum state estimator with application on a distillation process. *AIChE Journal*, 58(2):480–492, 2012.

I. Olsen, G. O. Endrestøl, and T. Sira. A rigorous and efficient distillation column model for engineering and training simulators. *Computers & Chemical Engineering*, 21(0): 193–198, 1997.

Ž. Olujić, M. Jödecke, A. Shilkin, G. Schuch, and B. Kaibel. Equipment improvement trends in distillation. *Chemical Engineering and Processing: Process Intensification*, 48 (6):1089–1104, 2009.

A. Opler and R. G. Heitz. Punched card calculation of six-component distillation columns with heat balancing. *Industrial & Engineering Chemistry*, 43(11):2465–2471, 1951.

M. Osman and M. Ramasamy. Neural network based soft sensor for inferential control of a binary distillation column. *Journal of Applied Sciences*, 10:2558–2564, 2010.

G. Pannocchia and A. Brambilla. How to use simplified dynamics in model predictive control of superfractionators. *Industrial & Engineering Chemistry Research*, 44(8):2687–2696, 2005.

R. K. Pearson. Selecting nonlinear model structures for computer control. *Journal of Process Control*, 13:1–26, 2003.

R. K. Pearson. Nonlinear empirical modeling techniques. *Computers & Chemical Engineering*, 30(10-12):1514–1528, 2006.

R. K. Pearson and M. Pottmann. Gray-box identification of block-oriented nonlinear models. *Journal of Process Control*, 10(4):301–315, 2000.

D.-Y. Peng and D. B. Robinson. A new two-constant equation of state. *Industrial & Engineering Chemistry Fundamentals*, 15(1):59–64, 1976.

O. Perron. Über Stabilität und asymptotisches Verhalten der Lösungen eines Systems endlicher Differenzengleichungen. *Journal für die reine und angewandte Mathematik (Crelles Journal)*, 1929(161):41–64, 1929.

R. H. Perry and D. W. Green, editors. *Perry's Chemical Engineers' Handbook*, volume 8. McGraw-Hill, 2008.

W. Peters, Jr. The efficiency and capacity of fractionating columns. *Industrial and Engineering Chemistry*, 14(6):476–479, 1922.

Process Systems Enterprise. *gPROMS*. www.psenterprise.com/gproms, 1997-2013.

Process Systems Enterprise. *gPROMS Model Developer Guide, Release v3.2.0*. www.psenterprise.com/gproms, 2009.

E. Quintero-Marmol, W. L. Luyben, and C. Georgakis. Application of an extended Luenberger observer to the control of multicomponent batch distillation. *Industrial & Engineering Chemistry Research*, 30(8):1870–1880, 1991.

O. Rademaker, J. E. Rijnsdorp, and A. Maarleveld. *Dynamics and Control of Continuous Distillation Units*. Elsevier Science Inc., New York, NY, USA, 1975.

O. Redlich and J. N. S. Kwong. On the thermodynamics of solutions. V. An equation of state. Fugacities of gaseous solutions. *Chemical Reviews*, 44(1):233–244, 1949.

H. Renon and J. M. Prausnitz. Local compositions in thermodynamic excess functions for liquid mixtures. *AIChE Journal*, 14(1):135–144, 1968.

B. Retzbach. *Mathematische Modelle von Destillationskolonnen zur Synthese von Regelungskonzepten*. Number 126 in Fortschritt-Berichte VDI / 8. VDI-Verlag, Düsseldorf, 1986.

B. Roffel, B. H. Betlem, and R. de Blouw. A comparison of the performance of profile position and composition estimators for quality control in binary distillation. *Computers & Chemical Engineering*, 27(2):199–210, 2003.

J. Rommes and N. Martins. Efficient computation of multivariable transfer function dominant poles using subspace acceleration. *IEEE Transactions on Power Systems*, 21(4): 1471–1483, 2006.

J. A. Rossiter. *Model-Based Predictive Control: A Practical Approach*. CRC Press LLC, Boca Raton, FL, first edition, 2004.

H. Sadeghifar. An applicable method for efficiency estimation of operating tray distillation columns and its comparison with the methods utilized in HYSYS and Aspen Plus. *Heat and Mass Transfer*, 51(10):1393–1402, 2015.

A. A. Safavi and J. A. Romagnoli. Application of wave-nets to modelling and optimisation of a multidimensional chemical process. In *IEEE International Conference on Neural Networks*, volume 4, pages 1724–1728, 1995.

A. A. Safavi, A. Nooraii, and J. A. Romagnoli. A hybrid model formulation for a distillation column and the on-line optimisation study. *Journal of Process Control*, 9(2):125–134, 1999.

R. Scattolini. Architectures for distributed and hierarchical model predictive control – a review. *Journal of Process Control*, 19:723–731, 2009.

H. Scheu and W. Marquardt. Sensitivity-based coordination in distributed model predictive control. *Journal of Process Control*, 21(5):715–728, 2011.

J. D. Seader. The B. C. (before computers) and A. D. of equilibrium-stage operations. *Chemical Engineering Education*, 19(2):88–103, 1985.

J. Shin, M. Lee, and S. Park. Design of a composition estimator for inferential control of distillation columns. *Chemical Engineering Communications*, 178(1):221–248, 2000a.

J. Shin, H. Seo, M. Han, and S. Park. A nonlinear profile observer using tray temperatures for high-purity binary distillation column control. *Chemical Engineering Science*, 55(4): 807–816, 2000b.

A. Sirohi, , and K. Y. Choi. On-line parameter estimation in a continuous polymerization process. *Industrial & Engineering Chemistry Research*, 35(4):1332–1343, 1996.

S. Skogestad. Dynamics and control of distillation columns – a critical survey. *Modeling, Identification and Control*, 18(3):177–217, 1997.

S. Skogestad. Control structure design for complete chemical plants. *Computers & Chemical Engineering*, 28(1–2):219–234, 2004.

S. Skogestad and I. Postlethwaite. *Multivariable Feedback Control*. John Wiley & Sons, 1996.

G. Soave. Equilibrium constants from a modified Redlich-Kwong equation of state. *Chemical Engineering Science*, 27(6):1197 – 1203, 1972.

E. Sorel. *La rectification de l'alcool*. Gauthiers-Villais et fils, 1893.

M. Stuckert, B. Pluymers, and W. Marquardt. A novel method for monitoring of separation performance in distillation columns. In D. Bogle and M. Fairweather, editors, *22nd European Symposium on Computer Aided Process Engineering*, Computer Aided Chemical Engineering, pages 907–912. Elsevier, 2012.

R. Taylor. (Di)still modeling after all these years: A view of the state of the art. *Industrial & Engineering Chemistry Research*, 46(13):4349–4357, 2007.

R. Taylor and R. Krishna. *Multicomponent Mass Transfer*. John Wiley & Sons, 1993.

R. Taylor, R. Krishna, and H. Kooijman. Real-world modeling of distillation. *Chemical Engineering Progress*, pages 28–39, 2003.

The MathWorks, Inc. MATLAB and Optimization Toolbox Release 2011b, 1994–2016.

H. L. Toor. Prediction of efficiencies and mass transfer on a stage with multicomponent systems. *AIChE Journal*, 10(4):545–548, 1964.

S. Tronci, F. Bezzo, M. Barolo, and R. Baratti. Geometric observer for a distillation column: Development and experimental testing. *Industrial & Engineering Chemistry Research*, 44(26):9884–9893, 2005.

J. van den Berg. *Model Reduction for Dynamic Real-Time Optimization of Chemical Processes*. PhD thesis, Technische Universiteit Delft, 2005.

V. Venkatasubramanian, R. Rengaswamy, and S. N. Kavuri. A review of process fault detection and diagnosis: Part II: Qualitative models and search strategies. *Computers & Chemical Engineering*, 27(3):313–326, 2003a.

V. Venkatasubramanian, R. Rengaswamy, S. N. Kavuri, and K. Yin. A review of process fault detection and diagnosis: Part III: Process history based methods. *Computers & Chemical Engineering*, 27(3):327–346, 2003b.

V. Venkatasubramanian, R. Rengaswamy, K. Yin, and S. N. Kavuri. A review of process fault detection and diagnosis: Part I: Quantitative model-based methods. *Computers & Chemical Engineering*, 27(3):293–311, 2003c.

Online-Buchshop für Ingenieure

BUCHSHOP

Online-Shops

Fachliteratur und mehr - jetzt bequem online recherchieren & bestellen unter: www.vdi-nachrichten.com/Der-Shop-im-Ueberblick

Täglich aktualisiert: Neuerscheinungen VDI-Schriftenreihen

Im Buchshop von vdi-nachrichten.com finden Ingenieure und Techniker ein speziell auf sie zugeschnittenes, umfassendes Literaturangebot.

Mit der komfortablen Schnellsuche werden Sie in den VDI-Schriftenreihen und im Verzeichnis lieferbarer Bücher unter 1.000.000 Titeln garantiert fündig.

Im Buchshop stehen für Sie bereit:

VDI-Berichte und die Reihe **Kunststofftechnik:**

Berichte nationaler und internationaler technischer Fachtagungen der VDI-Fachgliederungen

Fortschritt-Berichte VDI:

Dissertationen, Habilitationen und Forschungsberichte aus sämtlichen ingenieurwissenschaftlichen Fachrichtungen

Newsletter „Neuerscheinungen":

Kostenfreie Infos zu aktuellen Titeln der VDI-Schriftenreihen bequem per E-Mail

Autoren-Service:

Umfassende Betreuung bei der Veröffentlichung Ihrer Arbeit in der Reihe Fortschritt-Berichte VDI

Buch- und Medien-Service:

Beschaffung aller am Markt verfügbaren Zeitschriften, Zeitungen, Fortsetzungsreihen, Handbücher, Technische Regelwerke, elektronische Medien und vieles mehr – einzeln oder im Abo und mit weltweitem Lieferservice

Die Reihen der Fortschritt-Berichte VDI:

1 Konstruktionstechnik/Maschinenelemente
2 Fertigungstechnik
3 Verfahrenstechnik
4 Bauingenieurwesen
5 Grund- und Werkstoffe/Kunststoffe
6 Energietechnik
7 Strömungstechnik
8 Mess-, Steuerungs- und Regelungstechnik
9 Elektronik/Mikro- und Nanotechnik
10 Informatik/Kommunikation
11 Schwingungstechnik
12 Verkehrstechnik/Fahrzeugtechnik
13 Fördertechnik/Logistik
14 Landtechnik/Lebensmitteltechnik
15 Umwelttechnik
16 Technik und Wirtschaft
17 Biotechnik/Medizintechnik
18 Mechanik/Bruchmechanik
19 Wärmetechnik/Kältetechnik
20 Rechnerunterstützte Verfahren (CAD, CAM, CAE CAQ, CIM ...)
21 Elektrotechnik
22 Mensch-Maschine-Systeme
23 Technische Gebäudeausrüstung

ISBN 978-3-18-525308-9